

ANASTASIA KOIVIKKO

Grippers and Sensors for Soft Robots

ANASTASIA KOIVIKKO

Grippers and Sensors for Soft Robots

ACADEMIC DISSERTATION

To be presented, with the permission of
the Faculty of Medicine and Health Technology
of Tampere University,
for public discussion in the auditorium S2
of the Sähköotalo, Korkeakoulunkatu 3, Tampere,
on 21 January 2022, at 12 o'clock.

ACADEMIC DISSERTATION

Tampere University, Faculty of Medicine and Health Technology
Finland

<i>Responsible supervisor and Custos</i>	Associate Professor Veikko Sariola Tampere University Finland	
<i>Supervisor</i>	Professor Pasi Kallio Tampere University Finland	
<i>Pre-examiners</i>	Professor Herbert Shea École Polytechnique Fédérale de Lausanne Switzerland	Research Fellow Fares Abu-Dakka Aalto University Finland
<i>Opponent</i>	Reader Adam Stokes The University of Edinburgh Scotland, United Kingdom	

The originality of this thesis has been checked using the Turnitin OriginalityCheck service.

Copyright ©2022 author

Cover design: Roihu Inc.

ISBN 978-952-03-2274-8 (print)
ISBN 978-952-03-2275-5 (pdf)
ISSN 2489-9860 (print)
ISSN 2490-0028 (pdf)
<http://urn.fi/URN:ISBN:978-952-03-2275-5>

PunaMusta Oy – Yliopistopaino
Joensuu 2022

Hemmille

PREFACE

The work was done in the Bioinspired Materials and Robotics Group (BioMaRo) in the Faculty of Medicine and Health Technology in Tampere University during the period 2017–2021. Overall, it has been a rewarding but demanding journey with high ups and downs. The highlight of my path to become Doctor of Technology was my research visit to Prof. Metin Sitti's Department of Physical Intelligence in Max-Planck Institute for Intelligent Systems in Stuttgart, Germany in 2018-2019. It was a great opportunity to work with talented people, learn new skills and see the world. I am deeply grateful for Prof. Metin Sitti for hosting me and for him and Dr. Dirk-Michael Drotlef for supervising me during my visit.

At first, I want to thank Assoc. Prof. Veikko Sariola for being my supervisor. It has been a real privilege to prepare this thesis and grow as a researcher under his supervision. Thank you for endlessly supporting and guiding me during these years.

I am also grateful for Prof. Pasi Kallio for being my second supervisor and for Prof. Arri Priimägi being a follow-up group member, their support has motivated me during the studies. Additionally, I thank the pre-examiners Prof. Herbert Shea and Dr. Fares Abu-Dakka. Their feedback helped me to improve the quality of this work. I am also grateful for Reader Adam Stokes for being the opponent in the public examination of my thesis.

I am grateful to all the people of Biomicrosystems joint research groups in Sähköotalo C and D corridors. Our summer and winter seminars have been important events to practice presentation skills and discuss our research. I am lucky to call many of you my friends nowadays. Especially, I am thankful for M.Sc Kaisa Tornberg for all the support during the long nights in the lab. I want to also thank Dr. Marika Janka and Mr. Jouni Niemelä for all the support in the lab with experiment setups.

I am deeply grateful to all the co-authors of my publications for all your help with the experiments and research questions. I want to also thank all the present and past colleagues of BioMaRo group: Vilma, Vipul, Kyriacos, Mika, Ahmed, Ehsan, Nur, and Katriina, our discussions in the group meetings and coffee breaks have motivated and helped me a lot. Moreover, I want to thank my office mates Kyriacos and Anum for inspiration, peer support and excellent coffee breaks.

I am grateful to all the funding I have got for my doctoral studies. I want to thank all the foundations that have supported me: The Finnish Cultural Foundation, The Finnish Science Foundation for Technology and Economics (KAUTE), The Finnish Foundation for Technology Promotion (TES), Walter Ahlström Foundation and Finnish Automation Society. I am also grateful for Assoc. Prof. Veikko Sariola for hiring me to his Academy of Finland projects.

Last, I am grateful to my parents Jyrki and Sari, brother Pietari, all my dear friends, and husband Risto. Thank you for always being there and reminding me of the life outside the lab.

Tampere, December 2021

A handwritten signature in cursive script, reading "Veikko Sariola". The signature is written in black ink on a white background.

ABSTRACT

Our lives in modern society are easier in many ways due to the ongoing revolution of robotics. Robots perform endless tasks in assembly lines and in factories making our work lighter and decreasing the need for human labour. To repeat these precise and heavy tasks millions of times, the robots—including actuators, sensors, and control and power units—are made of hard and tough materials. The hard robots are needed in factories but at the same time the hardness of the robots limits the safety and the comfort while working near humans. The research in soft materials has opened new possibilities in robotics, creating a new field called soft robotics. By shifting from the hard robot materials to soft ones, the robots can be 1) made safer: they cause less damage, even in collision; 2) made to conform to objects; and 3) made to feel comfortable against the skin.

Many of the manufacturing methods of soft robots have been adapted from the field of microfluidics. Silicone casting has been widely used to fabricate chips with detailed small structures. The method is efficient for replicating small features. However, complex structures, such as overhangs and buried channels, are particularly difficult to fabricate since the elastomer piece must be removed from the mould. In soft robotics, these kinds of structures are often desired for creating moving actuators and grippers. An efficient and fast way to fabricate fully three-dimensional soft structures is still needed.

Grippers made of soft materials can conform to objects, which can enable the picking of fragile objects without damaging them. However, it can limit the holding forces while carrying the object. During the object transport it can be beneficial if the gripper material is stiff or even rigid. Materials and mechanisms with controllable stiffness could be used to achieve this effect.

In addition to the soft body of the robot, the sensors need to also be stretchable and soft. One of the most important types of sensors used in soft robots is the strain sensor which in different configurations can measure exteroceptive and proprioceptive information. Many methods for fabricating soft strain sensors have been proposed, such as liquid metals and ionic conductors. However, many of these methods involve multiple fabrication steps or materials which are difficult to handle, so they are not suitable for mass manufacturing. Additionally, these sensors are

usually electrical, unlike soft actuators which are often pneumatic. Using pneumatics also for the sensing would simplify the overall structure of the robot.

This thesis explores different methods of designing and fabricating soft robots and sensors for them. First, we studied whether sacrificial 3D printing was a suitable method of fabricating soft devices moulds with overhanging structures. We were able to demonstrate that the proposed method is straightforward and can be used to fabricate buried channels in soft silicone elastomer structures. Second, we developed soft robotic grippers. We fabricated two different 3D printed suction-based grippers: a pneumatic one and a magnetically switchable hydraulic one. 3D printing was found to be a suitable method for soft gripper fabrication. We also found that the grippers outperformed commercial suction grippers with small, unevenly loaded and fragile objects. We propose using magnetorheological fluid, embedded inside a soft robotic gripper, to control the stiffness of the gripper. Last, the sensors were fabricated and integrated into soft robots. Two different approaches were proposed for strain and curvature sensing: screen-printed stretchable sensors and soft pneumatic strain sensors. We propose that screen-printing is a low-cost method suitable for mass manufacturing electric strain sensors, whereas soft pneumatic strain sensors are a step towards fully pneumatic soft robots.

To conclude, this dissertation describes new methods of fabricating soft robots and sensors for them, aiming at simpler ways to fabricate smarter soft robots with perception.

TIIVISTELMÄ

Elämämme modernissa yhteiskunnassa on monin tavoin helpompaa kuin ennen, ja yksi suuri syy tälle on robottien nopea yleistyminen. Ne ovat täyttäneet tehtaat ja valmistuslinjat ja työskentelevät siellä taukoamatta tehden työstämme fyysisesti kevyempää. Jotta robotit voisivat toistaa pikkutarkkoja ja raskaita liikkeitä miljoonia kertoja, täytyy robottien sekä niiden toimielinten, antureiden, ohjausyksiköiden ja voimalähteiden olla kovia ja kestäviä. Tällaisia kovia robotteja tarvitaan tehtaissa, mutta toisaalta kovuus rajoittaa niiden turvallista ja miellyttävää käyttöä ihmisten lähellä. Pehmeiden materiaalien tutkimus on avannut uusia mahdollisuuksia robotiikan alalle luoden uuden alan: pehmorobotiikan. Kovista materiaaleista pehmeisiin siirtymällä 1) roboteista tulee turvallisempia: ne eivät vahingoita, vaikka törmäisivät ihmiseen, 2) robotit mukautuvat pinnan muotoihin ja 3) ne tuntuvat mukavammilta ihoa vasten.

Monet pehmorobottien valmistusmenetelmistä on otettu mikrofluidistiikan alalta, jossa on käytetty silikonivaluja pienien ja yksityiskohtaisten mikrofluidististen testausalustojen valmistukseen. Tämä tekniikka mahdollistaa erittäin pienien rakenteiden tarkan kopioimisen muotista lopputuotteeseen, mutta monimutkaiset rakenteet, kuten ulokkeet ja upotetut kanavat, ovat haasteellisia valmistaa, koska muotti pitää saada irrotettua pehmeän rakenteen ympäriltä. Pehmoroboteissa tällaisia monimutkaisia rakenteita kuitenkin tarvitaan liikkuvien toimielinten ja tarttuvien aikaansaamiseksi, ja siksi tarvitaan valmistustapa, jolla voidaan tehdä tehokkaasti aidosti kolmiulotteisia rakenteita.

Pehmeistä materiaaleista tehdyt tarttujat mukautuvat kohteen muotoihin, mikä mahdollistaa hauraiden asioiden poimimisen vahingoittamatta niitä. Pehmeys voi kuitenkin rajoittaa sitä, kuinka suuria voimia tarttujat pystyvät käsittelemään. Tarttujan kovuus tai jäykkyys voi kasvattaa sen kykyä käsitellä suuria voimia kappaleen kuljetuksen aikana. Materiaalit ja mekanismit, joiden jäykkyyttä voi kontrolloida, voisivat mahdollistaa tällaisen säädettävän tarttumisen ja jäykkyyden.

Pehmeiden runkojen lisäksi roboteissa käytettävien antureiden tulee olla venyviä ja pehmeitä. Yksi tärkeimmistä pehmoroboteissa käytetyistä anturityypeistä on venymäanturi, jonka eri kokoonpanoilla voi mitata robotin ulkoista ja sisäistä informaatiota. Venymäantureiden valmistamiseen on ehdotettu monia erilaisia

menetelmiä, kuten nestemäiset metallit ja ionijohteet. Monissa menetelmissä tarvitaan kuitenkin useita valmistusvaiheita tai niissä käytettyjä materiaaleja on vaikea käsitellä, joten ne eivät sovellu massavalmistukseen. Tämän lisäksi ehdotetut anturit ovat usein sähköisiä toisin kuin toimielimet, jotka ovat usein pneumaattisia. Siirtymällä pneumaattisiin antureihin voitaisiin robotin kokonaisrakennetta yksinkertaistaa.

Tässä väitöskirjassa tutkimme eri menetelmiä pehmorebottien tarttujen ja antureiden valmistamiseksi. Ensiksi tutkimme, voiko uhri-3D-tulostuksella valmistaa pehmeille materiaaleille valumuotteja, joissa on ulkonevia rakenteita. Näytimme, että tapa oli vaivaton ja että sillä pystyttiin valmistamaan upotettuja kanavia pehmeisiin silikonirakenteisiin. Toiseksi me kehitimme pehmotarttuvia. Valmistimme kaksi erilaista 3D-tulostettua imukuppitarttujaa: pneumaattisen sekä magneettisesti ohjattavan hydraulisen tarttujan. Totesimme 3D-tulostuksen sopivaksi tavaksi valmistaa pehmotarttuvia. Huomasimme myös valmistettujen tarttujen suoriutuvan haasteellisten kohteiden, kuten pienien kappaleiden, epätasaisten kuormien ja hauraiden esineiden, poimimisesta paremmin kuin kaupallisten imukuppitarttujen. Ehdotamme myös, että magnetoreologisen nesteen käytöllä tarttujan jäykkyyttä voidaan säädellä. Viimeiseksi valmistimme ja integroimme antureita pehmorebottihin. Ehdotimme kahta erityyppistä ratkaisua venymän ja käyryyden mittaamiseen: silkkipainettuja resistiivisiä venyviä antureita sekä pneumaattisia venymäliuskoja. Esitämme, että silkkipainotekniikka on edullinen ja massavalmistukseen soveltuva valmistustapa sähköisten venymäantureiden valmistukseen, kun taas pneumaattiset venymäliuskat ovat askel lähemmäs kokonaan pneumaattisia pehmorebottia.

Kaiken kaikkiaan tämä väitöskirja käsittelee uusia pehmorebottien tarttujen ja antureiden valmistusmenetelmiä. Tavoitteena on löytää yksinkertaisempia tapoja valmistaa älykkäämpiä pehmorebottia.

CONTENTS

1	Introduction	1
2	Soft robotics.....	4
2.1	Fabrication of soft robots.....	5
2.2	Actuation of soft robots	8
2.3	Soft manipulators.....	11
3	Sensors for soft robots.....	16
3.1	Strain sensing methods	16
3.2	Integration stretchable strain sensors into soft robots.....	19
3.3	Soft strain sensor performance.....	21
4	Aims of the study	25
5	Experimental work.....	26
5.1	Castable soft elastomers	26
5.2	3D printing.....	28
5.3	Screen-printing	28
5.4	Coating and casting soft silicone elastomers	29
5.5	Design and fabrication of soft grippers	31
5.6	Integration of sensors into soft pneumatic actuators	33
5.7	Soft pneumatic gripper fabrication	34
5.8	Characterization methods.....	34
5.8.1	Suction gripper characterization	34
5.8.2	Surface roughness measurements.....	36
5.8.3	Pneumatic actuation.....	36
5.8.4	Curvature measurements	37
5.8.5	Resistance measurement	37
5.8.6	Pneumatic resistance measurement.....	38
5.8.7	Statistical analysis.....	38
6	Summary of main results	39
6.1	Sacrificial 3D printing for complex mould fabrication (Publication I).....	39
6.2	Compliant gripping (Publications II and III).....	42

6.3	Screen-printed stretchable strain sensors for soft robotics (Publication IV)	49
6.4	Stretchable pneumatic strain sensors (Manuscript V).....	54
7	Discussion.....	61
7.1	Alternative and more capable fabrication of soft robot components.....	61
7.2	Grippers with switchable adhesion and stiffness.....	62
7.3	Stretchable strain sensors for soft robots	65
7.4	Future of all-pneumatic soft robots	68
8	Conclusions	70

ABBREVIATIONS AND SYMBOLS

2D	Two-dimensional
3D	Three-dimensional
ABS	Acrylonitrile butadiene styrene
CNC	Computer numerical control
DE	Drift error
DLS	Digital light synthesis
eGaIn	eutectic Gallium Indium
ER Fluid	Electrorheological fluid
FDM	Fused deposition modelling
GF	Gauge factor
GF _{silver}	Gauge factor for silver-ink based sensor
HIPS	High-impact polystyrene
MEMS	Medical microelectromechanical system
MR fluid	Magnetorheological fluid
PET	Polyethylene terephthalate
PMMA	Polymethyl methacrylate
PVA	Polyvinyl alcohol
PVB	Polyvinyl butyral
PDMS	Polydimethylsiloxane
SD	Standard deviation
SE	Standard error
SLA	Stereolithography
TPU	Thermoplastic polyurethane
UV	Ultraviolet
A_0	Initial area of cross section
A_r	Cross sectional area of the conductive sensing films
a	Loss in the output power
C	Capacitance
$C_{1,2,3}$	Pneumatic actuators 1,2,3

c	Concentration of chemical species in the medium that attenuate light
d_c	Thickness of the dielectric layer
d_{np}	Distance from the neutral plane
E	Young's Modulus
e	Absorptivity of the material
F	Applied force
F_{off}	Pull-off force
F_{pre}	Preload
L	Elongated length
L_0	Initial length
L_r	Length of the conductor
L_w	Initial length of the wave guide
L_c	Length of the capacitor
P_{act}	Pressure inside the pneumatic actuator
P_{atm}	Atmospheric pressure
P_{gauge}	Pressure in pneumatic strain sensor
P_{neg}	Negative pressure inside the gripper chamber
P_{supply}	Supply pressure for the pneumatic strain gauge
r	Radius
R	Pneumatic resistance of the pneumatic strain sensor
R_1	Resistance at the beginning of the period
R_2	Resistance at the end of the period
$R_{1,2,3}$	Pneumatic resistance of the pneumatic strain gauges 1,2,3
$R_{c1,c2,c3}$	Pneumatic resistance of the constant restrictors 1,2,3
R_r	Resistance of the conductor
R_c	Pneumatic resistance of the constant restrictor
R_{carbon}	Resistance of the carbon ink-based strain sensor
R_{silver}	Resistance of the silver ink-based strain sensor
R_{rms}	Root mean squares surface roughness
R_z	Maximum peak to valley depth in single sampling rate
S	Shore hardness
V	Withdrawal volume
W_T	Tensile work

$\Delta C/C_0$	Relative change in the sensor output capacitance
$\Delta R/R_0$	Relative change in sensor output resistance
$\Delta R/R_c$	Relative change in pneumatic resistance
δ	Resistivity of the material
ε	Engineering strain
ϵ_0	Vacuum permittivity
ϵ_r	Relative permittivity of the dielectric layer
κ	Curvature
σ	Tensile stress
ν_d	Poisson's ratio of the dielectric
ν_e	Poisson's ratio of the electrodes
ω_c	Width of the capacitor

ORIGINAL PUBLICATIONS

- Publication I **Koivikko A.** & Sariola V. Fabrication of Soft Devices with Buried Fluid Channels by Using Sacrificial 3D Printed Molds. In *RoboSoft 2019 - 2019 IEEE International Conference on Soft Robotics*. IEEE: Seoul, Korea, 2019, pp 509–513.
- Publication II **Koivikko A.**, Drotlef D-M., Dayan C. B., Sariola V. & Sitti M. 3D Printed soft suction gripper for rough and small objects. *Advanced Intelligent Systems*, **3**, 2100034 (2021).
- Publication III **Koivikko A.**, Drotlef, D-M., Sitti M. & Sariola V. Magnetically switchable soft suction grippers. *Extreme Mechanics Letters*, **44**, 101263 (2021).
- Publication IV **Koivikko A.**, * Sadeghian Raei E., * Mosallaei M., Mäntysalo M. & Sariola V. Screen-printed curvature sensors for soft robots. *IEEE Sensors Journal*, **18**, 223-230 (2017).
- Manuscript V **Koivikko A.**, Lampinen V., Pihlajamäki M., Yiannacou K., Sharma V., Sariola V., Highly stretchable pneumatic strain gauges. MANUSCRIPT

*These authors contributed equally.

AUTHOR'S CONTRIBUTION

- Publication I The study was designed by the author and V. Sariola. The author conducted the experiments and wrote the conference paper together with V. Sariola.
- Publication II The author designed the gripper together with D-M. Drotlef. The experiments were done by the author and C. B. Dayan. The paper was written by the author with inputs from all three other authors.
- Publication III The author designed the gripper together with D-M. Drotlef and V. Sariola. The author fabricated, characterized, and analysed the data and wrote the paper together with V. Sariola.
- Publication IV The author and E. Sadeghian Raei fabricated and characterized the actuators with integrated sensors, manufactured the soft pneumatic gripper and conducted the demonstrations. Moreover, the author was responsible for writing the paper together with E. Sadeghian Raei and V. Sariola.
- Manuscript V The study was planned by V. Sariola and the author. The author conducted the fabrication, design, and characterization of the pneumatic strain sensors together with V. Lampinen, M. Pihlajamäki and K. Yiannacou. The paper was written by the author and V. Sariola.

1 INTRODUCTION

Nowadays, autonomous machines, *robots*, perform various tasks in assembly lines of the factories and other repetitious well-defined jobs like weaving clothes. For other kinds of tasks human labour is still needed, for example lifting elderly people in nursing homes, operating patients in operating theatres and giving physiotherapy to paralysed people. These tasks consist of several sub steps, with several alternative ways to complete them and still they are often heavy for the humans executing them.

The automatization of such complex tasks has been predicted to become reality since the 90s, by then newly developed moving field robots, which were not stationary machines anymore. The development and fast progress of artificial intelligence and machine learning in the 2000s made the hopes of automated healthcare even more realistic, as the robots took first steps simulating human interaction.¹ Nevertheless, to make the robots suitable for working near humans, the robots should be not only intelligent, but also safe and comfortable to use.

To address this, the materials of the robots should be examined. Traditionally, the robots have been built by soldering hard electronic components, injection moulding thermoplastics, welding steel parts together or by using carbon fibres. By shifting from these hard materials to *soft*, the robots can be made safer: even in collision, they produce less damage, they conform to target objects and feel comfortable against the skin.

Manufacturing of these *soft robots* is not straightforward since the previously used manufacturing methods do not apply anymore: soft parts cannot be milled and joined with gears. Since many animals are entirely or partly soft, the inspiration was sought from nature; how plants grow,^{2,3} animals move^{4,5} and grasp objects,⁶ and respond to different stimuli?⁷ For example, an octopus can move nimbly, grasp objects and squeeze through confined spaces⁸ even with an entirely soft body.

Many of the proposed soft robot fabrication methods have been adapted from the field of microfluidics.⁹ There, silicone replica moulding has been widely used to manufacture chips with detailed small structures. Although the method is efficient for replicating small features, complex structures—overhangs and buried channels—are particularly difficult to fabricate since the elastomer must be removed from the

mould. In soft robotics, these kinds of structures are often desired for creating moving actuators and grippers. Thus, an efficient and fast way to fabricate fully three-dimensional (3D) soft structures is needed.

The soft materials conform to surface they are pressed against which can simplify the grasping.⁹ However, while the compliance simplifies the picking, the achieved maximum gripping forces can be smaller in comparison with hard grippers. After the object picking and transportation, the objects should be able to release controllably. A gripper with adhesion and stiffness switching would conform the surface shapes, be stiff during the transportation and release the object in a controlled way.

To create a soft robot with perception, sensing needs to be added to the soft body. For preserving the soft nature of the robot, the sensors must be also soft and stretchable. These kinds of soft sensors have been used in wearable electronics and many sensing methods have been transferred from there into soft robots. One of the most popular sensors being a strain sensor, which in different configurations can measure exteroceptive or proprioceptive information. Many methods of fabricating soft and stretchable strain sensors have been proposed, such as liquid metals¹⁰ and conductive nanocomposites.¹¹ However, many of these examples involve multiple fabrication steps or materials which are difficult to handle, so they are not suitable for mass manufacturing. Additionally, these sensors are usually electrical, unlike the often-used soft pneumatic actuators. To shift the sensing also from electrical to pneumatic, would simplify the overall structure of the robot.

The aim of this thesis is to develop faster and easier fabrication methods for a soft robot, a gripper, and a sensor manufacturing, allowing more complex designs and easy integration. First, we studied if sacrificial 3D printing was suitable method for fabricating soft devices with overhanging structures. We were able to demonstrate that the proposed method is straightforward and can be used to fabricate soft silicone elastomer structures with buried channels. Second, we developed two types of soft robotic grippers. We fabricated 3D printed suction-based grippers: a pneumatic one and a magnetically switchable hydraulic one. 3D printing was found out to be suitable method for soft gripper fabrication. We also found out that the grippers outperformed a commercial suction gripper with small, unevenly loaded, and fragile objects. Additionally, we propose using magnetorheological (MR) fluid, embedded inside a soft robotic gripper, to control the stiffness of the gripper. Last, the sensing functionality was integrated into soft robots. Two different approaches were proposed for strain and curvature sensing: screen-printed strain sensors and soft pneumatic strain sensors. We show that

screen-printing is a simple, a low-cost method suitable for mass manufacturing of electric strain sensors. Whereas soft pneumatic strain sensors are a stable, non-hysteric way to capture small and large strains, leading the way towards fully pneumatic soft robots.

The key novelty of the **Publication I** is the comprehensive comparison of the suitability of different commercial 3D printing materials for sacrificial mould fabrication. In **Publication II**, the novelty is the shift from elastomer casting to 3D printing which enables higher pull-off forces and simpler fabrication. The principle to use MR fluid for stiffness switching in a suction gripper is novel in **Publication III**. In **Publication IV**, the key novelty is to demonstrate that different inks can be used to fabricate curvature sensors. We also prove that the sensor is measuring the curvature, not pressure by decoupling the pressure from the sensor output. In the **Manuscript V**, the principle of the pneumatic resistance is a novel approach to be used in the strain sensing.

2 SOFT ROBOTICS

Soft robots have been defined as 1) machines made of compliant, soft materials or 2) hard actuators that operate in concert, having soft material properties.¹² In this thesis only soft bodied robots are discussed. Figure 1 shows the softness of some common biological (blue) and engineering (pink) materials. The biological materials tend to be softer than commonly used materials in robotics like steel and fibreglass. The robots, which primarily consist of materials which softness is close to soft biological materials, such as skin and fat, are considered soft robots in this thesis.⁹

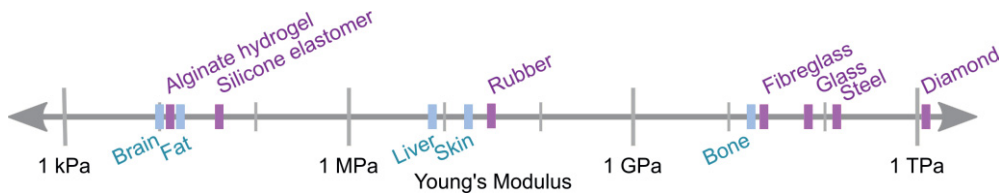


Figure 1. Mechanical properties (Young's modulus) of some common biological (blue) and engineering (pink) materials, modified from Rus and Tolley.⁹

The soft robots consist of the same key components as hard robots: logic, power source, actuators, including end-effectors, and sensors. In traditional hard robots, these components are usually rigid and electrical. In soft robots, the components should be soft, or they should be placed outside the robot. For the soft logic, soft pneumatic circuits have been proposed^{4,13,14} in addition to traditional electrical logic circuits. The power source type depends on the used actuators, logic, and sensors. One of the most common actuator type in soft robots is the fluidic elastomer actuator which moves in response to pressure change.^{15,16} Thus, the power source is often pneumatic. In addition to traditional pneumatic power sources, untethered solutions, such as combustion,¹⁷ have been developed.

In addition to soft actuators, robots also need grippers for picking and handling objects. Soft and compliant grippers allow the robots to conform to the manipulated objects, which makes it easy to grip objects of varying size, material, and shape. Soft grippers based on different physical principles such as adhesion and grasping have been demonstrated,¹⁸ each gripper type having its own advantages, like high holding

forces¹⁹ or adaptive sealing.²⁰ However, there are still several not fully solved challenges, such as switchable adhesion or easy integration into robotic body. Thus, there is a need for versatile grippers, which are easy to integrate into the soft robot bodies.

Another key component of the robot is the sensor which gives feedback from the posture of the robot and its surroundings. These sensors must be also soft since they are located inside the robot body. Different sensors technologies have been proposed for soft sensing, but they are often complicated to manufacture, include materials challenging to handle (e.g., liquid metals) or cannot be fully integrated into soft robot body.

In this chapter literature related to soft robots is discussed, followed by the next Chapter 3 about stretchable sensors for soft robots.

2.1 Fabrication of soft robots

Many of the fabrication methods of soft robots have been adapted from the field of microfluidics,⁹ where structures have been manufactured by casting soft elastomers into moulds. The chosen fabrication method of the soft robot depends on desired material and design. Table 1 shows some materials commonly used for fabricating soft robots.

Table 1. Common materials and suitable fabrication methods used in soft robots manufacturing

Soft body materials	Fabrication into soft actuator	Selected references
Silicone elastomers	Casting, 3D printing	6,15,21,22
Hydrogels	Casting, 3D printing	23,24
Polyurethanes	Casting, sculpting	25
Printable elastic resins	3D printing	17,26
Liquid crystal elastomers	Casting, Laser cutting	5,27
Protein-based materials	Casting, Laser cutting	28

Soft silicone elastomers and polyurethanes are traditionally cast into computer numerical control (CNC) milled or 3D printed moulds to create different shaped actuators,¹⁵ grippers²¹ and logic^{4,13} for soft robots. The silicone elastomers are usually two component materials, other one being the curing agent.²⁹ Initially, the components are liquids, which enables degassing (the removal of air bubbles) and pouring the silicone elastomer also into narrow moulds. However, the designs of

parts that can be moulded at a time are limited: for example, a part cannot contain cavities inside.

Silicone elastomers are not the only castable materials that have been used in the fabrication of soft robots.³⁰ Hydrogels have also been cast into moulds, to make soft actuators. Hydrogels are hydrophilic crosslinked polymer networks that also contain water molecules. The polymer network mesh size is ~ 10 nm, which is much larger than the water molecule size. Thus, the water molecules maintain the same chemical and physical properties as in liquid water.³¹ Some hydrogels are extremely soft (Young's Modulus ≈ 10 kPa⁹) and biocompatible³² which could allow the fabrication of biocompatible soft robots. The actuation of hydrogels is usually based on the uptake or release of water which causes the actuators to either swell or shrink in response of different stimuli, such as pH or humidity. However, this actuation method is often relatively slow.³⁰ In response to that limitation, Yuk et al.³³ proposed a cast hydrogel actuator that is hydraulically driven providing faster actuation speed and higher forces.

Other materials that are cast to create soft robots include liquid crystal polymers and protein-based materials, both recombinant and natural ones. Liquid crystals are materials that can have the properties of liquids and solid crystals. The liquid crystals can be loosely crosslinked with elastomers to form elastic materials that are responsive to different stimuli like light⁷ or temperature.³⁴ Recently, recombinant protein materials have been also introduced to soft robotic fabrication. Penafrancesch et al.²⁸ reported synthetic biomimetic squid ring teeth material that can self-heal micro and macro scale damages.

Another fabrication method proposed for soft robot manufacturing is sculpting. Argiolas et al.²⁵ proposed a method for creating a sculptable material, by mixing silicone elastomer with salt. The sculpting was done freely by hand, so it is more suitable for demonstrations and fast prototyping.

All the fabrication methods can be used to create the entire soft robot body or just parts of it, which are later bonded together. The bonding method depends on the materials used. Some silicone elastomers, especially polydimethylsiloxane (PDMS), can be bonded by cleaning the surface with oxygen plasma and pressing the treated parts together. This method is widely used in the field of microfluids.³⁵ The attached surfaces must be smooth and clean to achieve a durable bond. One of the limiting factors for the use of plasma bonding is the softness of the elastomer. The reason is likely the silicone oils which soften the silicone structure but interfere with the plasma bonding.³⁶ Such elastomers are usually attached by wet bonding, where a thin layer of uncured elastomer is spread between the parts and let cure.^{12,15,21}

Recently, 3D printing has become more versatile with different material options and better resolution. Many 3D printing technologies allow direct printing of soft and stretchable materials. They can be used to 3D print the whole soft robot in one run.¹⁴ Filament based 3D printers, often called fused deposition modelling (FDM) printers, use thin filaments which are extruded through a heated nozzle and printed layer by layer to form a 3D object. The filaments are often thermoplastics which melt in the nozzle and, while still partly melted, bond well to the previously printed and cooled layer. Many manufacturers offer different flexible filaments, but thermoplastic polyurethane (TPU) has been the most successful (Young's modulus ≈ 10 MPa). In FDM printing, the printing resolution is determined by the nozzle diameter, but due to the heterogeneities in the print, the wall thickness should be triple the nozzle size.³⁷

In resin-based 3D printing techniques, like in stereolithography (SLA) and in digital light synthesis (DLS), the resin is photosensitive and solidifies in ultraviolet (UV) or near-UV light. In SLA technique, a near-UV beam scans two-dimensional (2D) cross-sections on thin resin layers and the 3D structure is formed layer-by-layer. The DLS technique is similar but uses a digital projector to illuminate the entire 2D cross-section at once, resulting in faster 3D printing time.³⁷ Flexible and elastic resins are available for both methods, such as Elastic 50A, Formlabs Inc. and EPU 40, Carbon Inc.

Custom built SLA printers have been also proposed for printing soft and stretchable materials. Patel et al.³⁸ developed UV-curable elastomer, which was the mix of monofunctional monomer consisting of epoxy aliphatic acrylate and a cross-linker consisting of aliphatic urethane diacrylate diluted with isobornyl acrylate. They were able to achieve up to 1100% strains and 3D print different structures.

3D printing of silicone elastomers²² and hydrogels²³ have been also proposed. The soft silicone elastomers were 3D printed with direct ink writing technique and by adding nano silica to the elastomer ink.²² Mishra et al.²³ proposed SLA printing technique for the printing of hydrogels to create hydraulically actuated hydrogel actuators, which had autonomic perspiration ability.

In conclusion, casting is a suitable fabrication method for the variety of the soft materials. High replication resolution can be achieved and the method is suitable for mass manufacturing. The 3D structure of the cast part is limited since the part must be demoulded after curing, limiting overhanging structures and buried channels. If the robot is assembled from many parts, the bonding of the soft elastomer pieces can be challenging. For plasma bonding, the surfaces must be clean and smooth to achieve a strong bond. If wet bonding is used, the adhesive (e.g. uncured elastomer)

can block the small and thin structures. 3D printing allows the fabrication of the whole soft robot at once. Complex structures such as overhangs and buried channels can be fabricated but they might require supporting structures during 3D printing. Removing the support structures can damage the surface of the 3D printed object. 3D printing of soft materials has developed fast recently, but the resolution is not yet as high as with cast parts. In layer-by-layer 3D printing (FDM and SLA), delamination between layers can occur where the material strength is not the same as by using casting.

2.2 Actuation of soft robots

The actuation method of a soft robot depends on the robot design and the desired robot tasks such as locomotion, manipulation or human-machine interaction.⁹ One of the most common actuation methods is to use pneumatic or hydraulic actuation^{39,40} because it can achieve high grasping forces, fast operation speeds and the control is relatively simple. However, the power units tend to be large and heavy so miniaturization can be difficult.

The main idea is that the generated pressure difference expands the compliant robot material, while the asymmetric structure or strain limiting parts causes the part to move in a desired way. Pneumatic and hydraulic actuation-based robots have been proposed for locomotion (e.g., crawling,^{15,41} and jumping¹⁷), manipulation,²¹ and human-machine interaction.^{42,43} One example of the linear pneumatic actuators is the pneumatic artificial muscle, also known as the McKibben actuator, developed already in 1950's.⁴⁴⁻⁴⁹ They consist of a soft inflatable elastomer tube and a strain limiting mesh sleeve around it, fixed from both ends of the tube. When the soft elastomer tube is pressurized, it expands but the sleeve restricts it and forces the actuator to shorten (Figure 2a).

Another widely used actuator type is the fluidic elastomer actuator which is usually made of silicone elastomer and driven by pneumatics or hydraulics. One of the most popular fluidic elastomer actuator type is the pneumatic network actuator. It consists of soft elastomer with a fluidic network and/or chambers, attached to a strain limiting layer.^{15,16,23,50,51} When the chambers are pressurized, they expand and push each other away. The strain limiting layer limits the expansion and elongation of the actuator forcing the actuator to bend instead (Figure 2b). These fluidic elastomer actuators have been used to build various soft walking robots^{15,50} and manipulators.¹² For instance, Shepherd et al.¹⁵ proposed a completely soft crawling

robot built of five pneumatic actuators, which was able to navigate through difficult obstacles.

Another type of the fluidic elastomer actuator is a fibre-reinforced actuator.⁵² It consists of an extensible pneumatic chamber attached to a strain limiting layer. The soft and stretchable chamber is covered with fibre mesh for limiting the expansion in the radial direction. When the chamber is pressurized, the strain limiting layer forces the actuator to bend, similarly than with the pneumatic network actuator. Fibre-reinforced actuators have been used in various manipulators, for instance in a soft robotic hand.⁵³ Wang et al.⁵⁴ combined pneumatic networks and fibre-reinforced actuators for developing a robotic hand with a human-inspired soft palm.

In addition to positive pressure actuation, negative pressure can be also used. When negative pressure is applied, vacuum chambers in the soft elastomer collapse which causes a linear actuator to shrink (Figure 2c).^{55,56} Fatahillah et al.⁵⁷ combined both negative and positive pressures on their soft actuators and demonstrated that this increased the overall blocking force of the actuator.

Another widely used way to actuate soft robots is integrated tendons, where a cable is integrated into the soft body of an actuator. They can achieve high operation speed and accuracy, but the external motors add the overall size and weight of the robot. The cable is connected to an external motor. By withdrawing the cable, the length of the tendon inside the soft actuator shortens forcing the actuator to bend (Figure 2d).^{6,58–60}

Different actuation methods based on materials that respond to external stimuli (active materials) have also been proposed. These include shape memory materials such as shape memory alloys and polymers.⁶¹ The shape memory materials response to external stimuli (often heat) by returning to their initial shape. In soft actuators, shape memory materials are often used as springs and wires (Figure 2e). Simone et al.⁶² built a three-fingered prosthetic hand by using shape memory alloy wires (nickel-titanium) as tendons. Villoslada et al.⁶³ used shape memory alloy wires in a wearable soft robot wrist exoskeleton. The limitations to shape memory materials are the low response speed (seconds) and hysteresis.¹⁸

Polymers that react to electrical stimulus are called electroactive polymers. The most common ones are dielectric elastomers and ionic-polymer metal composites.¹⁸ Dielectric elastomer actuators consist of a soft elastomer film sandwiched between two electrodes forming an elastomeric capacitor.⁶⁴ When a high voltage is applied between the electrodes, they attract to each other (Maxwell stress). This squeezes the elastomer dielectric while its area expands (Figure 2f). The actuators have typically fast response time and are light weighted but they cannot pick heavy objects and

need a high voltage for actuation.⁴⁰ Actuators based on this phenomenon have been used for example to build soft robotic grippers⁶⁴ and swimming soft robots.⁶⁵

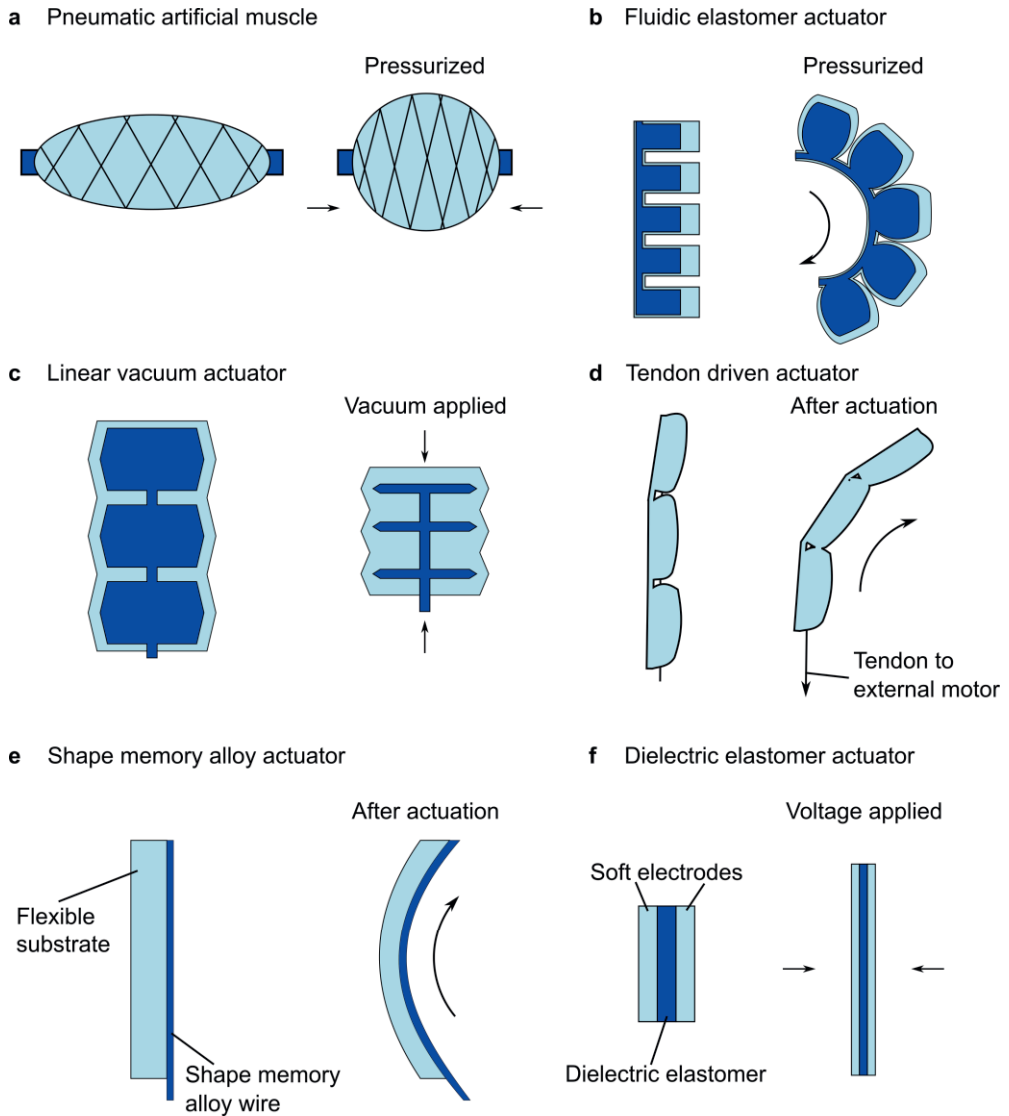


Figure 2. Actuation methods of the soft actuators. a) Linear pneumatic artificial muscle actuator b) bending pneumatic network actuator, c) linear vacuum actuator, d) bending tendon driven actuator, e) bending shape memory alloy wire actuator and f) linear dielectric elastomer actuator.

Ionic-polymer metal composites are also capacitors but here the dielectric layer is an electrolyte-swollen polymer membrane. When a low voltage is applied, anions and cations start to migrate towards an anode and a cathode, respectively which leads to swelling of the actuator on the other side of the structure.¹⁸ Bending actuators using this phenomenon have been proposed,^{66,67} but the method has limitations with slow response speed and produced forces.¹⁸

There are various other materials that are responsive to different stimuli. One big group are different gels and hydrogels. They can be actuated for example by light,⁶⁸ pH change,⁶⁹ temperature change,²⁴ and magnetically and electrically.⁷⁰ In addition to gels and hydrogels, liquid crystals^{5,7} and nature based materials⁷¹ have been proposed.

2.3 Soft manipulators

One crucial task for soft robots is the manipulation—picking, carrying and placing—of target objects. For soft manipulators, variety of different grippers have been proposed.¹⁸ One way to categorize the grippers is by the grasping method they use. The first approach is to use the bending soft actuators: gripping by grasping the object (Figure 3a). These grippers can be fluidically actuated,^{12,72,73} tendon driven,^{6,58} or the material can be externally actuated: grippers made of electroactive polymers,⁶⁴ hydrogels²⁴ and shape memory alloys,⁶² as discussed in Chapter 2.2. The grasping-based grippers can typically handle heavy loads and pick different shaped objects, but flat and deformable objects can be difficult for them.¹⁸ One of the first soft fluidic grippers was proposed in 1992 by Suzumori et al.⁷⁴ They fabricated fluidic elastomer actuators with seven degrees of freedom and combined them to build a four-fingered gripper.

In addition to tendon driven grippers, external motors are also used in fish fin deformation inspired grippers, called Fin Ray grippers.¹⁸ The gripper has a passive structure that bends conforming the object when in contact, and external motors are used to provide the movements of the grasping parts. Tawk et al.⁷⁵ combined the Fin Ray structure with fluidic elastomer actuators to build gripper that can handle different shape and size objects.

The other proposed grasping method is to control the stiffness of the gripper (Figure 3b). This can be made by using shape memory materials,⁷⁶ granular jamming,¹⁹ low melting point alloys⁷⁷ or electrorheological (ER) and MR fluids.⁷⁸ Granular jamming is familiar phenomenon from the vacuum sealed coffee packages:

they become soft once they are opened. This is due the pressure-change between the granules inside the package. This phenomenon has been used to fabricate universal soft grippers^{19,79,80} which can be actuated rapidly. However, the target object must be smaller than the diameter of the gripper for the gripping to succeed. Thus, also flat objects are difficult for this gripping method.

Low melting point alloys respond to heat (47-62 °C) by changing from solid to liquid. In soft grippers, such alloys can be encapsulated with soft silicone elastomers or foams. They have been also combined with dielectric elastomer⁷⁷ and fluidic elastomer⁸¹ actuators to create a switchable stiffness structure. The main limiting factor for the usage of this phenomenon is the slow response speed (30–40 s).¹⁸

ER and MR fluids are also used in the stiffness switching grippers. These fluids change their stiffness under electric or magnetic field. ER fluids consist of dielectric fluid (often oil) and polarizable particles (0.1-100 μm), which form chains under electric field.¹⁸ This chain structure leads to an increase in the stiffness of the fluid. MR fluids are also oils and they contain ferromagnetic particles (3-5 μm).⁸² Grippers made of soft silicone elastomer with a cavity filled with MR^{78,83} or ER⁸⁴ fluids have been proposed. Both of these have been also mixed with soft silicone elastomer to create stiffness switchable grippers, but the stiffness change is greatly decreased.¹⁸

The gripping can also be produced by controlling the adhesion between the gripper and the target object (Figure 3c). These grippers do not have the limitation of the target object being too large to grip since they do not envelope the object. First way to control the adhesion is to mimic the controllable adhesion in gecko's foot (dry adhesion). Geckos can climb up the walls without falling due to the special microfibrillar structures on their feet. The microfibrillar structures are responsible for the ability of geckos to adhere to walls: each tiny fibre adhering to the wall contributes a small force (van der Waals and capillary forces⁸⁵), yet together millions of these fibres provide strong enough adhesion for a gecko to even hang upside down from the ceiling. This structure has been mimicked in the gecko-adhesive grippers. These grippers^{86–88} can pick loads multiple times their own weight but struggle with wet, dirty and complex shaped surfaces. Song et al.⁸⁶ proposed gecko-inspired film attached to the suction based gripper allowing controllable load sharing. The method allows to control the gripping strength during the picking process. Ruffato et al.⁸⁹ proposed hybrid gripping technique where they combine an adhesion controlled surface with a grasping based gripper.

Another method of controlling the adhesion is called electroadhesion. This gripping method is based on the Coulomb force: the attraction between positive and negative charges. In soft gripping, a high electric field is used to control the electric

charges on the gripper and the object surfaces. Shintake et al.⁹⁰ proposed a soft gripper which combined electroadhesion (adhesion switching) and dielectric elastomer actuators (grasping). Guo et al.⁹¹ reported a soft wall climbing robot, which used electroadhesion to attach to the wall. Overall, electroadhesion can have challenges with dirty surfaces since this can reduce the adhesion force.¹⁸

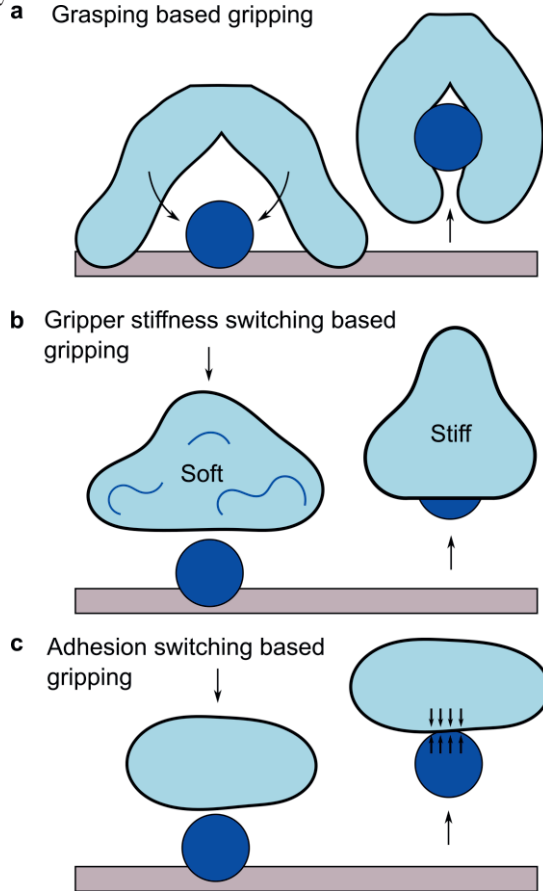


Figure 3. The different gripping methods commonly used is soft manipulators. a) Gripping based on object grasping, b) gripping based on switching the gripper stiffness and c) gripping based on switching the adhesion between the gripper and the object.

Finally, suction based soft grippers have been proposed. The inspiration for these grippers can be found in the nature: octopi can handle various objects and attach different surfaces due to their multiple suction cups in their tentacles. Those are fully soft but can generate strong adhesion to the target objects. The principle of the suction cup gripper is based on the pressure difference between the ambient pressure and the pressure under the suction cup. This difference can be created by two ways:

passively by pressing the cup against a surface (Figure 4a) and actively by using an external vacuum unit (Figure 4b).

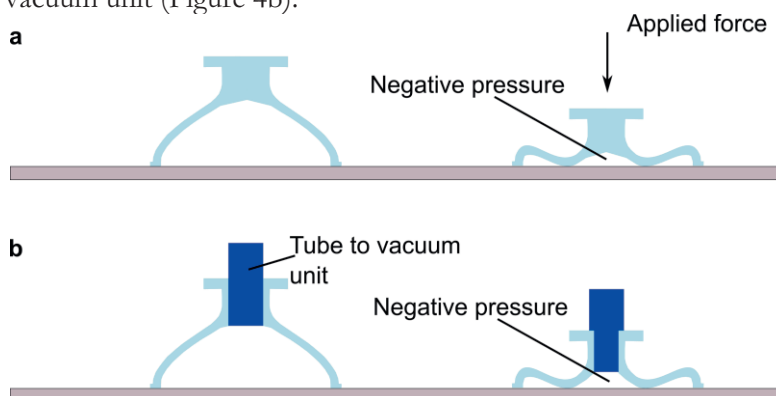


Figure 4. Actuation of the suction-based gripper. a) passive method: negative pressure applied by pressing the suction cup manually and b) active method: negative pressure applied by using an external vacuum unit.

Researchers have proposed many grippers based on the suction principle.⁹² Horie et al.⁹³ proposed a miniature size octopus inspired gripper for picking medical microelectromechanical systems (MEMS). However, the masses the gripper could handle were relatively small compared the pressures needed. Takahashi et al.⁹⁴ presented an octopus inspired suction gripper with a film underneath it, which used a combination of vacuum and jamming phenomena for gripping. They fabricated 14 mm wide gripper which had glass beads inside the gripper body (for granular jamming) and the film included multiple suction cups. They reported a maximum pull-off force (the force needed to separate the object from the gripper) of 2.1 N. The same group also reported the enhancing effect of liquid on the surface⁹⁵ with the same gripper design. Mazzolai et al.⁶ presented an octopus inspired actuator with suction cups. The suction cups had three different designs (without a film under the body, with the film under the body and with the curved film under the body) depending on the desired function. They reached 3.3 N pull-off forces with the gripper combined with the tentacle shaped soft actuator. Recently, Iwasaki et al.⁹² reported a suction gripper with an attached magnet which enabled the magnetic control of the gripper.

In our previous work²⁰, we used the design of a controllable load sharing gecko gripper by Song et al.⁸⁶ but without the gecko-inspired film. We found that the flat film without microstructure adheres better to rough surfaces. Table 2 lists the examples of previously proposed soft grippers and their properties. The results from

Publications II and **III** are also presented in Table 2 and will be discussed in detail in the Results section and comparisons will be made in the discussion.

Table 2. Selected soft grippers and their properties, adapted from **Publications II** and **III**

Gripper type	Ref.	Max. Preload (N)	Gripper Diameter (mm)	Max. Pull-off force (N)	Max. lifting ratio ¹	Diameter ratio limits ²	Surface Conditions			Max. Surface Roughness tested R _z (μm)	Time to acquire grip (s)	Power required to maintain grasp (W)
							Dry	Watery	Oily			
Fluidic elastomer actuator gripper	12	-	9-14	-	-	< 0.7	Yes	-	-	-	-	3
Granular jamming	19	150	86	100	-	0.1-0.85	Yes	-	-	-	-	3
MR fluid jamming	96	40	108	50	1.7	0.2-0.4	Yes	-	-	-	< 0.1	75
Bioinspired suction gripper	6	0.5-1	9-14	3.3	3.9	> 2 ⁴	Yes	Yes	Yes	36.5	20 ⁵	-
Soft suction gripper	20	0.5	18	2.7	476 ⁶	-	Yes	-	-	1.6 ⁷	-	0
Magnet-embedded suction cup	92	0.3	10	0.9	-	> 3	Yes	Yes	-	-	140 ⁸	0
Same size commercial suction cup for uneven workpieces	97	-	20	11	~ 48	> 1	Yes	Yes ⁹	Yes ⁹	-	< 0.1 ¹⁰	3
Gecko-inspired gripper	87	-	180 ¹¹	43	200	> 0.5 ¹²	Yes	-	-	-	< 0.1	0
Pneumatic suction gripper	Publication II	1	20	7.4	-	> 0.3	Yes	-	-	5.66 ⁷	1	0
Magnetically and hydraulically actuated grippers	Publication III	1.5	20	7.5	80	> 0.4	Yes	Yes	Yes	17.7	10	0

¹ Object mass/gripper mass

² Object diameter/gripper diameter

³ Power the vacuum unit needs

⁴ Estimated from Fig. 5 in ⁶

⁵ Estimated from the video in ⁶

⁶ Only the gripper mass excluding holder was reported

⁷ R_{rms} value

⁸ Estimated from the video in ⁹²

⁹ Separated filtering system for liquids is needed

¹⁰ Depends the vacuum system used

¹¹ Estimated from the Fig. 1 in ⁸⁷

¹² Estimated from the Figures in ⁸⁷

3 SENSORS FOR SOFT ROBOTS

The soft bodies and actuators are hardly robots without sensing. The robots need to get feedback about their position, movements, and surrounding environment to work safely and precisely. Since the robot bodies are soft, the sensors integrated them also need to be soft. Different kind of soft and stretchable sensors have been studied intensively during past decades in the fields of wearable electronics^{98–101} and health monitoring.^{32,102–104} Many of the sensors used in the aforementioned applications have been integrated into soft robotics,¹⁰⁵ strain sensors being ones of the most common ones.

3.1 Strain sensing methods

The strain is suitable quantity to measure in soft robots since many of the actuators are based on elongation or bending of soft materials.^{15,21} The strain during the elongation or bending can be measured based on different phenomena. Classic metal foil strain gauges, proposed by E. Simmons and A. Ruge already in 1940s,¹⁰⁶ are based on change in resistance of the meandering metal foils while they are stretched. The strains in these traditional strain gauges are often limited to only 5% and they are used for measuring small strains, such as deformations in rigid objects.¹⁰⁵ In soft robots, the strains are often a lot higher. Thus, different stretchable and soft strain sensors have been proposed.^{10,107,108}

Measuring the strain based on the change in the resistance was the idea used in the first strain gauges and the idea has been used also in many new strain sensors.^{109,110} The change in the strain sensor resistance can be generated in multiple ways: by the intrinsic resistive response of the material, the geometrical effects, the tunnelling effect, the disconnection of micro-/nanomaterial and the controlled microcrack creation.¹⁰⁵

The first one, intrinsic resistance response of the material, is the method used in the traditional strain gauges and more recently in the semiconductor-based strain sensors. In semiconductor strain sensors, the external deformation changes the bandgap on interatomic spacing, leading to dramatic change in the resistance.¹⁰⁵

The geometrical effect is based on the deformation of the material while stretching. When the material is stretched it will deform based on its Poisson's ratio: its length will increase, and its cross-sectional area will decrease. The resistance of the conductor can be given by

$$R_r = \delta \frac{L_r}{A_r}, \quad (1)$$

where δ is the resistivity of the sensor material, L_r is the length of the conductor and A_r is the cross-sectional area of the conductive sensing films. Thus, in elongation the resistance of the conductor would increase. The resistance difference in liquid metal-based strain sensors is mainly caused by geometrical effects.¹⁰⁵

Tunnelling is the third mechanism to produce resistance change. When nonconductive material is sandwiched between conductive nanomaterials, the electrons can pass through the nonconductive material with a certain cut-off distance. The tunnelling was found out to be the dominant mechanism of the resistance change in the strain sensors based on graphene or carbon nanotubes-polymer nanocomposites.¹¹¹

The resistance change can also be based on the disconnection mechanism. In a conductive nanomaterial network, there is a certain threshold for the minimum number of nanomaterials for electrons to pass through the network based on the percolation theory. In stretching, the resistance of the conductive material increases since some of the nanomaterials loses their overlapping area. The disconnection is mainly caused by the mismatch between the stiffer conductive material (often nanowires or flakes) and stretchable scaffold material (soft silicone elastomer).

In conductive brittle films, the change in the resistance is mainly based on crack generation. When the conductive ink printed on stretchable elastomer substrate is stretched, microcracks are generated in the film. The cracks restrict the electrical conductivity by increasing the resistance of the strain sensor. Crack generation has been reported in carbon nanotube, graphene, metal nanowire and nanoparticle-based sensors.¹⁰⁵

The strain can also be measured based on the change in the sensor capacitance. The capacitance change is often based on geometrical effect. Many of the capacitive strain sensors are fabricated by sandwiching a dielectric layer (an insulating film) between stretchable electrodes and the sensors can be considered as plate capacitors. The capacitance for a plate capacitor can be calculated as

$$C = \epsilon_0 \epsilon_r \frac{L_c \omega_c}{d_c}, \quad (2)$$

where ϵ_0 is the vacuum permittivity, ϵ_r is the relative permittivity of the dielectric layer, L_c is the length of the capacitor, ω_c is the width of the capacitor and d_c is the thickness of the dielectric layer. Upon stretching, the thickness of the dielectric layer decreases and the overlapping area increases which increases the capacitance of the strain sensors.¹⁰ Larson et al.¹⁰ fabricated highly stretchable (395%) capacitive strain sensors which also change their illumination upon stretching.

Optical sensing has been also proposed for measuring the strain in soft robots.^{107,112} The sensors are stretchable soft wave guides composed of a cladding with lower reflective index and a core with higher reflective index, connected to a light emitter and a photo detector. When elongated, the geometry of the wave guide changes according to its Poisson's ratio. This changes the transmission of the wave guide which can be measured by the light power difference. The loss in the output power caused by the stretching can be given by

$$a = 10e\epsilon L_w \epsilon, \quad (3)$$

where e is the absorptivity of the material and c is the concentration of chemical species in the medium that attenuate light, L_w is the initial length of the wave guide and ϵ is the engineering strain.¹⁰⁷ Zhao et al.¹⁰⁷ integrated stretchable waveguide strain sensors into a soft prosthetic hand for posture and tactile sensing.

Recently stretchable strain sensors based on piezoelectric¹¹³ and triboelectric¹¹⁴ effects have been proposed. In piezoelectric effect, external deformations generate a voltage due to the dipole moments in the piezoelectric materials.¹¹³ In triboelectric sensors, external mechanical deformations are converted to electricity which can be used to fabricate self-powered strain sensors.¹¹⁴

In addition to electrical based strain sensing, the strain can be measured based on the change in the pressure. This method is potentially beneficial since many of the soft robots are actuated pneumatically. By shifting from electric sensing to pneumatic, the overall structure of the robot simplifies. Researchers have proposed that by measuring the pressure difference in the pneumatic chamber integrated in the soft robot structure, the strain in the robot can be reported. Yang et al.¹¹⁵ integrated pneumatic sensing bodies into a soft gripper to measure tactile force and curvature. Other groups demonstrated similar pressure chambers in the robot force sensing¹¹⁶ and human-machine interface.¹¹⁷

This pressure chamber-based method suffers from the permeability of the silicone elastomers: in long-term measurements, air slowly diffuses through

elastomer. The method is also vulnerable to any leakages in the chamber or connecting tubes since they will change the sensor output.

Kusuda et al.¹¹⁸ proposed strain measurement based on the change in the fluid flow rate in the microfluidic channel integrated into a soft robot. With constant flow rate in the channel, slow diffusion or small leakages do not have major effect on the sensor output which makes this method more stable in long term measurements. However, Kusuda et al. did not study the behaviour in long term measurements nor behaviour under large strains.

3.2 Integration stretchable strain sensors into soft robots

Different materials and fabrication methods have been proposed for soft stretchable strain sensors. Usually, the sensor includes a conductive material integrated into soft elastomer, rubber, or natural based materials such as wool. The conductive materials that have been proposed include graphene, carbon black particles, carbon nanotubes, metallic nanowires, ionic liquids and conductive polymers.¹⁰⁵ In this sub chapter some selected examples of the materials and fabrication methods of the strain sensors integrated into soft robots are discussed.

First approach to measure strains in soft robots is to use commercial bending sensors. Gerboni et al.¹¹⁹ integrated commercial resistive bending sensors into a fluidic elastomer actuating system. The system consists of two pneumatic actuators symmetrically placed respect to the central plane. The strain sensors were placed into specific flat channels next to pneumatic chambers. The sensors were fixed only from the other end of the actuating system, so they were free to slide inside the flat channels while the actuators bend. Elgeneidy et al.¹²⁰ proposed the usage of the commercial bend sensor. They integrated a resistive bend sensor onto the neutral plane of the fluidic elastomer actuator and used the sensory feedback to control the bending. A commercial bend sensor was used also in Homberg et al.¹²¹ together with a commercial force sensor to measure the curvature and force of the pneumatic gripper. The commercial bend sensors in soft robotic devices were also tested and compared in Kim et al.¹²² The above-mentioned commercial sensors are limited in measuring small strains (bending) due to their material being not highly stretchable.

Other common way to measure strains in soft robots is to use different conductive nanoparticles.¹¹ The conductive particles are mixed in the soft and stretchable material, often silicone elastomer, to form stretchable and conductive composites. Thuruthel et al.¹¹ mixed conductive carbon nanoparticles to PDMS,

added wires, and encapsulated the structure with softer silicone elastomer. Then they cut sensors by hand and placed them arbitrary along the fluidic elastomer actuator to simulate neural networks. They were able to model the kinematics of soft robot in real time and estimate applied forces when in contact with objects.

By using liquid metals as conductors, extreme strains can be achieved. In this method, microchannels in soft silicone elastomer are filled with liquid metals e.g. eutectic gallium-indium (eGaIn), to form a conductive path. The microchannels are often fabricated with the same silicone casting methods used in soft robot fabrication. Hamaguchi et al.¹²³ proposed eGaIn-based inductive strain sensor, which was used in bending and tactile sensing of the pneumatic actuator. The eGaIn was encapsulated with soft silicone elastomer. An external spiral coil circuit was used to measure the displacement of the eGaIn to measure the bending and force. Park et al.¹²⁴ fabricated resistive strain sensors by filling microchannels with eGaIn. The sensors were used for the proprioceptive sensing of the soft pneumatic gripper. Similar resistive eGaIn sensors were also used for strain sensing inside the soft robot fish in the study from Lin et al.¹²⁵ The main challenges for these types of sensors are the potential leakages and bubbles in the channels.

Hydrogels have been also used in strain sensing in soft robots. Wang et al.¹²⁶ proposed a resistive ultra-stretchable (1200%) hydrogel strain sensor for curvature, twisting and tactile sensing for the soft pneumatic actuator. The mixed hydrogel was cast into a 3D printed mould, degassed and cured in UV light. Then the sample was placed in moist environment for stabilization. Last, wires were attached to the sample and it was sealed with tape to minimize the water evaporation.

The soft optical waveguides proposed by Zhao et al.¹⁰⁷ were used in curvature and haptic sensing in a soft prosthetic hand application. The wave guides were fabricated by four step casting process. First, the cladding (silicone elastomer) was cast into a 3D printed mould, and then cured and demoulded. Next, the cladding was filled with a core material (urethane rubber) and let cure. Finally, the wave guide was sealed with cladding material to form uniform cladding. In the prosthetic hand, each finger included three optical waveguides. In the study from Sareh et al.,¹¹² three commercial macrobend optical fibres were sewn onto the surface of the continuum robot with three pneumatic actuators. The fibres were used for measuring the bending, elongation, and compression of the robot.

Different printing technologies have been also used to fabricate sensors for soft robots. Pinto et al.¹⁰⁹ used two-phase manual screen-printing to fabricate resistive curvature sensors for fluidic elastomer actuators. First, they printed carbon nanotube-based ink onto PDMS substrate for creating a distributed sensor array.

Then, a second mask was placed onto the cured ink and silver nanowire-based ink was applied to create conductive paths for the sensor array. Finally, copper wires were attached with silver paste and the sensor was encapsulated with PDMS. This sensor was bonded onto the bottom of a fluidic elastomer actuator and the sensor was able to measure the curvature of the actuator. Yeo et al.⁴³ proposed also screen-printing for stretchable sensor fabrication. They printed silver nanoparticle ink onto silicone elastomer substrate and added connectors to both ends of the sensor. Then, the sensor was bonded to the fluidic elastomer actuator and sealed with fabric glove. The sensors were used to measure the curvature of the actuator. In a study from Ozel et al.,¹²⁷ solid printing was used to fabricate magnetic curvature sensors for a soft robot snake. They printed the circuit on two substrates: copper clad and copper foil laminated polyethylene terephthalate (PET) film. The substrate was then etched, and the conductive paths were drawn manually. A magnet is bonded on the finished circuit and the whole structure is sealed with silicone elastomer and integrated in the middle of the snake robot. The curvature can be measured contactless by using Hall effect with an embedded magnet and a Hall sensor.

3.3 Soft strain sensor performance

Strain sensors can be exposed to extreme strains and long-lasting measurements if used in soft robots. Thus, it is important to evaluate the sensors performance in these conditions. Table 3 lists selected strain sensors used in soft robots and some common criteria to evaluate their performance. Table 3 also includes the sensors from **Publication IV** and **Manuscript V**, but they will be reported in detail in the results section in Chapter 6.

The first important criterion for soft strain sensor is its stretchability. It is usually reported by the maximum engineering strain the sensors can be used to measure. Engineering strain ε is defined as

$$\varepsilon = \frac{L-L_0}{L_0}, \quad (4)$$

where L_0 is the initial length of the strain sensor and L is the strained length. It depends heavily on the sensor material type and the used fabrication process.¹¹¹ The maximum strains of recently proposed strain sensors vary from 2% to 1400%.¹⁰⁵

The hysteresis of the strain sensors becomes a crucial factor especially in dynamic measurements. The hysteresis of the strain sensor can be defined 1) as the difference

in the output between loading and unloading (in this thesis) or 2) as the dependency of the output of the sensor on its history, e.g. the output of the current cycle to the output of the previous cycle.¹⁰⁵ Hysteresis is often reported as a percentage of the full range of the output of the sensor. In general, capacitive and optical strain sensors show less hysteresis than resistive strain sensors.^{105,107,128}

In soft robots, the strain sensors are possibly used for long times and thus the stability of the sensor is important. The stability can be studied by calculating the drift during certain period. For the resistive type strain sensor, the drift error DE of the sensor can be defined as

$$DE = \frac{R_1 - R_2}{R_1}, \quad (5)$$

where R_1 is the resistance at the beginning and R_2 is resistance at the end of the measurement. Resistive strain sensors are known to be temperature sensitive¹²⁹ which causes drift in the output. It is often compensated by using them in Wheatstone circuits. They show also larger overshooting behaviour than capacitive and optic type strain sensors.

The stability in the dynamic measurements is also important in soft robotic applications. The dynamic stability represents the sensor response in long term cyclic loading.¹⁰⁵ It is often recorded by cyclically loading the strain sensors thousands of times and studying the drift during the experiment.

Sensitivity of the strain sensor is often reported as its gauge factor GF . It is the relative change in the output signal versus the applied strain. For resistive-type sensors, the gauge factor GF is defined as

$$GF = \frac{\Delta R/R_0}{\varepsilon}, \quad (6)$$

where $\Delta R/R_0$ is the relative change in the output resistance of the sensor. The GF values for recently proposed resistive-type strain gauges vary a lot from 1.2 to over 100,000. For capacitive-type sensor GF is given by

$$GF = \frac{\Delta C/C_0}{\varepsilon}, \quad (7)$$

where $\Delta C/C_0$ is the relative change in the output capacitance. The change in the capacitance due the deformation (Eq. (2)) can be also expressed with the relative contraction of the thickness and width of the dielectric ν_d and electrodes ν_e , respectively. For an isotropic material, $\nu_d = \nu_e$, and thus:

$$C = \frac{\epsilon_0 \epsilon_r (1 + \epsilon) l_c (1 - \vartheta_e) \omega_c}{(1 - \vartheta_d) d_c} = (1 + \epsilon) C_0. \quad (8)$$

By using equation (2) and (7), the theoretical maximum of the GF for the capacitor is:

$$GF = \frac{\Delta C}{C_0 \epsilon} = \frac{(1 + \epsilon) C_0 - C_0}{C_0 \epsilon} = 1. \quad (9)$$

The achieved GF is usually smaller than 1 with capacitive type strain sensors. However, recently researchers have reported capacitive type strain sensors with higher GF.⁹⁸ For instance Nur et al.¹³⁰ developed a capacitive strain sensor which has a wrinkled form when no strain is applied. In strain, wrinkled capacitor unfolds and has an additional degree of freedom perpendicular to strain direction. This enhanced the change in capacitance and increased GF.

For the optical strain sensors, the GF is defined as the stretch-dependent power loss of the optical waveguide under deformation, such as bending or straining and reported in dB/ ϵ .^{105,107}

Table 3. Selected stretchable strain and curvature sensors used in soft robots, their materials, sensing method and some common factors for performance evaluation

Fabrication method	Materials	Stretchability (%)	Hysteresis (%)	Sensing type	Gauge factor, GF	Reference
Commercial	Bend sensor®	<10	10	Resistive	40 ¹	119,122
Commercial	Flex sensor®	<10	13	Resistive	7 ¹	120,122
Two-phase screen-printing	Carbon nanotube and silver nanowire inks, silicone elastomers	5	29 ²	Resistive	250 ³	109
Screen-printing	Silver nano ink, silicone elastomer	200	-	Resistive	50,000	43
Casting and mixing nanoparticles	Carbon nanotubes, silicone elastomer	-	-	Resistive	-	11
Silicone casting, filling microchannels	eGaln, silicone elastomer	23	5 ⁴	Resistive	2 ⁵	131
Casting, mixing components, taping	Hydrogel, tape	1200	-	Resistive	1.3	126
Silicone casting, filling microchannels	eGaln, silicone elastomer	-	-	Resistive	-	124
Silicone casting, mixing components	ZnS phosphor-doper silicone elastomer, hydrogel	490	-	Capacitive	0.7 ⁶	10
Casting	Silicone elastomer, polyurethane rubber	85	~0	Optical	18.75 dB/ε ⁷	107
Commercial fibre	Polyethylene optical fibre	400	~0	Optical	-	112
Silicone casting, filling channel	Silicone elastomer, liquid metal	-	-	Inductive	-	123
Solid ink printing, elastomer casting	Copper clad, PET film, magnet, silicone elastomer	-	~0	Magnetic	-	127
Screen-printing	Silver flake ink, TPU	74⁸	17	Resistive	6	Publication IV
Screen-printing	Carbon ink, TPU	-	27	Resistive	7	Publication IV
Silicone casting	Silicone elastomer	300	~0	Pneumatic	~0.7-1	Manuscript V

¹ From Table 1 in ¹²² and using relation $\varepsilon = \theta r / L_0$, $L_0 = 50.8$ mm, $r = 10$ mm

² Estimated from Fig. 9a in ¹⁰⁹

³ Estimated from Fig. 6a in ¹⁰⁹

⁴ Estimated from Fig. 5 in ¹³¹

⁵ Value from ¹³²

⁶ Estimated from Fig. 2b in ¹⁰

⁷ Value from Table 1 in ¹⁰⁵

⁸ Value from previous work ¹³³

4 AIMS OF THE STUDY

The main aim of this thesis was to develop new fabrication methods for sensors and grippers used in soft robots. The specific objectives and hypotheses were:

1. To develop more capable fabrication methods for soft robotic devices including soft actuators, grippers, and sensors. The first hypothesis was that sacrificial manufacturing of the elastomer casts provide a simple and fast method for manufacturing soft devices (**Publication I**). The second hypothesis was that 3D printing can be used to create easily adaptable end-effectors (grippers) for soft robots (**Publications II and III**). Third hypothesis was that elastomer casting can be used in soft sensor manufacturing to simplify the overall manufacturing process of the soft robot (**Manuscript V**).
2. To manufacture adhesion switchable soft grippers by using the fabrication methods proposed in this thesis. The hypotheses were that the switching can be done by using pneumatic actuation (**Publication II**) and the combination of fluidic and magnetic actuation (**Publication III**).
3. To integrate stretchable sensors into soft robots. The first hypothesis was that printed electronics can be integrated into soft actuators providing fast and easy way to add sensing to soft robots (**Publication IV**). The second hypothesis was that the same pneumatics used in actuation can be used for sensing by fabricating soft pneumatic strain sensors (**Manuscript V**).

5 EXPERIMENTAL WORK

In this chapter, methods related to experimental work are described. First, the materials and the fabrication methods of the soft devices and sensors are discussed, following the characterization methods used in this thesis work.

5.1 Castable soft elastomers

The soft silicone structures used in this thesis were castable two component silicone elastomers (Table 4). The silicone elastomers were chosen based on their material properties, e.g., transparency or softness. The softness of the material can be defined by its Young's modulus¹³⁴

$$E = \frac{\sigma}{\epsilon} = \frac{\frac{F}{A_0}}{\frac{L-L_0}{L_0}}, \tag{10}$$

where σ is tensile stress, F is the applied force, L_0 is the initial length of a prismatic (uniform cross-section) bar and A_0 is the initial area of the cross-section. E scales with the ratio of the applied force to the percent elongation of the prismatic bar.

Table 4. Properties of the castable soft silicone elastomers used in this thesis based on their datasheets

Trade name	Shore Hardness A	Shore Hardness 00	100% Modulus (kPa)	Elongation at break (%)	Viscosity (Pa·s)
Sylgard 184	50	85 ¹	-	140	4
Dragonskin 30	30	70 ¹	592	364	20
Sorta-Clear 18	18	60 ¹	241	545	21
Ecoflex 50	10 ¹	50	82	980	8

¹Estimated by using Table I in Qi et al.¹³⁵

Figure 1 in Chapter 2 showed Young's modulus values for some common materials. Young's modulus is often measured by calculating the initial slope in the stress strain curve. For soft materials that behave linearly, Young's modulus is usually calculated

at 100% strain. However, soft silicone elastomers often have nonlinear hyperelastic behaviour. Then the modulus at 100% strain is only a rough estimate of Young's modulus.¹³⁶ Nevertheless it is a useful tool for describing the softness of the materials together with Shore Hardness (S) scales, which will be explained next.

Shore (durometer) hardness test is a commonly used method to evaluate the hardness of the elastomeric materials. It is measured with a calibrated spring loaded indenter.¹³⁶ The value depends on the depth the needle penetrates in the material and is dimensionless, varying from 0 to 100, the hardness increasing with the value. The spring calibration and shape of the durometer define the scale used, and in soft robotics often used scales are Shore D, A or 00, which are partially overlapping. Shore classes and Young's modulus are correlated, but the relation between them is not perfect. One way to approximate Young's modulus from Shore hardness is by A. Gent:¹³⁷

$$E = \frac{0.0981(56+7.62336S)}{0.137505(254-2.54S)} \quad (11)$$

where E is in MPa and S is A type Shore hardness. Figure 5 also shows a rough estimate between Shore scales and Young's modulus.

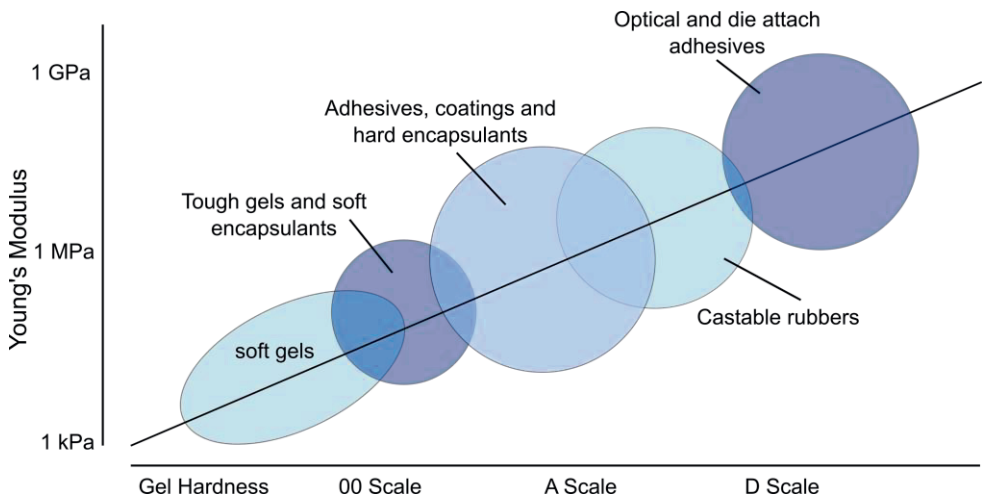


Figure 5. Rough estimate of Shore hardness scales and Young's modulus, adapted from Larson.¹³⁶

5.2 3D printing

In **Publication I**, the sacrificial moulds were 3D printed with a FDM 3D printer (Prusa i3 MK2, Prusa Research s.r.o.). The filament materials were selected based on their solubility. We used filaments that were intended to use as dissolvable support structures. Table 5 shows the used filaments, their manufacturers, main material components and solvent used to dissolve them.

Table 5. Filaments used in sacrificial 3D printing, adapted from **Publication I**

Trade name	Manufacturer	Main Material	Solvent
HIPS	Orbi-Tech ¹	High impact polystyrene (HIPS)	Limonene
ABS	miniFactory ²	Acrylonitrile butadiene styrene (ABS)	Acetone
PVB	Polymaker ³	Polyvinyl butyral (PVB)	Isopropanol
Ethy-Lay	CC-Products ⁴	PVB	Ethanol
Hydrosupport	3D-Fuel ⁵	Polyvinyl alcohol (PVA)	Water
PVA	MatterHackers ⁶	PVA	Water
LAYaPVA	CC-Products ⁴	PVA	Water
Lay-Cloud	CC-Products ⁴	Undisclosed ⁷	Water
High-t-Lay	CC-Products ⁴	Undisclosed ⁷	Water

1. Orbi-Tech GmbH, Moltkestrasse 25, 42799 Leichlingen, Germany

2. miniFactory Oy LTD, Kampusranta 9 C 60320, Seinäjoki, Finland

3. Polymaker, Suzhou, Jiangsu, China

4. CC-PRODUCTS, Auenweg 173 / Halle 10, 51063 Köln, Germany

5. 3D-Fuel, Units 8/10 Moville Business Park, Glencrow, Moville, Co. Donegal, F93 DF84 Ireland

6. MatterHackers, Lake Forrest, California, USA

7. The exact material component was a trade secret

In **Publication II**, the gripper bodies were 3D printed with a DLS 3D printer (M2 Printer, Carbon, CA, USA) by using a soft silicone urethane resin (SIL 30, Carbon, CA, USA. Shore hardness: A 35). In **Publication III**, the gripper bodies were 3D printed with SLA 3D printer (Form 2, Form Labs, MA, USA) by using Elastic V1 50A resin (Shore hardness A 50).

5.3 Screen-printing

In **Publication IV**, stretchable curvature sensors were fabricated for the soft actuators. The sensors were screen-printed onto soft TPU substrate by using conductive inks: silver ink (ECM / CI-1036) and carbon ink (ECM / CI-2051) (II in Figure 6). First, the substrate (IV in Figure 6) was slightly stretched, attached to an aluminium plate, and cleaned with isopropyl alcohol. Then, the sensor structures

were printed in two continuous printing cycles with a semi-autonomous screen-printing machine (TIC / SCF-300). The squeegee (V in Figure 6) spreads the conductive ink onto the substrate through the mesh (III in Figure 6) on top the substrate. After this, the samples were placed in an oven for annealing process (silver ink: 30 min at 125 °C, and carbon: 10 min at 90 °C) and after cooling downs, the wires were attached with conductive glue (8331–14G, MG Chemicals).

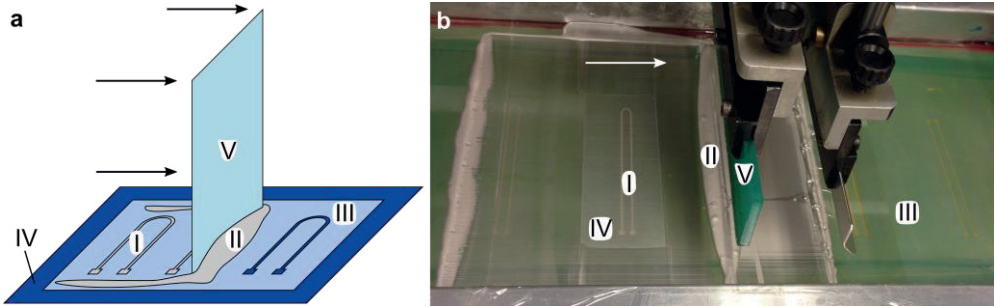


Figure 6. Screen-printing process a) a schematic and b) a photograph. Substrate (IV) is attached to the aluminium plate and a squeegee (V) spreads the conductive ink (II) onto the substrate through the mesh (III) creating the screen-printed sensors (I).

5.4 Coating and casting soft silicone elastomers

The soft silicone elastomers used in this thesis were two component elastomers (Table 4), which were mixed and degassed (Figure 7) before using them in coating or casting. To create a thin film for the grippers (Figure 7a) used in **Publications II** and **III**, uncured elastomer (Ecoflex 00-50, Smooth-On Inc., PA, USA) was spread onto a flat PET substrate. In **Publication II**, a thin film was created by using a bar coater. In **Publication III**, a thin film was created but by using a universal film applicator. In both methods, the applicator moves onto silicone elastomer on certain height and pushes the excess elastomer out of the way.

In **Publications I** and **IV** and **Manuscript V**, the elastomer was cast into a 3D printed mould to create soft structure (Figure 7b and c). In the first publication, the moulds were made from sacrificial material, which allows them to be dissolved after the curing of the cast silicones (SortaClear 18, Smooth-On Inc., PA, USA and Sylgard 184, Dow Inc.) (Figure 7c). Thus, the moulds do not need to be removed by hand and overhanging structures can be created inside the silicone cast. In **Publication IV** and **Manuscript V**, the soft actuators and grippers were cast by

using 3D printed moulds (Figure 7b). Thus, the moulds were removed by hand after the silicone (Dragon skin 30, Smooth-On Inc., PA, USA) was cured.

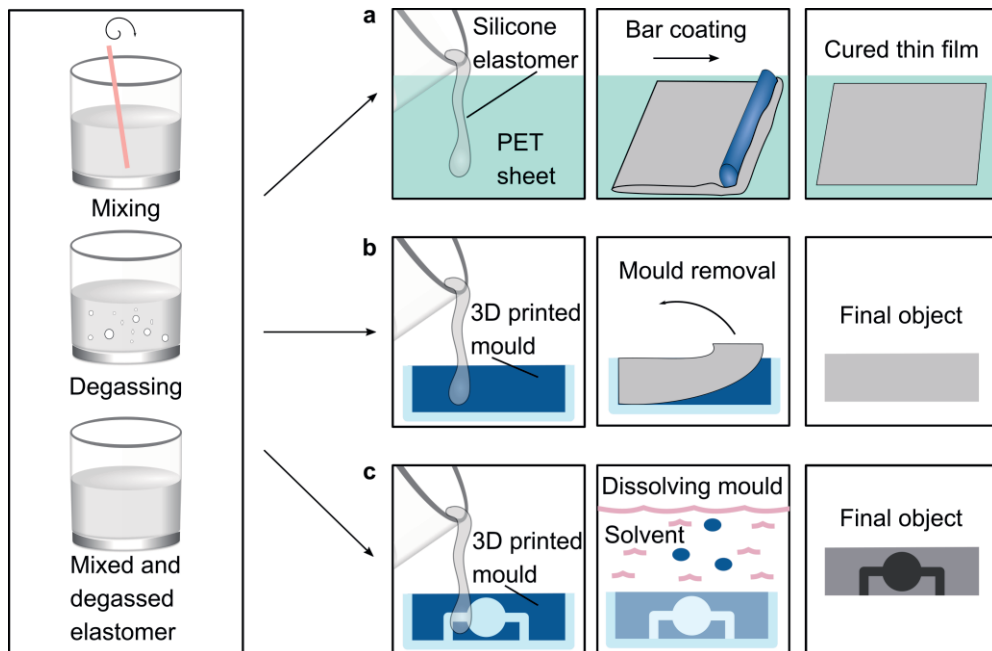


Figure 7. Two component silicone elastomer casting: parts are mixed and degassed before application. a) Uncured elastomer is poured onto a flat substrate and spread using a bar coater to form a thin film, b) uncured elastomer is poured into a 3D printed mould and cured elastomer piece is demoulded by tearing it from the mould, c) uncured elastomer is poured into a sacrificial 3D printed mould and the mould is dissolved by placing in into a solvent bath.

The moulds used for soft pneumatic strain sensors in **Manuscript V** (Figure 8) were made by photolithography (negative photoresist SU-8 3050, Microchem). The moulds were treated with trichloro(1H,1H,2H,2H-perfluorooctyl)silane before casting, to ease the mould removal. The elastomer piece (Eco-Flex 00-50 and Dragon skin 30, Smooth-On Inc., PA, USA) including the channels was then bonded to a flat silicone elastomer piece by spin coating a thin layer of uncured elastomer onto the flat elastomer substrate and then pressing the elastomer pieces together.

After curing, the strain sensor was cut to the desired shape and holes for the inlets were made with a needle. Then metal inlets were inserted into the holes and sealed with silicone glue (Sil-Poxy, Smooth-On Inc., PA, USA). Figure 8 shows the detailed fabrication process of the pneumatic strain sensors.

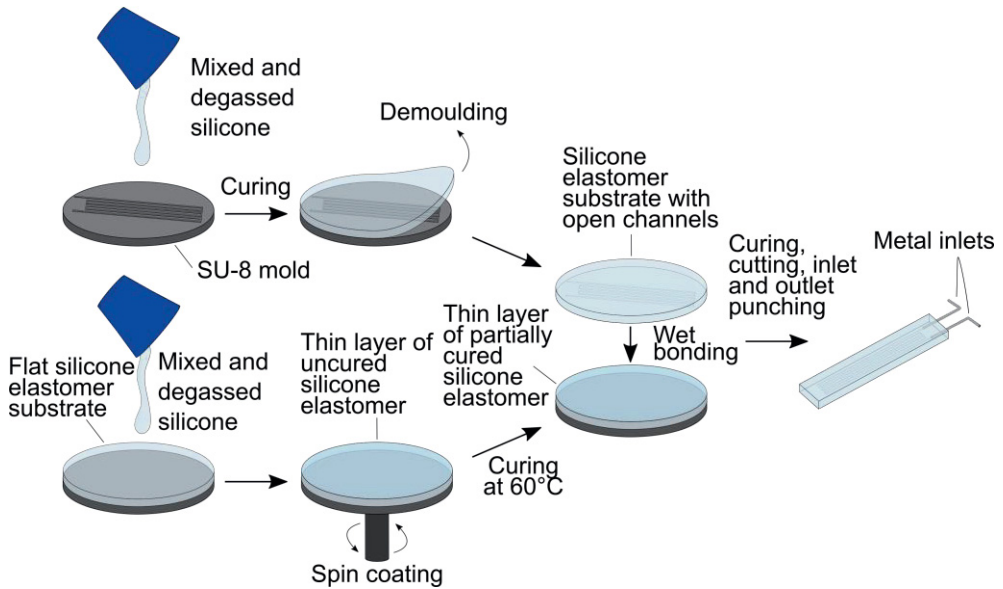


Figure 8. Fabrication of the soft pneumatic strain sensors. First, two elastomer sheets are fabricated: one with open channels and the other one without any structures. After curing, the sheet with channels is demoulded. The flat elastomer sheet is placed in the spin coater and thin layer of uncured elastomer is coated on top of it. Then, the flat sheet with uncured elastomer is placed in the oven for 40 s at 60°C. Then the elastomer sheet with channels is placed on top of the uncured elastomer and let cure. The strain sensors are then cut from the elastomer piece. Holes for the inlet and the outlet are made with a needle and metal inlets are inserted into them.

5.5 Design and fabrication of soft grippers

In **Publications II and III**, soft suction grippers with thin film were designed and fabricated by 3D printing (Figure 9). In both publications, the gripper body has a hollow bell-like structure, with an inner diameter of 20 mm, a height of 12.5 mm and a wall thickness of 700 μm . In **Publication II**, the inlet diameter was 2 mm and in **Publication III** it was 4 mm. In both publications, the inlet was situated at the apex of the bell-like structure.

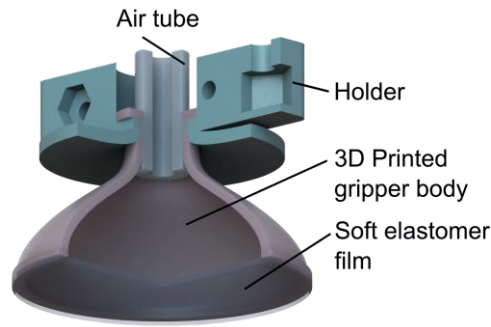


Figure 9. Schematic of the 3D printed gripper, including a soft 3D printed gripper body, a soft and thin elastomer film, an air tube and a rigid 3D printed holder.

Then, the 3D printed gripper bodies were treated with oxygen plasma (Figure 10) to get them more hydrophilic and easier to bond to 400 μm thick silicone film (Ecoflex 00–50, Smooth-On Inc., PA, USA). The gripper bodies and silicone films were bonded with silicone glue (Sil-Poxy, Smooth-On Inc., PA, USA) by dipping the gripper body in the silicone glue and then pressing it on the silicone film (Figure 10). After the glue was cured, the same glue was used to attach a silicone tube to the gripper body for the pneumatic and hydraulic connection. Then the gripper was attached to the 3D printed rigid holder (Figure 9).

In **Publication III**, the sealed gripper was also filled with MR fluid (122EG and 140CG, Parker Lord, PA, USA). This was done by first sucking a near vacuum inside the gripper chamber with an empty syringe. Then the vacuum was let to suck MR fluid inside the gripper chamber by attaching a syringe filled with MR fluid to the gripper (Figure 10). Then, the gripper was let to set in a vertical position so that all the small air bubbles moved from the gripper body to the syringe and could be later removed.

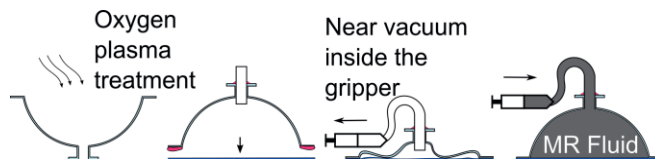


Figure 10. The fabrication process of the magnetically and hydraulically actuated soft gripper. First, the gripper body is treated with oxygen plasma to have stronger bonding with silicone glue. Then the body is attached to the thin silicone film and let cure. After the glue is cured, a near vacuum space is applied inside the gripper chamber with an empty syringe. Then, the vacuum is let to suck the MR fluid inside the gripper chamber by attaching a syringe filled with MR fluid to the tube.

5.6 Integration of sensors into soft pneumatic actuators

The fabricated stretchable sensors with wires (**Publication IV**) were integrated into soft pneumatic actuators.¹⁶ The actuators consist of two soft silicone components (Dragon skin 30, Smooth-On Inc., PA, USA, Shore hardness A 30): an upper part including the pneumatic chambers and a lower flat one (Figure 11). The strain limiting layer made from glass fibre was attached to the lower part during the silicone casting. The printed sensor was glued onto the lower silicone part on top of the strain limiting layer by using the same uncured silicone elastomer. Then the upper part was placed on the lower part and bonded also with uncured silicone elastomer (Figure 11).

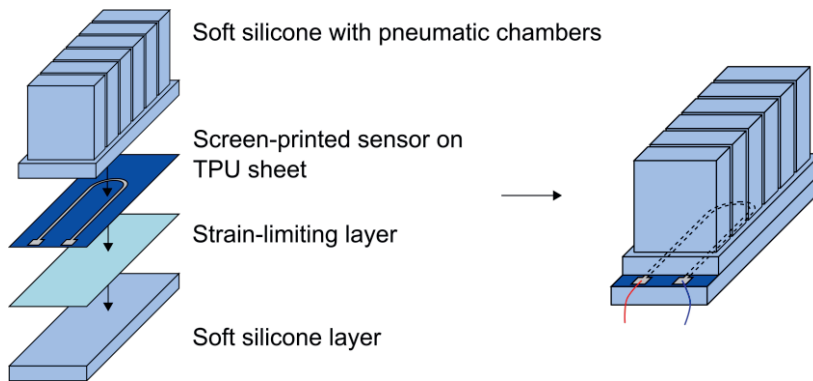


Figure 11. Integration of the screen-printed sensor into a soft pneumatic actuator. The screen-printed sensor on TPU sheet is placed on top of the strain-limiting layer between the upper and the lower soft silicone components.

The pneumatic connection to the actuator was made by using 2 mm diameter biopsy puncher to make a hole in the silicone wall at one end of the actuator. Then 4 mm diameter tube was connected into the hole.

The pneumatic strain sensors (**Manuscript V**) were also integrated into similar soft pneumatic actuators. The sensors were placed in the middle of the bottom of the pneumatic actuator. The bonding was done by using uncured silicone elastomer (Dragon skin 30, Smooth-On Inc., PA, USA) as glue.

5.7 Soft pneumatic gripper fabrication

In **Publication IV** and **Manuscript V**, soft pneumatic grippers were fabricated. Both grippers were built from pneumatic actuators¹⁶ presented in previous Chapter 5.6. In **Publication IV**, the gripper was made by bonding the upper parts of the pneumatic actuators to the common three-fingered base part, which included the strain limiting layer and the screen-printed strain sensors (Figure 29a in Chapter 6.3). Then, separate inlets for all the actuators were connected and the gripper was attached to the 3D printed rigid holder.

In **Manuscript V**, three similar pneumatic actuators were connected by a 3D printed rigid piece. The 3D printed piece included a common pneumatic source to all the actuators (Figure 35a in Chapter 6.4). In this gripper, the upper parts of the actuators were bonded to the lower parts, which included the strain limiting layers and the pneumatic strain sensors integrated in the structure.

5.8 Characterization methods

The fabricated grippers and sensors were characterized to compare them with previously reported relevant research. The following chapters describe the relevant characterization methods used in this thesis.

5.8.1 Suction gripper characterization

The grippers were characterized by assembling them into a mechanical tester (**Publication II**: a custom measurement set up with GSO-1K, Transducer Techniques and LPS-65 2", Physik Instrumente GmbH & Co. KG, **Publication III**: TA.XT Plus, Stable Micro Systems, Figure 12a and b). The systems used in the **Publications II** and **III** were different, but the working principle was similar.

The gripping force measurements for the soft suction grippers (**Publications II** and **III**) were done by measuring the force necessary to retract and detach the gripper from the substrate. The following steps were included in the gripping force measurement, shown in Figure 12c:

- I. The gripper approaches the target surface.
- II. In contact, preload F_{pre} is applied.

- III. A negative pressure P_{neg} is created by withdrawing either air (**Publication II**) or liquid (**Publication III**) from the gripper chamber.
- IV. The movable magnet is placed on top of the gripper once the desired amount of MR fluid has been withdrawn (only in **Publication III**).
- V. The gripper starts to retract from the surface.
- VI. The gripper detaches from the surface and the peak of the force is recorded. We call it the pull-off force, F_{off} .

Figure 12c illustrates the measurement sequence for the magnetically switchable gripper. For the pneumatic gripper, we were able to measure also P_{neg} during the force measurements. It was measured with a pressure sensor from inside the tube attached to the gripper.

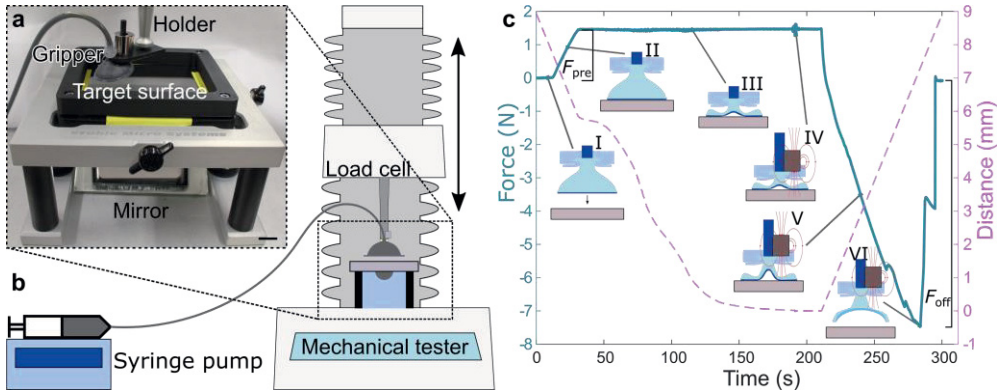


Figure 12. Measurement sequence for the magnetically switchable gripper. a) a photograph and b) a schematic of the force measurement set up, c) measurement cycle: I) The gripper approaches the target surface, II) The gripper reaches the target surface and F_{pre} is applied, then III) fluid is withdrawn from the gripper body and IV) a magnet is applied on top of the gripper (only in **Publication III**). Then V) the gripper is started to withdraw from the surface and the maximum force measured is when VI) the gripper is detached from the surface.

The tensile work W_{T} needed to detach the gripper from the surface was also calculated in **Publication III** by integrating the gripping force as a function of the distance of the gripper from the surface.

In **Publication II**, the repeatability of the gripper was studied. The gripper was attached to a six-axis torque sensor (Nano 17 Titanium, ATI Industrial Automation, USA) which was then attached to a seven degrees of freedom robotic arm (Franka

Emika, Panda Research, Germany) and a syringe pump, shown in Figure 13a and b. During the picking experiments, the forces were recorded, and a video was captured.

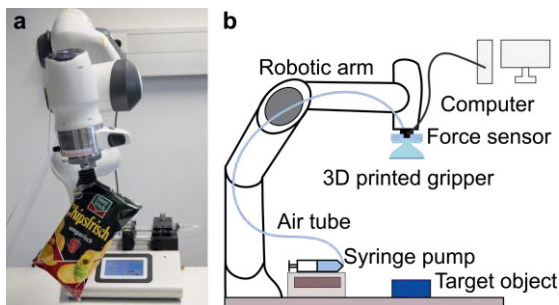


Figure 13. Repeatability experiment. A) Photograph of the robotic arm with the 3D printed suction gripper picking a chip bag, and a syringe pump connected to the gripper. b) Schematic of the robotic arm set up: Gripper is mounted at tip of the robotic arm and connected to the syringe pump using a silicone tube. A force sensor is placed between the gripper and the robotic arm, and the sensor is connected to a computer.

5.8.2 Surface roughness measurements

The surface roughness of the target objects in **Publications II** and **III** was measured to evaluate how rough surfaces the gripper was able to pick. The surface roughness is evaluated in this thesis by reporting either the root mean squares surface roughness (R_{rms}) or maximum peak to valley depth in single sampling rate (R_z). The measurements were done by using either a laser confocal microscope or an optical profilometer.

5.8.3 Pneumatic actuation

To characterize the stretchable strain sensors in **Publication IV** and **Manuscript V**, the actuators were connected to a fluidic control board. The instructions to assemble the board are available in the Soft Robotics Toolkit (<http://softroboticstoolkit.com/>).¹³⁸ The control board includes four solenoid valves (VQ11OU-5M, SMC), driven by Arduino microcontroller (Arduino MEGA 2560) using pulse-width modulation. The pressure P_{act} supplied for the actuator is controlled by changing the duty cycle of the valves and measured with a pressure sensor (100PGAA5, Honeywell, 100 PSI GAGE 5V).

5.8.4 Curvature measurements

To study the bending degree of the pneumatic actuator in **Publication IV** and **Manuscript V**, we calculated the curvature κ of the actuator. The curvature measurements were conducted by taking pictures from the bending actuator (Figure 14a and b) and then analysing these pictures by custom designed MATLAB script, which found the circular arc best fitting the bottom edge of the actuator. The inverse of the arc radius r is the curvature of the actuator at that time point. It should be noted that the curvature is not constant along the length of the actuator and thus curvature values should be understood only as the best-fit estimate.

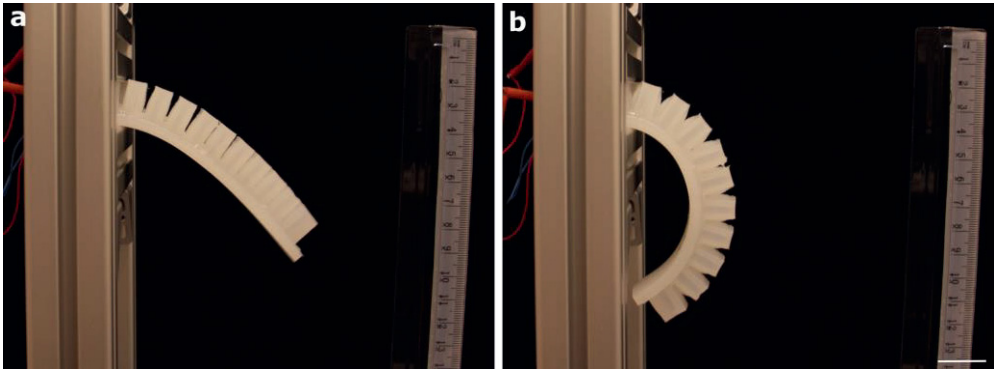


Figure 14. Curvature measurement of a) an unpressurized actuator and b) a pressurized actuator. Scale bar: 1 cm.

5.8.5 Resistance measurement

The resistances of the screen-printed curvature sensors were measured during the bending experiments with a data acquisition device (USB-4065, National Instruments). In the gripper application with multiple sensors measured simultaneously, we used strain/bridge input modules (National Instruments / NI-9237). In bridge circuits $100\ \Omega$ or $102\ \Omega$ resistors were in series with the sensors while the quarter-bridge was made into a half-bridge with $120\ \Omega$ resistors.

5.8.6 Pneumatic resistance measurement

The stretchable pneumatic strain sensors fabricated in **Manuscript V** were characterized by measuring the change in pressure inside the strain sensor while stretching or bending them. The strain applied to the strain sensor was produced with a mechanical tester (TA.XT Plus, Stable Micro Systems, in Figure 12b). The pressure inside the actuator was measured with pressure sensors (015PDAA5, Honeywell, 15 PSI Differential 5V) and recorded with a data acquisition device (USB-6356, National Instruments).

5.8.7 Statistical analysis

The data analysis in **Publication II** was performed with Origin software by calculating average and standard deviation (SD) values for the measurement data. In **Publications III**, the analysis was done with MATLAB Software. We calculated the average values and standard errors (SE) for the measured force data. We also calculated the P-values for the force data with and without a magnetic field applied by using Welch's unequal variances t-test. In **Publication IV** and **Manuscript V**, we used MATLAB software to calculate average values, SDs, SEs and interquartile ranges for the measured data.

6 SUMMARY OF MAIN RESULTS

In this chapter, the main results of the thesis are summarized. First, sacrificial 3D printing as a fabrication method of soft device moulds is presented. Nine different 3D printing materials were characterized and four the most suitable ones were selected for soft device fabrication.

Second part of the results chapter reports the results from soft suction grippers, both pneumatic and magnetohydraulic. The fabricated grippers were characterized by measuring the force needed to retract them from various surfaces and by handling various objects with them.

Last sub-chapter describes the novel sensing methods for soft actuators and robots. First, screen-printed stretchable curvature sensors integrated into soft actuators were characterized and discussed. Then, we integrated these sensors into a soft pneumatic gripper and demonstrated the actuation of three independent fingers with curvature sensors. In second approach we demonstrated that pneumatic microchannels in soft silicone elastomer can be used as pneumatic strain sensors. The pneumatic strain sensors were used under extreme strain (up to 300%), and in curvature sensing of a pneumatic actuator. We also integrated them into a three-fingered pneumatic gripper and demonstrated that the picked object shape can be inferred with proposed pneumatic sensors.

6.1 Sacrificial 3D printing for complex mould fabrication (Publication I)

The first aim of this thesis was to develop more capable fabrication methods for soft robotics. Our first hypothesis of this aim was that sacrificial manufacturing of the elastomer casts would provide a simple and fast fabrication method for soft robots. Traditionally, soft devices are cast into moulds and demoulded after curing. The design of the mould is limited since one should be able to remove the cast from the mould without damaging the soft silicone. Therefore, overhanging structures or buried channels inside the silicone elastomer are particularly challenging to fabricate. In **Publication I**, moulds for elastomer casting were fabricated by using FDM 3D

printing with dissolvable filament materials which enables the fabrication of sacrificial moulds for soft elastomer casting. Since the mould material can be dissolved after the elastomer has cured, the design of the moulds can be more complex.

To find out the most suitable materials to use in sacrificial mould fabrication, we studied the solubility of nine different commercially available 3D printing materials, which are listed in Table 6. Standard sized test pieces were 3D printed by using the selected filaments, and then the pieces were dissolved in the specific solvents (presented in Table 5 in Chapter 5.2) for 24 hours and their solubility was visually observed. The dissolving times are listed in Table 6 below.

Table 6. Dissolving times under different conditions for the filaments used for sacrificial 3D printing

Filament trade name	Dissolving time (h)		
	Static	Stirring	Ultrasound bath
HIPS	6	3.5	4
ABS	11	10	4.5
PVB	>24	-	-
Ethy-Lay	11	18	3
Hydrosupport	24	6	5
PVA	24	6	5
LAYaPVA	24	6	6
Lay-Cloud	>24	-	-
High-t-Lay	>24	-	-

Then we selected six materials for further studies, since three of the materials did not dissolve in 24 hours. The tradenames of these filaments were HIPS, ABS, Ethy-Lay, Hydrosupport, PVA and LAYaPVA. The same solubility experiments were done for these materials under two different conditions: with stirring the solution and in an ultrasound bath, and again the dissolving was visually observed. The times required to dissolve the materials are presented also in Table 6. Overall, the fastest dissolving times were reached with ultrasound and the pictures from that experiment are shown in Figure 15.

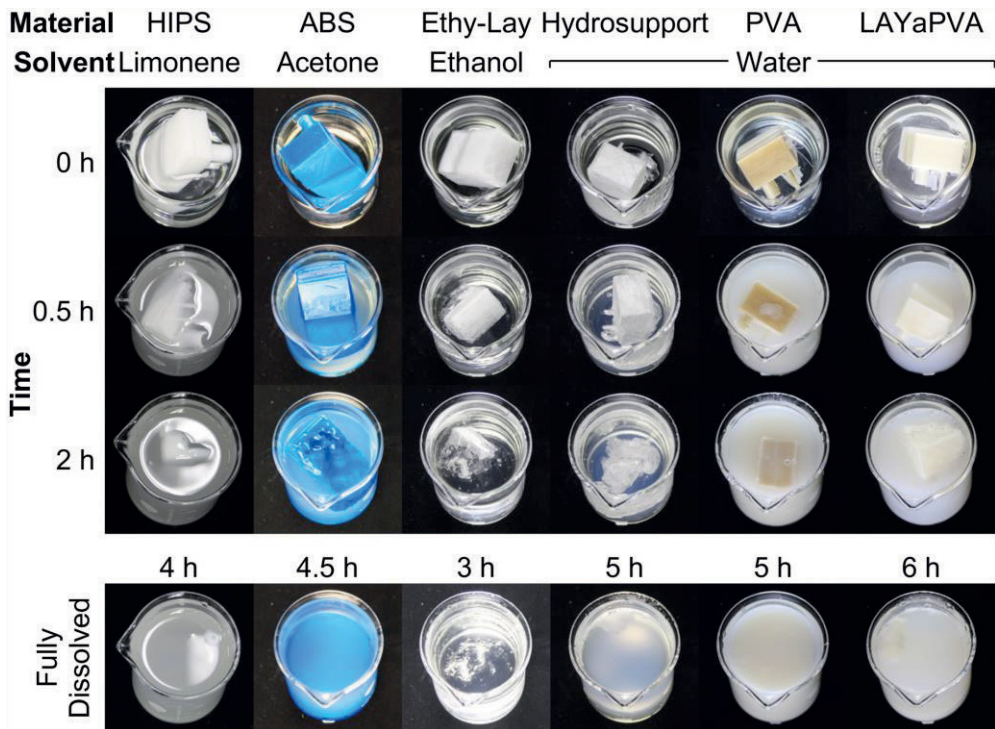


Figure 15. Solubility experiment for six different 3D printing filament materials (HIPS, ABS, Ethy-Lay, Hydrosupport, PVA and LAYaPVA) in an ultrasound bath.

The fastest filament material to fully dissolve (3 h) was Ethy-Lay (PVB), which was dissolved in ethanol. HIPS (dissolved in limonene) and ABS (dissolved in acetone) were also dissolved under five hours unlike water-soluble filaments which all needed five hours or more.

To show that these filaments can be used in the mould fabrication of soft devices, moulds including a buried channel were fabricated. Four fastest filaments dissolved were selected for mould fabrication: ABS, Ethy-Lay (PVB), Hydrosupport (PVA) and HIPS. The fabricated moulds were filled with two visually clear silicone elastomers: the softer one (Sorta-Clear 18, Shore hardness A18) and the harder one (Sylgard 184, Shore hardness A50). After the curing, the moulds were dissolved by using an ultrasonic bath. The results of the soft silicone pieces including buried channels filled with dyed water are presented in Figure 16.

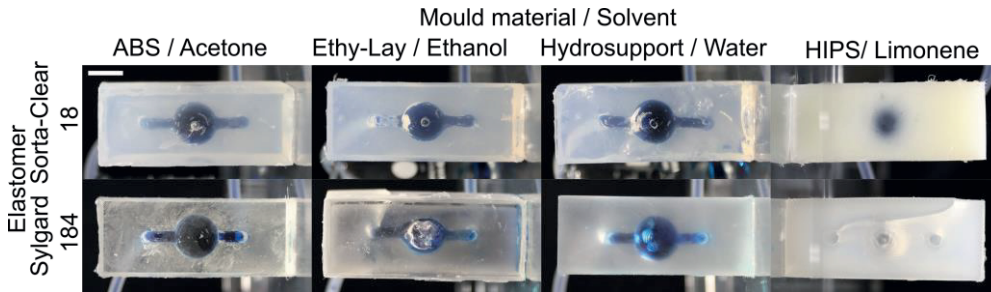


Figure 16. Buried channels in soft silicones, first row: the softer silicone elastomer (Sorta Clear 18) and second row: the more rigid one (Sylgard 184). The channels are filled with dyed water. Scale bar 1 cm.

Figure 16 shows the elastomers absorbed the limonene which was used as a solvent with HIPS filament. This caused the soft elastomer piece to swell and the more rigid one to rupture during the dissolving process. The buried channel structure was successfully 3D printed and dissolved with the other three materials. However, Ethy-Lay and Hydrosupport materials absorb water, making the 3D printing of them more challenging.

The fabricated buried channel structures showed that the mould material can be dissolved from the cavities inside the cured elastomer. However, it takes time, and in this study, the channels were relatively large.

6.2 Compliant gripping (Publications II and III)

The second aim of the thesis was to create delicate grippers with switchable adhesion for soft robots. **Publications II** and **III** present a soft suction cup gripper with a thin film attached underneath it (Figure 17). In our previous works, presented in Chapter 2,^{20,86} the gripper body was cast, and that fabrication process was time-consuming including several steps. Here the gripper body (\varnothing 20 mm) is 3D printed which makes the fabrication process faster and simpler, also allowing the easy modification of the gripper design. The gripper can be actuated pneumatically (**Publication II**) or with the combination of fluidic and magnetic actuation (**Publication III**).

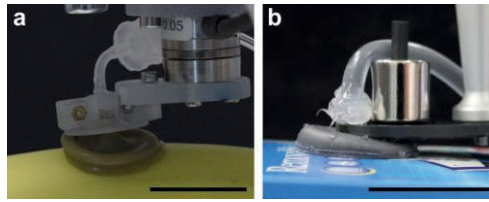


Figure 17. 3D printed suction-based grippers proposed in this thesis. a) a pneumatic gripper and b) a hydraulically and magnetically actuated gripper. Scale bars: 2 cm.

The pneumatic gripper (Figure 17a, **Publication II**) was characterized by measuring the pull-off force (F_{off}) with different applied negative pressures (P_{neg}) inside the gripper chamber. The negative pressure was generated by withdrawing different volume V of air from the gripper chamber by using a syringe pump. Additionally, to see the effect of the thin film, we did the same force measurement for a similar gripper without the thin film underneath it. Figure 18 shows that the gripping forces are significantly larger with the gripper including the film. We fitted first and second order polynomials to both force data and studied the fits with adjusted R^2 . We found out that second order polynomial fit is better for the gripper with film and first order fit for the gripper without film. Additionally, the achieved force values were more scattered with high negative pressures when the gripper without film was used.

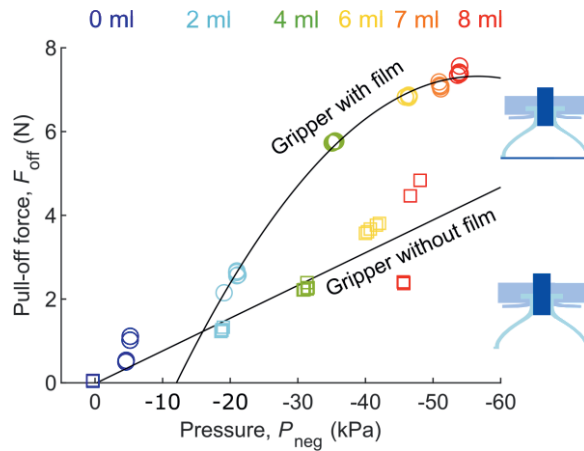


Figure 18. Maximum Pull-off forces for the 3D printed soft pneumatic suction gripper with different negative pressures on smooth glass plate. Colours are corresponding different withdrawal volumes. 2nd order polynomial (zero pressure excluded) was fitted in the data of the gripper including the film and 1st order polynomial to the data of the gripper without film.

To study if the roughness of the target surface has effect on the F_{off} values, we did the measurements with two different negative pressures (35 kPa and 47 kPa) and with five different surfaces with varying roughness. The surfaces were replicas of 2000 and 1000 grit sandpapers, a rough polymer, a rough steel, and a concrete. Surface replicas made of clear epoxy were used so that the material of the target surface is always the same and the effect of the material can be ruled out. The surface topographies and R_{rms} values are presented in Figure 19a and b.

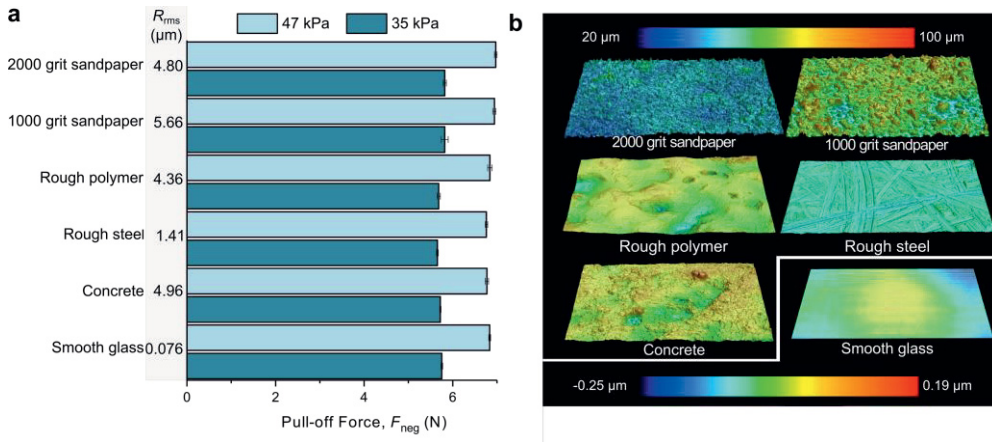


Figure 19. Maximum pull-off forces with different surface roughness. a) Pull-off forces with rough surface replicas (2000 and 1000 grit sandpapers, a rough polymer, a rough steel, and a concrete) and a smooth glass and their corresponding R_{rms} values. Each bar indicates an average of five measurements, and error bars show SD. b) The topographies of the used surface replicas, measured using a laser confocal microscope.

Figure 19 shows that the measured force values did not differ significantly from the smooth glass surface, which was used as a reference surface. The force depends on more the negative pressure used to retract the gripper which indicates that the operation principle of the gripper is mainly vacuum based. Hence, for the reliable gripping, P_{neg} has more significant effect than the roughness of the target object.

The repeatability of the gripper was tested by assembling it to the robotic arm including six axis force sensor (Figure 13 and Figure 20b) and picking and releasing objects 15 times. We were able to pick and place all the different surface replicas fabricated. Figure 20a shows the force data of the concrete replica. The force maintains stable during the picking and releasing process, and we concluded that the gripper conducted the tasks repeatably.

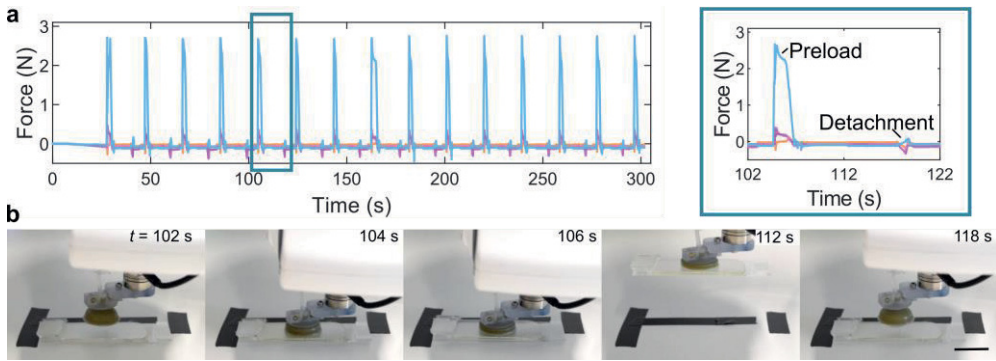


Figure 20. Repeatability tests for the pneumatic suction gripper. a) force data (x=orange, y=pink and z=blue) from 15 repeated measurements with a concrete replica and inset of the data. b) Snapshots from a repeatability measurement. At $t = 102$ s, the gripper approach the target object. The gripper contacts the object at $t = 104$ s, and a negative pressure is applied inside the chamber ($t = 106$ s). At $t = 112$ s, the object is carried, and then released ($t = 118$ s). Scale bar: 2 cm.

The traditional vacuum grippers cannot pick objects smaller than their diameter since they are sucked inside the vacuum system. Thus, we wanted to demonstrate the picking of such small objects. We fabricated small polymethyl methacrylate (PMMA) discs and picked them with a robotic arm system (Figure 21a). The gripper was able to pick 6 mm diameter disc, but not release it repeatably. The picking and releasing were repeatable with discs having a diameter bigger than 16 mm. We additionally noticed that the target object did not have to be exactly in the middle of the gripper during the picking. This can give more tolerance in the picking applications when the careful planning of the picking place can be removed reducing the complexity of the system.

Finally, we showed that our gripper, in addition to small and rough objects, can pick other objects that are usually challenging to traditional vacuum grippers: uneven loads, fragile and thin surfaces. Here, this is demonstrated by picking a glass bottle on edge (429 g, Figure 21b) creating torque to the gripper, a peach (170 g, Figure 21c) and a banana (130 g, Figure 21d), and by flipping pages of a book (Figure 21e). The commercial suction cup gripper (Bellow suction cup SPB4 20 SI-55 G1/8-AG, Schmalz GmbH, Germany) could not grip the glass bottle on edge, left marks to the fragile surfaces and crumpled the pages of the book. Therefore, the proposed gripper can have applications for example in warehouse industry where versatile gripping is needed.

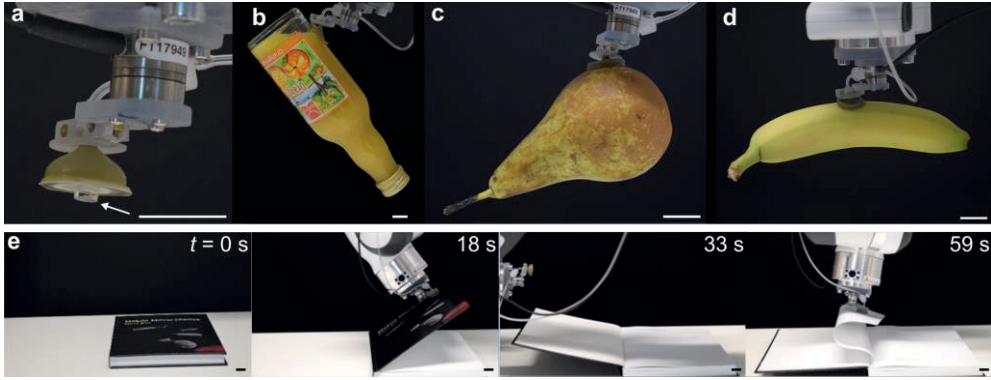


Figure 21. Demonstration with the 3D printed suction gripper. a-d) Photographs of the suction gripper holding challenging objects: a small object (6 mm), an orange juice bottle (429 g, highly uneven load), and soft fruits: a pear (167 g) and a banana (130 g). e) Snapshots of the experiment: Gripper turning the pages of the book. Scale bar in photographs: 2 cm.

To add stiffness switching to the proposed gripper, the same gripper design was used to fabricate a magnetically and hydraulically switchable soft gripper. The chamber of the gripper was filled with MR fluid, which turns into solid-like in an external magnetic field. In this study, a neodymium magnet was used for the switching, by bringing the magnet close to the gripper. The photograph of the magnetically switchable soft gripper is presented in Figure 17b.

The gripper was characterized by measuring F_{off} under varying withdrawal volumes V against smooth glass substrate without and with the external magnetic field applied, shown in Figure 22a. The force increased as a function of withdrawal volume, but started to saturate after 1.5 ml. There is a difference between the forces with and without the external magnetic field applied in all the cases, but the difference is the largest with bigger withdrawal volumes. The largest increase was with 1.5 ml: 90%. We also calculated the work needed to detach the gripper from the surface (tensile work W_T). The work increased as a function of the withdrawn volume and was significantly higher when the magnetic field was applied, starting from the 1 ml volume. We concluded that the external magnetic field increases F_{off} if a sufficient volume is withdrawn.

In addition to the clean glass surface, we measured F_{off} with surfaces wet by water or oil. Figure 22b shows that with the same V the F_{off} does not change significantly between the surface conditions. The highest forces were achieved with dry surfaces and lowest with oily ones, but the drop was less than 20%. The picking of the watery surface was demonstrated also by wetting a beaker glass (116 g) and picking it with

the gripper, shown in Figure 23a. These results show that the adhesion of the gripper is not limited to dry surfaces.

One known challenge for the grippers is to grasp the soft surfaces.¹⁸ Therefore, we measured the forces against ~ 0.7 cm thick, soft surfaces with Shore hardness varying from 00-10 to 00-80. The forces decreased as a function of the softness. Figure 22c shows that even with Shore 00-30 hardness (close to the softness of the human skin), the gripper can achieve almost 5 N forces. We further demonstrated the ability to pick soft objects with mango (418 g, Figure 23b) and banana (143 g, Figure 23c) which have soft surfaces. Thus, we conclude that our gripper can also pick extremely soft objects though with a reduced pull-off force.

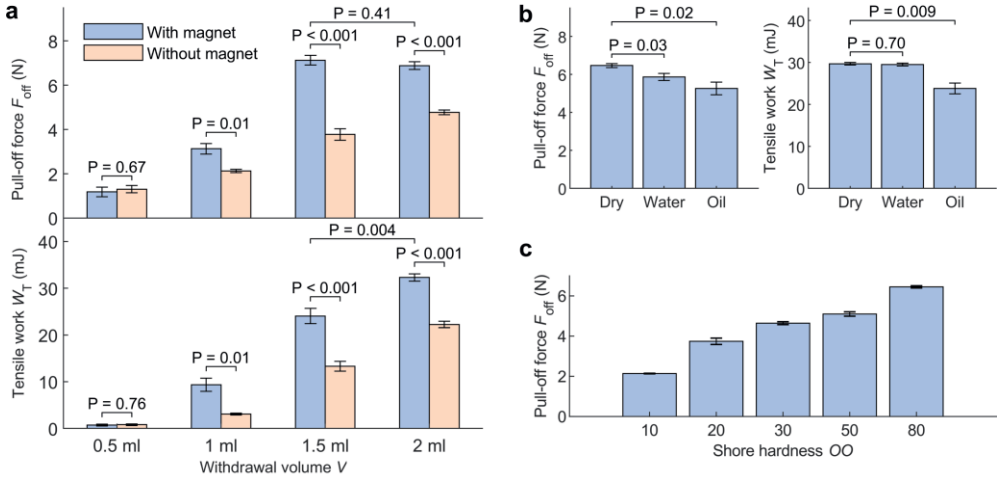


Figure 22. Maximum pull-off forces for the magnetohydraulic gripper. a) Pull-off forces and tensile works for the gripper with different withdrawal volumes on clean smooth surface. b) Pull-off forces and tensile works for different surface conditions: dry, deionized water and heavy mineral oil ($V = 1.5$ ml). c) Pull-off forces with different soft surfaces ($V = 1.5$ ml). The error bars show SE ($n = 5$) and the P-values are calculated using Welch's unequal variances t-test.

The gripper's ability of picking other typically challenging objects, such as rough, curved, or small objects, was tested by picking everyday objects. We picked a thin film (0.83 g, Figure 23d) which is known challenge for vacuum based grippers since the suction tends to crumple the films. A tape roll (164 g, Figure 23e) demonstrated that the gripper can adhere to the curved surfaces. Then, we demonstrated the picking of rough surfaces. A red grapefruit was selected, since its surface is rough ($R_z = 17.7 \mu\text{m}$) but the object is also relatively heavy (441 g), shown in Figure 23f. Finally, we picked small discs (8-16 mm diameter) to demonstrate that the gripper

diameter does not limit the picking like in traditional suction cup grippers. Photographs of the picking are shown in Figure 23g and h.

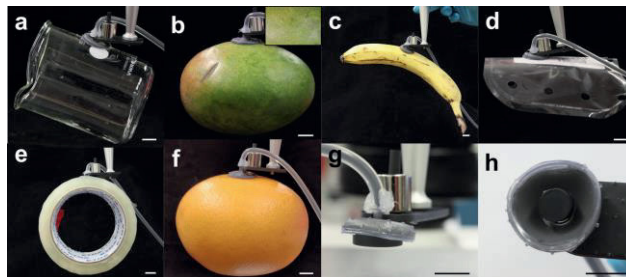


Figure 23. Gripping demonstrations: a) a wetted beaker (a wet object), b) a mango (a soft object, inset: a close-up of the surface of the mango), c) a banana (soft object), d) a thin plastic sheet, e) a tape roll (curved object), f) a red grapefruit (rough surface), g) \varnothing 16 mm 3D-printed disc, and h) \varnothing 8 mm 3D-printed disc. Scale bars: 1 cm.

To study how the external magnetic field affects the behaviour of the soft gripper, we recorded the film during the retraction with and without the external magnetic field applied, insets from the video shown in Figure 24. The insets in time 144 s and 219 s show that without the external magnetic field, the MR fluids moves more in the chamber. We conclude based on these results that the external magnetic field stiffens the fluid.

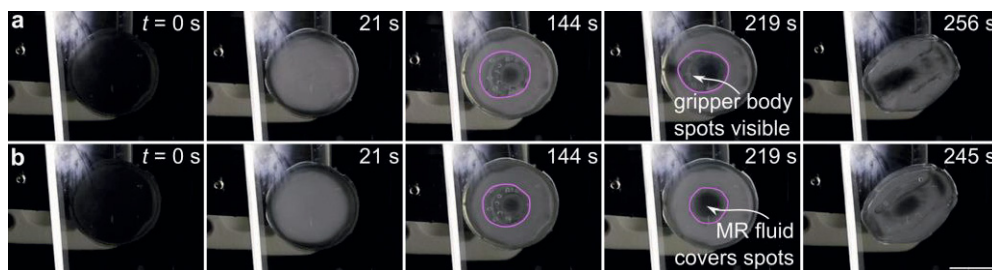


Figure 24. The soft film behaviour of the 3D-printed gripper. The snapshots of the video showing the film of the gripper a) under the magnetic field and b) without the magnetic field. Scale bar: 1 cm.

6.3 Screen-printed stretchable strain sensors for soft robotics (Publication IV)

The third aim of the thesis was to integrate sensors into soft robots. In **Publication IV** and our previous work in the 2017 IEEE Sensors conference,¹³⁹ we proposed that screen-printed strain sensors can be used for curvature sensing in soft pneumatic actuators. By placing the strain sensor inside the pneumatic actuator at distance from the neutral plane, the sensor would stretch while the actuator is bent, thus measuring the bending of the actuator.

To demonstrate that screen-printing with conductive inks can be used to produce resistive strain sensors for soft robots, we fabricated silver and carbon ink-based strain sensors onto TPU sheets. The design of the sensor is shown in Figure 25a, a photograph of it in Figure 25b and scanning electron micrograph of the silver ink in Figure 25d. The sensor was then integrated into the soft pneumatic actuator on top of the neutral plane (Figure 25c).

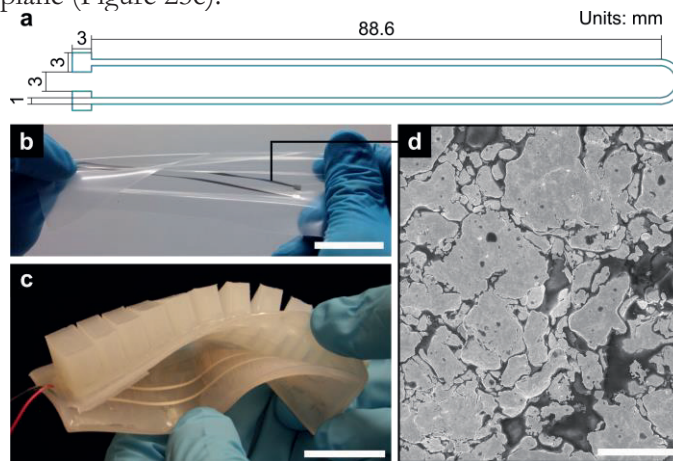


Figure 25. Screen-printed curvature sensor for the soft pneumatic actuator. a) Design of the printed resistive strain sensor. b) A photograph of the sensor. c) A photograph of the actuator with integrated strain sensor. Scale bars in photographs 3 cm. d) A scanning electron micrograph of the screen-printed silver sensor. Scale bar 10 μm .

To characterize the strain sensors as curvature sensors, we measured the resistance of the strain sensor, curvature of the actuator, and pressure inside the actuator during 30 repeated bending cycles. The cycles were slow (~ 5 min) to avoid viscoelastic effects of the soft structures. First, we studied the silver ink-based sensors. Figure 26 shows the results. The initial resistance of the silver ink-based sensor R_{silver} was 15.8 Ω , pressure in the actuator P_{act} was 12 kPa and the curvature of the actuator κ

was 7 m^{-1} , and at the maximum bending $R_{\text{silver}} = 1.7 \text{ } \Omega$, $P_{\text{act}} = 12 \text{ kPa}$ and $\Delta\kappa = 21 \text{ m}^{-1}$. The overall behaviour of the sensors was linear but hysteric (17% of full range). A linear estimate ($R^2 = 0.92$) was fitted to the resistance curvature data to calculate the sensitivity of the sensor ($0.075 \text{ } \Omega/\text{m}^{-1}$).

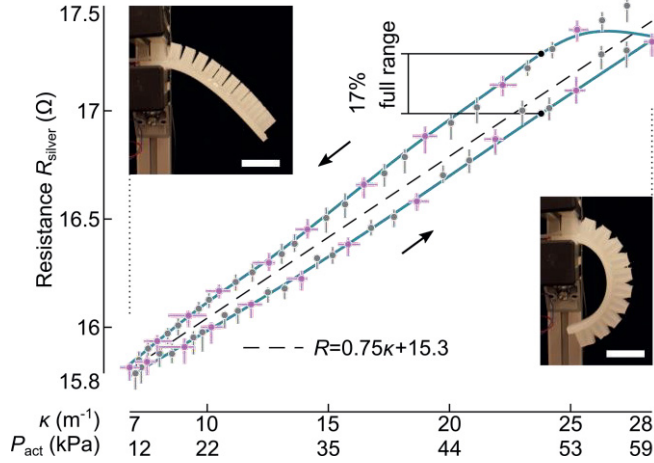


Figure 26. Characterization of the silver ink-based sensor. R_{silver} as a function of κ and P_{act} for the silver-based sensor. The data points are medians of 150 resistance measurements and 30 curvature measurements (pink points). The curvature was interpolated between frames (grey data points). The error bars are interquartile range. The cycle was repeated 30 times. Scale bars: 3 cm.

The resistance change of the sensor is based on the change in the applied strain. We wanted to estimate the linear strain of the sensors during the bending and first we used the ideal bending relationship

$$\Delta\varepsilon = d_{\text{np}}\Delta\kappa, \quad (12)$$

where d_{np} is the distance from the neutral plane. We assume that the neutral plane is half-way through the strain limiting fibreglass network. Then we get $d_{\text{np}} =$ half of the fibreglass thickness ($125 \text{ } \mu\text{m}$) + silicone adhesive ($500 \text{ } \mu\text{m}$) + TPU thickness ($50 \text{ } \mu\text{m}$) = $675 \text{ } \mu\text{m}$. Thus, using Eq. (12) $\Delta\varepsilon \approx 675 \text{ } \mu\text{m} \cdot 21 \text{ m}^{-1} \approx 1\%$. We estimated the strain also by using the relationship between ΔR_{silver} and previously reported GF for small strains: $\text{GF}_{\text{silver}} \approx 5.759$.¹³³

$$\Delta\varepsilon = \frac{\Delta R_{\text{silver}}}{R_{\text{silver}} \cdot \text{GF}_{\text{silver}}}, \quad (13)$$

which gives $\Delta\varepsilon \approx 2\%$. Since the distance from the neutral plane is challenging to measure, we consider that the GF based estimate is more trustworthy.

To show that also other conductive inks can be used in sensor fabrication, we made similar kind of sensor out of carbon-based ink. Similar characterization experiments were done than for silver-based ink, and Figure 27 shows the results. The initial resistance of the carbon-based sensor is higher ($R_{\text{carbon}} = 56.5 \text{ k}\Omega$). The overall behaviour of the carbon sensor is less linear ($R^2 = 0.64$) compared with the silver-based sensor. The maximum hysteresis of the carbon-based sensor is 27% and the sensitivity $0.31 \text{ k}\Omega/\text{m}^{-1}$. Since the silver-based sensor behaved more linearly and had less hysteresis, we selected it for the further experiments.

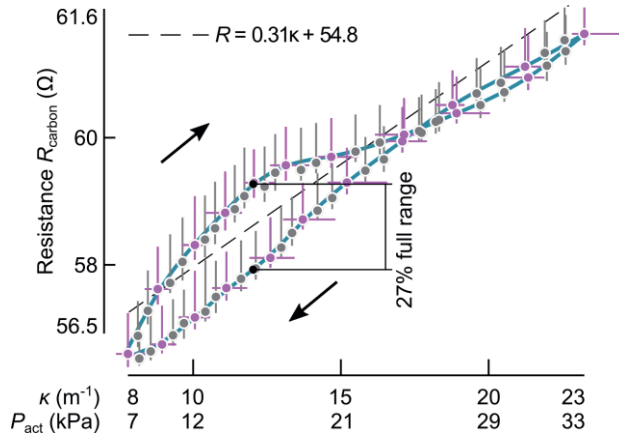


Figure 27. Characterization of the carbon ink-based sensor. R_{carbon} as a function of κ and P_{act} . Each datum point is the median of 150 resistance measurements and 30 curvature measurements (pink points). The curvature was interpolated for the grey data points. The error bars are interquartile range.

To make sure that the sensor measures the curvature of the actuator and not the pressure inside it, we measured the pressure and curvature of the actuator and resistance of the silver-based sensor in four different states: 1) neutral: no pressure or curvature is applied to the actuator, 2) driven: pressure and curvature are applied, 3) blocked: pressure is applied, but bending blocked by hand, i.e. curvature does not change, and 4) forced: no pressure is applied, but curvature change is created manually by hand.

Figure 28 shows the pressure of the actuator behaves like expected. The resistance of the sensor changes in driven, blocked and forced states. However, in the blocked state the change was significantly smaller when only the pressure was applied to the actuator. Therefore, we concluded that the sensor is measuring more

the curvature than the pressure of the actuator. The change during the blocked state is caused by the sensor responding to all the strains. Even though the actuator is prevented from bending, the actuator pressure applies some strain to the sensor. By using the method of least-squares, we estimated the curvature (pink line in Figure 28)

$$\kappa_{estimate} = \alpha R_{silver} + \beta P_{act} + \gamma, \quad (14)$$

where α , β and γ are the coefficients, having values of $\alpha = 17.1 \text{ m}^{-1}\Omega^{-1}$, $\beta = -0.230 \text{ m}^{-1}\text{kPa}^{-1}$ and $\gamma = -254 \text{ m}^{-1}$. The estimate (pink line) follows the measured curvature (turquoise line) well. Approximately

$$\frac{\kappa\Delta}{\alpha\Delta R} \approx 70\%, \quad (15)$$

of the sensor signal comes from the curvature changes alone.

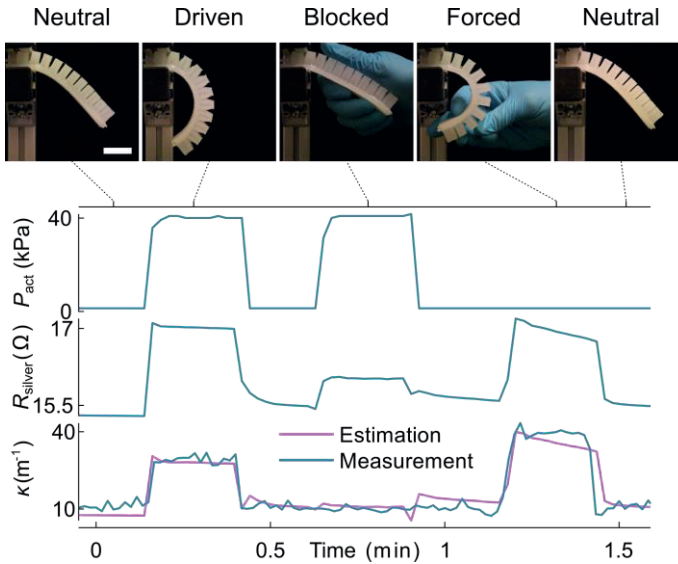


Figure 28. Decoupling pressure contribution from the curvature measurement. The snapshots are from the experiment: the actuator in four different states: neutral, driven, blocked, and forced. Pressure, resistance, and curvature recordings from the blocking experiment of a silver ink-based sensor. Scale bar: 3 cm.

Finally, we demonstrated that screen-printed strain sensors can be used in soft robot applications. We fabricated a three-fingered soft gripper with curvature sensing. The gripper was made by casting three pneumatic actuators onto common base part

(Figure 29a). All three fingers (Figure 29b) included curvature sensors, and they were independently actuated.

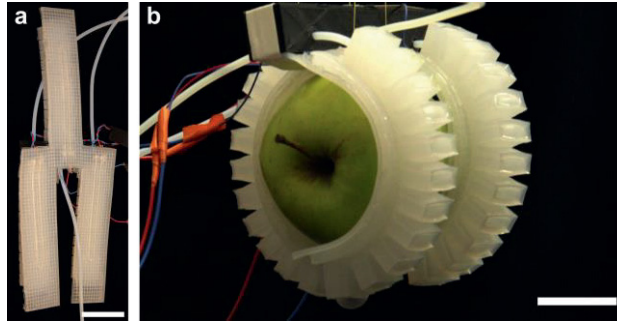


Figure 29. Soft pneumatic three-fingered gripper. a) Gripper in an open state, sensors showing inside the gripper and b) the gripper in the closed state holding an apple. Scale bar: 3cm.

To show that all three fingers can be independently actuated and measured, we recorded the pressures in the fingers and the resistances of the sensors while sequentially actuating the fingers. Figure 30 shows that sensors are mostly independent, but they have some response to the other fingers.

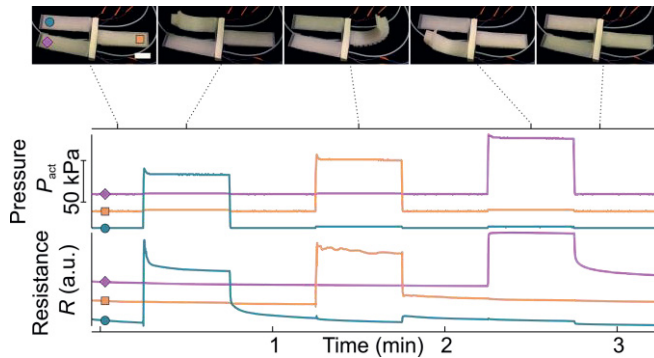


Figure 30. Gripper demonstration. Snapshots from the experiment show the actuation of all three fingers sequentially. The pressure and resistance data of the experiment are shown below the snapshots. Scale bar: 3 cm.

6.4 Stretchable pneumatic strain sensors (Manuscript V)

Third aim of this thesis was to integrate sensing into soft robots. Second hypothesis of that aim was that by shifting from electric sensors to pneumatic ones the overall structure of the soft robot would be simpler. In **Manuscript V**, we propose that the meandering microchannels in the soft silicone can be used as stretchable pneumatic strain sensors (Figure 31a, c and d).

To demonstrate the operation of the pneumatic strain sensors, we fabricated meandering microchannels (200 μm width and 200 μm height) in the soft silicone elastomer (Ecoflex 00-50). The channel was 183 mm long with five turns, creating 30 mm \times 3.84 mm sensing area. For measuring the change in the pneumatic resistance, we connected the pneumatic strain sensor R in series with a constant fluidic restrictor R_c . A constant positive pressure P_{supply} (60 kPa) was applied to the circuit and air pressure P_{atm} was used as a pneumatic ground. The pressure inside the strain sensor was called P_{gauge} and initially it was ~ 10 kPa and rose to ~ 24 kPa in 300% engineering strain ε .

To characterize the fabricated pneumatic strain sensors, we measured the relative pneumatic resistance $\Delta R/R_c$ under varying engineering strain ε from 0 to 300% (Figure 32a and b). We fabricated five similar samples and each of them was measured five time until 300% engineering strain. There was some variation between the samples, but the overall behaviour was very similar.

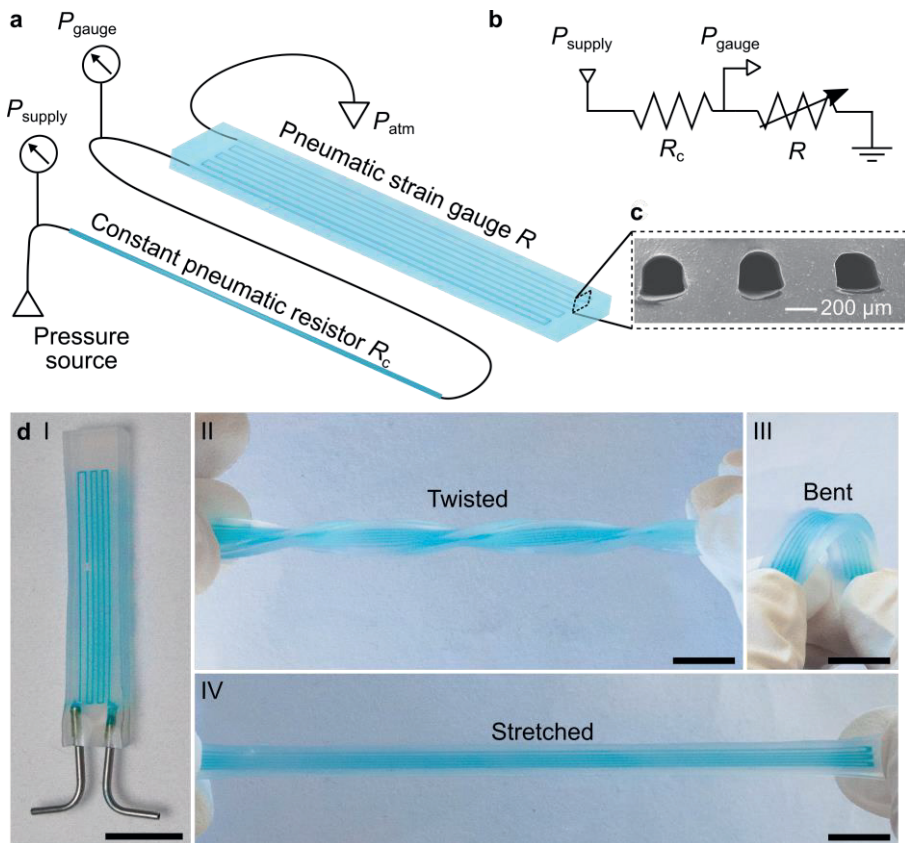


Figure 31. The concept of the soft pneumatic strain sensor. a) Schematic circuit for the soft pneumatic sensor. The measurement setup consists of a constant pneumatic resistor R_c and a pneumatic strain gauge R in series. A constant positive supply pressure P_{supply} is measured and applied to the constant pneumatic resistor R_c . The measured pressure between the resistor and the strain gauge is P_{gauge} . The strain gauge is vented to atmospheric pressure P_{atm} . b) Electric equivalent for the pneumatic circuit in a). c) A scanning electron micrograph of the channel cross-sections. d) Photographs of the pneumatic strain sensor when its relaxed (I), twisted (II), bent (II), and stretched (IV). Channels are filled with blue liquid. Scale bars: 1 cm.

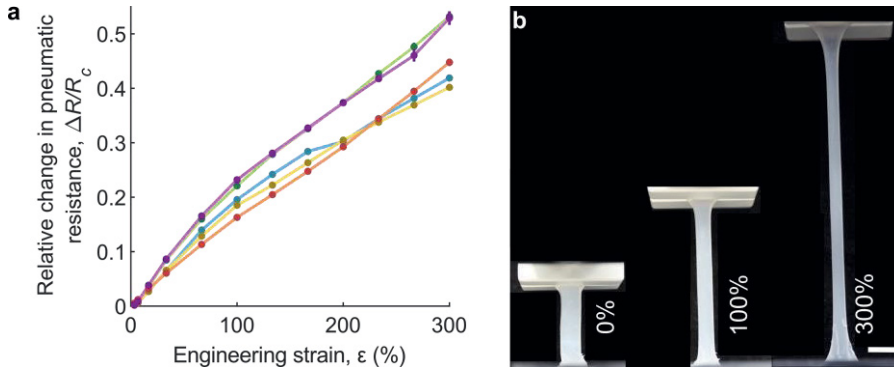


Figure 32. Relative change in the pneumatic resistance $\Delta R/R_c$ of the strain gauge as a function of the applied engineering strain ε . The five different coloured curves are from different samples and each curve is an average of five measurements with that sample. Error bars denote SD. b) Pneumatic strain sensor under 0%, 100%, and 300% engineering strain. Scale bar: 2 cm.

Then, we studied the overall performance of the pneumatic strain gauges. First, the stability during long-term measurement was studied (Figure 33a). We recorded the $\Delta R/R_c$ while 50% engineering strain was applied for 12 hours. The $\Delta R/R_c$ drifted from 0.127 to 0.119 and after the release the $\Delta R/R_c$ returned close to its initial value. Overall, the behaviour was reliable and reversible.

To investigate if the strain gauge has hysteric behaviour, we recorded $\Delta R/R_c$ while applying slowly (0.1 mm/s) 50% engineering strain five times (Figure 33b). The hysteresis was smaller than the noise level of the sensor (5% in tested range) and it cannot be observed even in the average curve of five repeats.

The sensitivity of the strain gauge was studied by calculating its gauge factor:

$$GF = \frac{dR}{dL} \frac{L}{R}. \quad (16)$$

We were not able to measure R , only R/R_c , due to our measuring configuration. Additionally, we wanted to study the gauge factor as a function of the engineering strain ε ($dL=L_0 d\varepsilon$). By substituting these variables into Eq. (16), we obtained

$$GF = \frac{d(R/R_c)}{d\varepsilon} \cdot \frac{R_c}{L_0} \cdot \frac{L}{R} = \frac{d\left(\frac{R}{R_c}\right)}{d\varepsilon}, \quad (17)$$

shown in Figure 33c. The GF is roughly 1: when the length is doubled, the $\Delta R/R_c$ is also roughly doubled.

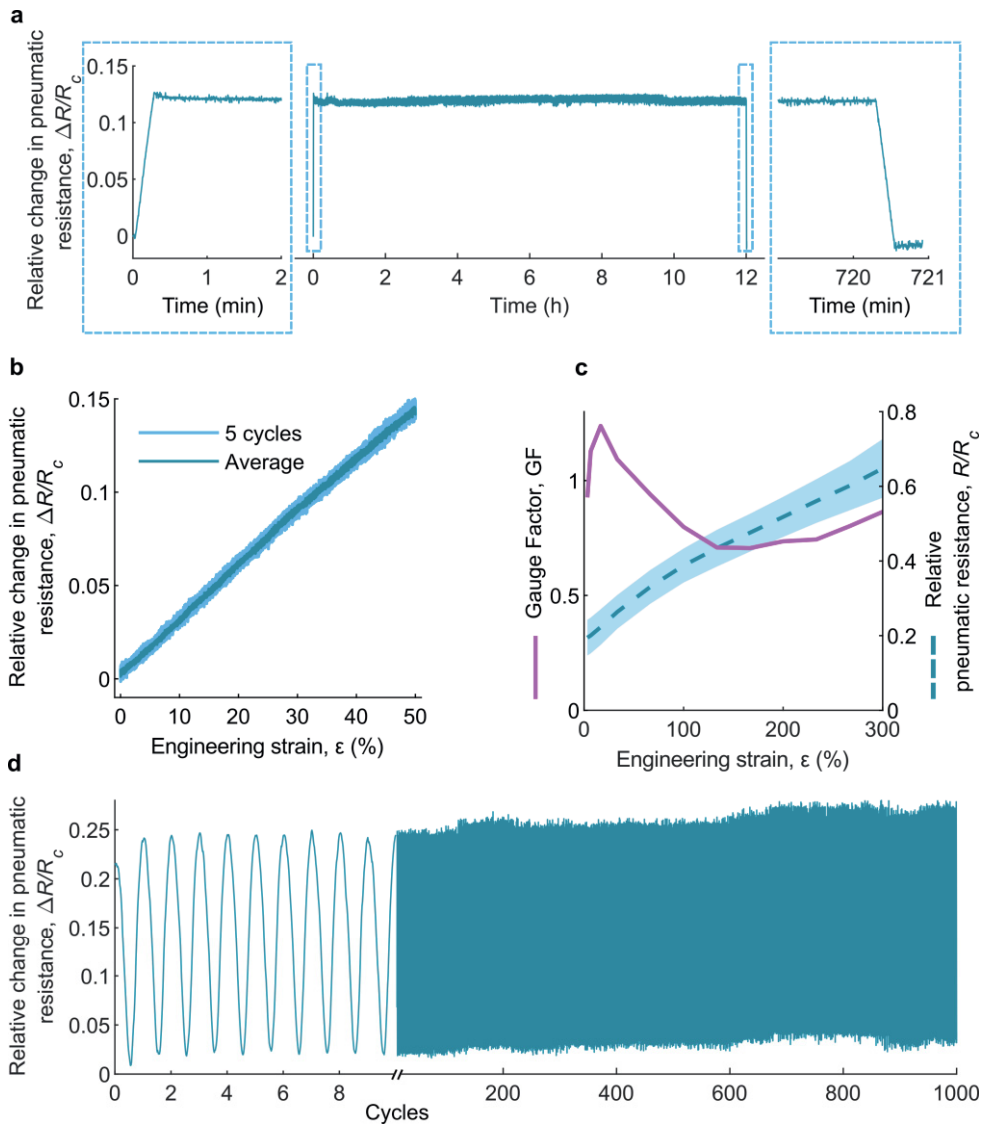


Figure 33. Pneumatic strain sensor characterization. a) Stability of the strain gauge when a static 50% engineering strain is held for 12 h. b) Hysteresis of the strain gauge when 50% engineering strain is applied for five cycles. c) Gauge factor of the pneumatic strain gauge. The solid line is the gauge factor, calculated using Eq. (17). The dashed line is the mean R/R_c of the five tested samples shown in Figure 32a, with the shaded area showing standard deviation. d) Stability of the strain sensor when a cyclic 67% engineering strain is applied for 1000 cycles.

The strain gauge behaviour under dynamic strain was also studied (Figure 33d). We applied 63% engineering strain 1000 cycles with a frequency of 0.25 Hz. Figure 33d shows some minor drift during the experiment but the overall behaviour is stable.

Bending pneumatic actuators are commonly used in soft robots for grasping and moving.^{15,18} To study if the pneumatic strain gauges can be used to measure the curvature of the bending actuator, we integrated the strain gauge on the bottom of the same pneumatic actuator than used in **Publication IV** (Figure 34a). The actuator and the strain gauge were fabricated of the same soft silicone elastomer (Dragon skin 30).

The behaviour of the pneumatic strain gauge as a curvature sensor was characterized by measuring the $\Delta R/R_c$ while bending the actuator 30 times (Figure 34b). At the initial stage, $\Delta R/R_c = -0.002$ and $\kappa = 3.5 \text{ m}^{-1}$, and at the maximum bending, $\Delta R/R_c = -0.022$ and $\kappa = 24 \text{ m}^{-1}$. The sensor was able to detect when the actuator was bent but the signal was noisy, suggesting that the strains were significantly smaller than in the tensile strain experiments. It should be noted that here the sensor is on the bottom of the actuator (i.e., compressing while bent). In **Publication IV**, the sensor was on top of the strain limiting layer and straining while bent.

The strain during the bending was estimated with the same ideal bending relationship (Eq. (12)) than in **Publication IV**. Here the distance from the neutral plane $d_{np} \approx 2 \text{ mm}$, which gives $\Delta \varepsilon \approx 4\%$. This value is roughly corresponding to the values in Figure 32a.

Similarly than in **Publication IV**, we cannot rule out the possibility that the sensor is measuring the pressure inside the actuator. Therefore, we did the same experiment as in Figure 28 and measured the curvature κ , pressure inside the actuator P_{act} and $\Delta R/R_c$ in four different states: neutral (Figure 34c, I), driven (Figure 34c, II), blocked (Figure 34c, III) and forced (Figure 34c, IV). Then we calculated the curvature $\kappa_{estimate}$ by using the method of least-squares (Eq. (14)). Here $\alpha = -1249.3 \text{ m}^{-1}$, $\beta = 0.0116 \text{ m}^{-1}\text{kPa}^{-1}$, and $\gamma = 2.66 \text{ m}^{-1}$. Thus, only $\left| \frac{\beta \Delta P_{act}}{\alpha \Delta R/R_c} \right| \approx 3\%$ of the strain sensor output is from the pressure change in the actuator. The sensor is primarily measuring the curvature of the actuator.

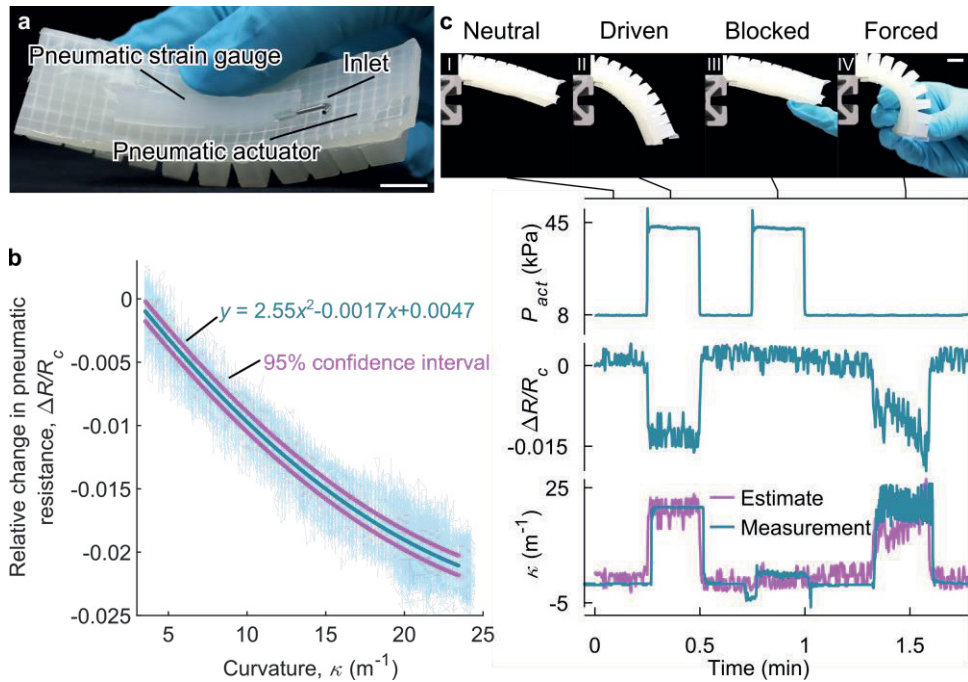


Figure 34. Pneumatic strain sensor as a curvature sensor. a) A photograph of the soft pneumatic actuator with an integrated strain sensor. b) Response of $\Delta R/R_c$ to curvature κ in repetitive cyclic bending. c) Decoupling the actuator pressure from the measured curvature. Actuator pressure P_{act} , relative change in pneumatic resistance $\Delta R/R_c$, and curvature κ versus time in four different states. The estimated curvature is calculated using Eq. (14). Scale bar: 1 cm.

To investigate if the pneumatic strain sensors integrated in the soft pneumatic actuators can be used in soft robot applications, we build a three-fingered soft pneumatic gripper (Figure 35a). The electric equivalent circuit for the gripper system is shown in Figure 35b. The fingers ($C_{1,2,3}$) are similar pneumatic actuators than used before, and they were connected to a 3D printed part, which also included connection to a vertical motor. All the fingers were actuated by the same pressure signal P_{act} so they opened and closed in unison unlike in **Publication IV**, where the fingers were independent. The lower part of each finger included an independent strain sensor ($R_{1,2,3}$) which was in series with constant pneumatic restrictor ($R_{c1,c2,c3}$) and they were all connected to a constant positive pressure source P_{supply} .

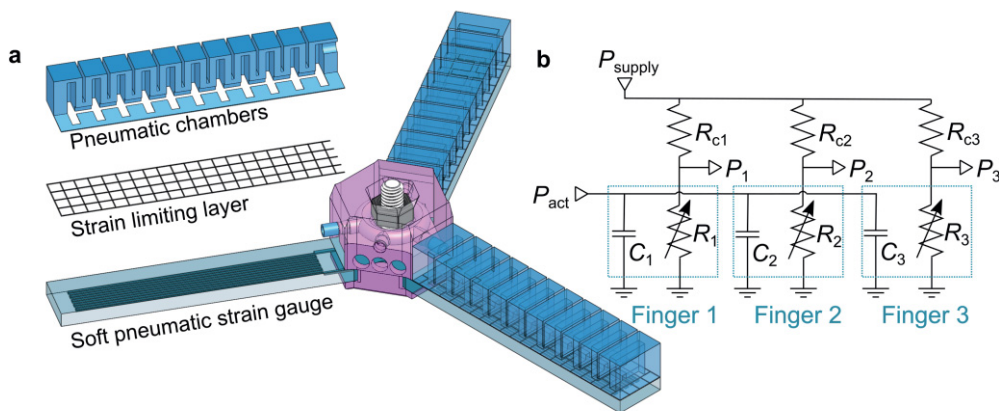


Figure 35. Pneumatic strain sensors in a soft pneumatic gripper. a) A schematic of the soft pneumatic gripper with three fingers, each including an independent strain sensor. b) Electrical equivalent circuit for the gripper.

The curvature of the fingers of the pneumatic gripper depends on the shape of the picked object. To study if the shape of the object can be inferred from the sensor signals alone, we picked up nine times three differently shaped objects: a bottle (25 g), a lemon (155 g) and a lime (82 g). From each experiment, we calculated the relative change in pneumatic resistance before and during gripping the object. The data are shown in Figure 36 as a 3D scatter plot, where each axis corresponds to a different strain sensor. The objects form clear clusters which suggest that the sensor data can be used to infer the information about the shape of the object picked.

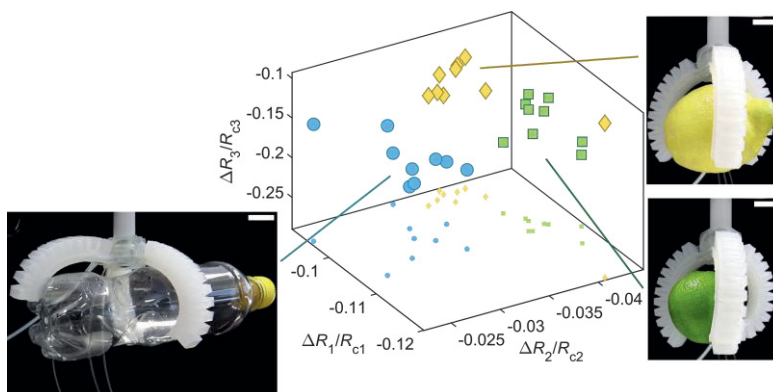


Figure 36. Soft pneumatic gripper with perception. $\Delta R/R_c$ for each pneumatic strain gauge when three different objects (a lemon, a lime, and a water bottle) are picked nine times, and photographs from the picking experiment. Scale bar: 2 cm.

7 DISCUSSION

In this chapter, the results are discussed and compared with previous related research. The structure follows three main aims proposed in Chapter 4 and last sub chapter is the outlook of the work.

7.1 Alternative and more capable fabrication of soft robot components

The fabrication methods of soft robot components depend heavily on the desired design and materials. The widely used soft silicone elastomers are often cast into 3D printed moulds. This method limits the design of the moulded part since the fabricated part have to be demoulded after curing. In **Publication I**, we showed that by using sacrificial 3D printing, silicone elastomer parts with complex structures, such as buried channels, can be cast at once.

The fabrication time of the sacrificial moulding is longer than by using traditional casting techniques since the moulds have to be fabricated separately for every cast and then dissolved. However, the moulds are fabricated with FDM filaments and 3D printers, which allow fabricating of multiple moulds at once and the filaments are relatively inexpensive. Compared to direct 3D printing of soft structures, the fabrication time of sacrificial moulds is also longer.

The main advantage of sacrificial mould fabrication is that the soft elastomer piece was fabricated in a single cast and it included a buried channel. In this work, the fabricated channel was relatively large (~ 3 mm) which can limit the future usage in the soft robot applications. However, the demonstrated technique has been also used in the field of microfluidics¹⁴⁰ to fabricate microchannels, so the fabrication method is not limited only to large structures.

The direct 3D printing of soft robot body is still limited with extremely soft (Shore 00 scale) materials which is not a case with traditional casting. Sacrificial moulds allow the fabrication of complex structures in extremely soft elastomer without bonding separate parts together. The softest commercial 3D printing

materials have softness of ~ 30 A Shore but softer materials have been demonstrated with custom 3D printers.³⁷

In the next two studies, **Publications II** and **III**, we demonstrated that by 3D printing the robot end-effectors, different designs can be fabricated fast at once. We were able to test and modify the fabricated grippers and eventually select the design most suitable for our purpose. 3D printing has been also used to fabricate soft actuators;¹⁴ thus, grippers and actuators of the robot can be potentially manufactured at once, simplifying the overall fabrication of the soft robot.

Soft pneumatic strain sensors were fabricated in **Manuscript V** by using the same silicone elastomer casting techniques with 3D printed moulds that are widely used in soft actuator manufacturing. The method has limitations in the bonding of the parts together due the uncured elastomer blocking and the small and thin structures. The sensors do not need any other materials, such as liquid metals¹⁰ or conductive inks¹⁰⁹ which is an advantage over the alternative proposed stretchable strain sensor fabrication methods. The same materials and fabrication methods also make possible to fabricate the actuators and sensors during the same process and integrate them into soft robots. Thus, the pneumatic strain sensors have potential to simplify the overall soft robot fabrication process.

The fabrication of sacrificial and traditional moulds for soft robot actuators and sensors is more feasible due the rapid development of 3D printing. This supports the outlook that 3D printing, in various ways, is a suitable and valid method to fabricate soft robot, sensor and gripper components in the future.

7.2 Grippers with switchable adhesion and stiffness

In **Publications II** and **III**, we proposed soft 3D printed suction grippers for switchable adhesion and compliant gripping. In **Publication II**, the pneumatic actuation was used, whereas in **Publication III** we proposed the combination of magnetic and hydraulic actuation.

In both publications, the maximum achieved pull-off forces were ~ 7 N with the same diameter grippers. Compared with previously reported suction grippers (in Table 2), the achieved pull-off forces and the diameter normalized pull-off forces were significantly higher. One exception being the gripper from Takahashi et al.⁹⁵ which had a higher pull-off force and a diameter normalized pull-off force. However, the measurements were done with a liquid surface, so the comparison was not straightforward. We attributed that the reason for higher pull-off forces is the

improved gripper design which was achieved by 3D printing the gripper bodies. Comparison of the maximum pull-off forces to other types of soft grippers was done in a lifting ratio (Table 2) because the gripper geometries vary. The hydraulic 3D printed suction gripper had a lifting ratio of ~ 80 when also the gripper holder and the connecting tube were included. The highest lifting ratio was achieved with the previously proposed soft suction gripper²⁰ (476) and the gecko inspired gripper⁸⁷ (200) but it was not clear if the whole gripping systems were included in the grippers' weights. Other gripper types had significantly lower values. The proposed 3D printed suction-based grippers achieve high pull-off forces compared to their masses which is in line with the previous reports of adhesion and suction based grippers.

Adhesion on rough surfaces is known to be challenge for suction and gecko inspired grippers whereas actuation and stiffness switching grippers usually do not have such challenges.¹⁸ Thus, the adhesion to the rough surfaces was tested for both proposed grippers (Table 2). In **Publication II**, we measured the pull-off forces against surface replicas and for both proposed grippers, we picked rough surfaced real-world objects (such as red grapefruit and a page of the book). The surface roughness did not have major effect on the achieved pull-off forces, but the applied negative pressure had a significant effect. This is promising results considering the practical applications of the gripper: the gripper can adhere on various surfaces.

The picking of small objects was tested for both proposed grippers (Table 2). The smallest picked objects were 30% of the gripper diameter for the pneumatic gripper and 40% for the hydraulic gripper. The other reported suction-based grippers were only tested with objects that were wider than the diameters of the gripper. Small objects can be a challenge for traditional suction grippers because they are sucked inside the gripper without filtering layers. Grasping and stiffness switching based grippers can also have challenges with small objects if there is a big size difference between the gripper and the target object. In addition to limitations with small objects, the large objects can be challenging for the grasping and the stiffness switching grippers since they need to enclose the picked object or at least a part of it to achieve a grasp.^{19,121} The suction and adhesion based grippers do not have such limitations and we showed that our proposed grippers can pick large films and parts.

Unevenly distributed loads can be a challenge for many robotic grippers since these loads produce torques, leading to uneven stress distribution between the gripper and the picked object. In **Publication II**, a glass bottle containing fluid was picked with the proposed 3D printed suction gripper and a traditional suction gripper. The traditional suction gripper failed to maintain the grasp while the 3D printed gripper was successful. We attribute that the soft silicone elastomer film of

the gripper maintains the seal, preventing a small opening for developing a catastrophic loss of vacuum. This result suggests that the gripping planning does not have to be detailed: the picking place or angle does not have to be exact which is beneficial especially in the situations visual inspection is limited.

Picking a wetted object is not a limitation for grasping⁶ or stiffness switching based grippers, but many adhesion based grippers have challenges with wet surfaces. In **Publication III**, the adhesion on watery and oily surfaces was tested for the proposed hydraulic suction gripper. The differences between the achieved pull-off forces were less than 20%, due to the merit of the gripper still working based on the vacuum principle. Thus, the gripper can adhere also on the watery surfaces like other vacuum based grippers.⁹⁵

Another challenge for grippers is the picking of soft and deformable objects.¹⁸ The grasping-based grippers can damage the target objects during the gripping by squeezing the deformable objects. Stiffness switching grippers cannot deform to the target objects after the stiffness switching which can lead the loss of the grasp. The adhesion-based grippers can adapt to the deformations of the target objects, but the soft and deformable objects are still a challenge. In **Publication III**, the adhesion on multiple soft and deformable surfaces was measured, and additionally we picked soft objects in both publications (such as a banana and a mango). The reached pull-off forces decreased with softer samples. However, even with Shore hardness A 30 sample, softness close to skin, the gripper was able to reach 5 N (68% of the maximum force against a smooth glass surface) pull-off force.

The target applications of the proposed suction-based grippers can be in the conveyer belts at the factories, where millions of picking cycles are repeated. Thus, the repeatability of the pneumatic suction gripper was tested in **Publication II**. The gripper was able to pick and release repeatable all the tested samples fifteen times. We conclude that the gripper is not limited to only smooth surfaces and can also release the objects. However, more thorough studies of repeatability are still needed.

The switching possibility of both grippers is important that reliable picking and releasing can be produced. The adhesion switching can be a challenge for adhesion-based grippers due to the sticky finger phenomenon: the object adheres to the gripper due van der Waals and capillary forces. Therefore, light objects were picked with both grippers: the grippers were able to also release light and small objects (80%) of the gripper diameter.

In **Publication III**, two different switching methods were possible: hydraulic and magnetic. The magnetic switching is used to control the stiffness of the gripper and hydraulic the adhesion. We showed that the by adding the stiffness switching to the

grippers, the achieved pull-off forces were significantly higher. This enables soft touch during picking, stiff gripper structure for the transport and controllable release in the end. Compared other stiffness switching grippers, such as granular jamming, the advantage of our gripper is that it is not limited by the size of picked object: the gripper does not have to enclose the object or part of it.

The operation speed is the main limitation to both demonstrated grippers. For the pneumatic one it was ~ 1 s and for the hydraulic gripper ~ 10 s (Table 2). The grasping and the stiffness switching grippers have faster operation speeds (< 0.1 s). However, we do not think the operation speed is a fundamental limitation of the gripper since faster syringe pumps can be used to achieve higher operation speeds. Another limitation to both proposed grippers is the risk of the raptures of the soft silicone elastomer used. The elastomer material is soft and sharp edges can cause raptures to the thin film which can lead to leakages in the gripper. The possible solution can be self-healing materials.

The magnetohydraulic gripper in **Publication III** has limitations because it uses MR fluid. The sedimentation of the MR fluid can clog the gripper. If the gripper is unused for several days, the MR fluid starts to sediment. This failure can be solved by resuspending the iron particles in the oil by applying a strong varying magnetic field or by repeatedly withdrawing the fluid from the cavity. Another limitation is the manually applied magnetic field. It takes a few seconds to place the magnet on top of the gripper which limits the gripper operation speed. The limitation can be solved in the future by using strong electromagnets which can change their state in less than milliseconds.

7.3 Stretchable strain sensors for soft robots

This dissertation explored two different methods for fabricating stretchable strain sensors for soft robots. In **Publication IV**, we showed that screen-printed resistive strain sensors are suitable for measuring the curvature of the pneumatic actuator. In **Manuscript V**, soft pneumatic strain sensors were fabricated and their suitability for curvature sensing in soft grippers as well as their ultra-stretchable nature were demonstrated.

The stretchability of the strain sensors is one of the crucial factors when their suitability for soft robots is considered. The soft pneumatic strain sensor demonstrated in **Manuscript V** could be used with extreme strains, up to at least 300%. The failure was observed at $\sim 500\%$ engineering strain. According to the

datasheet of the strain sensor elastomer, it breaks at 980%. However, this value is for bulk material and the cracks usually initiate from the microstructures in the elastomer which explains the lower reached strain values in the study. These kinds of microstructures exist also in the pneumatic logic⁴ and actuators¹⁵ so their stretchability would be the same than the proposed pneumatic strain sensors. The maximum strains of the previously reported electric strain sensors varied greatly, from 2% up to 1400%.¹⁰⁵ The reached 300% strain compares quite favourably to the hyper-elastic electric strain sensors.

In case the strain sensors are used for measuring the bending of the soft actuator, the changes in the strains are small. The strain sensors proposed in **Publication IV** were only tested in bending ($\sim 2\%$ strain). Suikkola et al.¹³³ have reported earlier that half of the 30 samples of similar resistive sensors withstood a single 74% strain but the strains reached with printed resistive strain sensors are still significantly lower than with pneumatic ones.

Especially when measuring small strains, the sensitivity of the sensor is in an important role. The sensitivity of the silver-based screen-printed sensor was $0.075 \Omega/m^{-1}$ and $GF \approx 5.759$, whereas GF of the pneumatic strain sensor (**Manuscript V**) was only ~ 1 . Some previously reported resistive strain sensors can reach GF values up to 100,000.¹⁴¹ Hence they can measure small strains accurately. When the strains are extreme ($\sim 300\%$), high GF can lead to the saturation of the output or even break the sensor. Thus, the sensor should be selected according to its target application. However, both our sensors were able to measure the bending of the actuator even the strains were small in bending.

The hysteresis of the sensors is especially important when the sensors are used in cyclic loading: the hysteresis leads to different output reading in loading and unloading. Generally, the resistive based strain sensors have larger hysteresis than capacitive and optical ones (Table 3). The screen-printed resistive sensors in **Publication IV** had quite hysteric behaviour: 17% for the silver-based, and 27% for the carbon-based sensor. These values are consistent with the previous reports of the hysteric behaviour of the printed inks.¹⁴² The pneumatic strain sensors demonstrated in **Manuscript V** did not show any hysteresis within the limit of its noise level. Thus, the pneumatic strain sensors have more potential in the dynamic soft robot applications, such as rehabilitation devices.

In soft robots, the strain sensors are potentially also used for long periods, for example in minimally invasive surgery.⁸ The stability in static and dynamic measurements are then crucial performance criteria. In **Publication IV**, the long-term stability or dynamic stability of the sensor were not studied. In the previous

study from Suikkola et al.¹³³ silver-ink based printed circuits were tested in 1000 cyclic loading with 10%, 15% and 20% strains. A significant drift was observed in the output: the normalized resistances increased 2.5, 4.3 and 5.3 times to initial their values with 10%, 15% and 20% strains, respectively. These results are in line with the previous reports of the electric strain sensors: resistive sensors often suffer from the drift. The pneumatic strain sensors in **Manuscript V** show minor drift (DE = 6.3%) during the 12-hour measurement and only minor variations between cycles. The previously reported pressure chamber strain sensors are prone to drift in long-term measurements since the air slowly diffuses from the structure.^{115–117}

Over-shooting behaviour is typical for resistive and capacitive type strain sensors, but the resistive type strain sensors have typically larger over-shooting behaviour. In the experiments with the three-fingered gripper in **Publication IV**, over-shooting after strain relaxation was not observed in the resistance, on the contrary, we observed slow creep in the output which is typical for elastomer based sensors.¹⁴³ The demonstrated pneumatic strain sensor did not show significant over shooting after 12-hour static 50% straining, so it also has potential in long term measurements.

Both sensors proposed in this thesis have their own limitations. The resistive strain sensors suffered from a high hysteresis and a creep. Moreover, the maximum demonstrated strains in **Publication IV** were only ~2% which is a limitation in soft robotic applications. The printed sensors were integrated into a pneumatic soft actuator on top of the neutral plane by gluing them. We noticed that in some cases the sensor delaminated from the actuator after multiple loadings which often happens in case of heterogeneous materials. The other possible failure point in our resistive sensors is the connection between the sensor and the wires. The wires were attached by using silver paint. To minimize the risk of delamination we placed the wire connection inside the pneumatic actuator. However, the connection between the wires and the sensors was the weakest point of the sensor. After multiple loading cycles, some sensors were found malfunctioning due to disconnected wires.

The demonstrated pneumatic strain sensor in **Manuscript V** did not have delamination limitations since the whole sensor actuator system was made of the same material. The inlets for the pneumatic channels were sealed with silicone glue and in some cases, leakages occurred which is a known limitation in pneumatic systems. If the strain sensor channels run too close to the robot surface, the channels can be blocked by external force. In this case, the sensor would act also as a tactile sensor and the strain measurement can be disturbed. This limitation can be solved by placing the channels deep in the soft robot structure.

The fluid used in the strain sensors was pressurized air. The usage of liquids can be desirable in some applications, such as underwater robotics as they use the liquids for their actuators and power. Liquids are also incompressible which would simplify the theoretical analyses. However, the usage of the pneumatics is attractive for land based soft robots since the availability of air in abundance and pneumatic power can be generated from chemical reactions.

Finally, both the resistive and the pneumatic strain sensors were used in soft pneumatic grippers for posture sensing. In **Publication IV**, the three-fingered pneumatic gripper with independent sensors and fingers was demonstrated, whereas in **Manuscript V**, three fingers had common pneumatic source, thus they were actuated in unison. In **Publication IV**, we showed that the fingers can be independently actuated and that the sensors are mostly independent. The sensors in the gripper in **Manuscript V** were suitable for inferring information about the shape of the picked object. The results are comparable to results in Homberg et al.¹²¹ where the experiment was done with electrical sensors. Thus, the pneumatic sensors can potentially replace the electrical sensors in practical soft robot applications.

7.4 Future of all-pneumatic soft robots

As discussed in Chapter 2, four key components of the robots are the actuators, the logic circuit, the power source, and the sensors. In soft robotics, the pneumatic actuation is one of the most used methods as the pneumatic actuators are capable of high grasping forces and operation speeds. This has inspired researchers to use the pneumatics also for the logic components of the soft robots such as pneumatic soft ring oscillators.^{4,13} In the future, all the needed logic components such as transistors and multiplexers should be researched and developed.

To power the soft pneumatic robots, an external pneumatic power source and connecting cables have been needed. This has limited the practical applications since it increases the size and weight of the robot. As a replacement for the pneumatic cables and fixed pressure power sources, untethered solutions have been proposed such as portable gas tanks⁴ and combustion.¹⁷ However, these power units are not entirely soft and they compromise the compliance of the soft robot. In the future, fully soft untethered pneumatic power units, such as combustion²⁶ should be further studied.

The soft pneumatic strain sensors demonstrated in this thesis are the fourth key component for all pneumatic, electronics free soft robots. Even though the strain

sensors were simple to fabricate since the used techniques (soft lithography and 3D printing) are well-known, the manufacturing included several steps and was time-consuming. In the future, the focus should be in simplifying and scaling up the current fabrication processes to mass manufacturing. The recent developments in 3D printing of soft elastomers and thus the soft robot structure directly at once is promising.¹⁴ In addition to scaling the fabrication process, the focus should be in the integration of the all the pneumatic robot components together.

The all pneumatic, electronics free soft robots can have future applications in the situations electronics cannot be used, for example in medical magnetic resonance imaging, inflammable environments and in strong radiation that can destroy electronics.

8 CONCLUSIONS

The main aim of this thesis was to develop fabrication methods for grippers and sensors used in soft robots. Together with the proposed three alternative techniques for fabrication, we successfully implemented switchable adhesion into soft grippers and integrated two different sensors into soft robots. Based on the results shown in this thesis the following conclusion can be drawn:

1. Three different fabrication methods were successfully used in different soft robot component manufacturing.
 - Sacrificial 3D printing is a suitable method of fabricating moulds including complex structures e.g., overhangs and buried channels for soft devices.
 - Multiple different gripper designs can be fabricated fast by 3D printing the soft gripper bodies by using either DLS or SLA printing. 3D printing enables to fast and easily modify the design to achieve the best design.
 - Soft highly stretchable strain sensors can be made by using the same traditional elastomer casting techniques and materials that are often used in soft body fabrication. This simplifies the overall soft robot manufacturing by reducing the needed fabrication steps and materials.
2. Switchable adhesion was successfully implemented into soft suction grippers.
 - 3D printed soft pneumatic suction-based grippers enable switchable adhesion together with high pull-off forces.

- By using magnetorheological fluid as medium in a soft hydraulic suction gripper, in addition to adhesion switching, the stiffness of the gripper can be switched magnetically.
3. Strain sensors were successfully integrated into soft pneumatic grippers to provide information about the gripper posture.
- Screen-printing is a suitable method of mass manufacturing curvature sensors for soft pneumatic actuators. They were successfully used in a three-fingered soft gripper to provide information about the finger posture.
 - Microchannels in soft silicone elastomer can be used as pneumatic strain sensors. By shifting from electric sensing to pneumatic one, the overall complexity of the pneumatic robot reduces since the actuation and sensing are both done pneumatically. The pneumatic strain sensors were also successfully demonstrated in a three-fingered soft gripper in which they could infer the information about the size of the picked object.

REFERENCES

- 1 Särkikoski T. Kaikki Itsestään-Automaatin jäljillä. In: Särkikoski T, Turja T, Parviainen J (eds). *Robotin Hoiviin?* Vastapaino: Tampere, Finland, 2020, pp 25–70.
- 2 Yang M, Cooper LP, Liu N, Wang X, Fok MP. Twining plant inspired pneumatic soft robotic spiral gripper with high-birefringence fiber optic sensor. *Opt Express* 2020; **28**: 35158–35167.
- 3 Sadeghi A, Mondini A, Del Dottore E, Mattoli V, Beccai L, Taccola S *et al.* A plant-inspired robot with soft differential bending capabilities. *Bioinspir Biomim* 2017; **12**: 015001.
- 4 Drotman D, Jadhav S, Sharp D, Chan C, Tolley MT. Electronics-free pneumatic circuits for controlling soft-legged robots. *Sci Robot* 2021; **6**: eaay2627.
- 5 Shahsavan H, Aghakhani A, Zeng H, Guo Y, Davidson ZS, Priimägi A *et al.* Bioinspired underwater locomotion of light-driven liquid crystal gels. *Proc Natl Acad Sci U S A* 2020; **117**: 5125–5133.
- 6 Mazzolai B, Mondini A, Tramacere F, Riccomi G, Sadeghi A, Giordano G *et al.* Octopus-Inspired Soft Arm with Suction Cups for Enhanced Grasping Tasks in Confined Environments. *Adv Intell Syst* 2019; **1**: 1900041.
- 7 Wani OM, Zeng H, Priimägi A. A light-driven artificial flytrap. *Nat Commun* 2017; **8**: 15546.
- 8 Zhu J, Lyu L, Xu Y, Liang H, Zhang X, Ding H *et al.* Intelligent Soft Surgical Robots for Next-Generation Minimally Invasive Surgery. *Adv Intell Syst* 2021; **3**: 2100011.
- 9 Rus D, Tolley MT. Design, fabrication and control of soft robots. *Nature* 2015; **521**: 467–475.
- 10 Larson C, Peele B, Li S, Robinson S, Totaro M, Beccai L *et al.* Highly stretchable electroluminescent skin for optical signaling and tactile sensing. *Science* 2016; **351**: 1071–1074.
- 11 Thuruthel TG, Shih B, Laschi C, Tolley MT. Soft robot perception using embedded soft sensors and recurrent neural networks. *Sci Robot* 2019; **4**: eaav1488.
- 12 Ilievski F, Mazzeo AD, Shepherd RF, Chen X, Whitesides GM. Soft Robotics for Chemists. *Angew Chemie - Int Ed* 2011; **50**: 1890–1895.
- 13 Preston DJ, Jiang HJ, Sanchez V, Rothemund P, Rawson J, Nemitz MP *et al.* A soft ring oscillator. *Sci Robot* 2019; **4**: eaaw5496.
- 14 Hubbard JD, Acevedo R, Edwards KM, Alsharhan AT, Wen Z, Landry J *et al.* Fully 3D-printed soft robots with integrated fluidic circuitry. *Sci Adv* 2021; **7**: eabe5257.
- 15 Shepherd RF, Ilievski F, Choi W, Morin SA, Stokes AA, Mazzeo AD *et al.* Multigait soft robot. *Proc Natl Acad Sci U S A* 2011; **108**: 20400–20403.
- 16 Mosadegh B, Polygerinos P, Keplinger C, Wennstedt S, Shepherd RF, Gupta U *et al.* Pneumatic Networks for Soft Robotics that Actuate Rapidly. *Adv Funct Mater* 2014; **24**: 2163–2170.
- 17 Bartlett NW, Tolley MT, Overvelde JTB, Weaver JC, Mosadegh B, Bertoldi K *et al.* A 3D-printed, functionally graded soft robot powered by combustion. *Science* 2015; **349**: 161–165.
- 18 Shintake J, Cacucciolo V, Floreano D, Shea H. Soft Robotic Grippers. *Adv Mater* 2018;

- 30: 1707035.
- 19 Amend JR, Brown E, Rodenberg N, Jaeger HM, Lipson H. A Positive Pressure Universal Gripper Based on the Jamming of Granular Material. *IEEE Trans Robot* 2012; **28**: 341–350.
- 20 Song S, Drotlef D-M, Son D, Koivikko A, Sitti M. Adaptive Self-Sealing Suction-Based Soft Robotic Gripper. *Adv Sci* 2021; **8**: 2100641.
- 21 Martinez R V., Branch JL, Fish CR, Jin L, Shepherd RF, Nunes RMD *et al.* Robotic Tentacles with Three-Dimensional Mobility Based on Flexible Elastomers. *Adv Mater* 2013; **25**: 205–212.
- 22 Zhou LY, Gao Q, Fu J-Z, Chen Q-Y, Zhu J-P, Sun Y *et al.* Multimaterial 3D Printing of Highly Stretchable Silicone Elastomers. *ACS Appl Mater Interfaces* 2019; **11**: 23573–23583.
- 23 Mishra AK, Wallin TJ, Pan W, Xu P, Wang K, Giannelis EP *et al.* Autonomic perspiration in 3D-printed hydrogel actuators. *Sci Robot* 2020; **5**: eaaz3918.
- 24 Zheng J, Xiao P, Le X, Lu W, Théato P, Ma C *et al.* Mimosa inspired bilayer hydrogel actuator functioning in multi-environments. *J Mater Chem C* 2018; **6**: 1320–1327.
- 25 Argiolas A, Mac Murray BC, Van Meerbeek I, Whitehead J, Sinibaldi E, Mazzolai B *et al.* Sculpting Soft Machines. *Soft Robot* 2016; **3**: 101–108.
- 26 Wehner M, Truby RL, Fitzgerald DJ, Mosadegh B, Whitesides GM, Lewis JA *et al.* An integrated design and fabrication strategy for entirely soft, autonomous robots. *Nature* 2016; **536**: 451–455.
- 27 Xiao Y-Y, Jiang Z-C, Tong X, Zhao Y. Biomimetic Locomotion of Electrically Powered “Janus” Soft Robots Using a Liquid Crystal Polymer. *Adv Mater* 2019; **31**: 1903452.
- 28 Pena-Francesch A, Jung H, Demirel MC, Sitti M. Biosynthetic self-healing materials for soft machines. *Nat Mater* 2020; **19**: 1230–1235.
- 29 Rosato D V., Rosato D V., Rosato M V. 2. Plastic Property. In: Rosato D V., Rosato D V., Rosato M V. (eds). *Plastic Product Material and Process Selection Handbook*. Elsevier, 2004, pp 40–129.
- 30 Le X, Lu W, Zhang J, Chen T. Recent Progress in Biomimetic Anisotropic Hydrogel Actuators. *Adv Sci* 2019; **6**: 1801584.
- 31 Yang C, Suo Z. Hydrogel ionotronics. *Nat Rev Mater* 2018; **3**: 125–142.
- 32 Xu H, Lv Y, Qiu D, Zhou Y, Zeng H, Chu Y. An ultra-stretchable, highly sensitive and biocompatible capacitive strain sensor from an ionic nanocomposite for on-skin monitoring. *Nanoscale* 2019; **11**: 1570–1578.
- 33 Yuk H, Lin S, Ma C, Takaffoli M, Fang NX, Zhao X. Hydraulic hydrogel actuators and robots optically and sonically camouflaged in water. *Nat Commun* 2017; **8**: 14230.
- 34 Xiao Y-Y, Jiang Z-C, Zhao Y. Liquid Crystal Polymer-Based Soft Robots. *Adv Intell Syst* 2020; **2**: 2000148.
- 35 Zhou J, Ellis AV, Voelcker NH. Recent developments in PDMS surface modification for microfluidic devices. *Electrophoresis* 2010; **31**: 2–16.
- 36 Park S, Mondal K, Treadway RM, Kumar V, Ma S, Holbery JD *et al.* Silicones for Stretchable and Durable Soft Devices: Beyond Sylgard-184. *Appl Mater Interfaces* 2018; **10**: 11261–11268.
- 37 Wallin TJ, Pikul J, Shepherd RF. 3D printing of soft robotic systems. *Nat Rev Mater* 2018; **3**: 84–100.
- 38 Patel DK, Sakhaei AH, Layani M, Zhang B, Ge Q, Magdassi S. Highly Stretchable and UV Curable Elastomers for Digital Light Processing Based 3D Printing. *Adv Mater* 2017; **29**: 1606000.
- 39 Rich SI, Wood RJ, Majidi C. Untethered soft robotics. *Nat Electron* 2018; **1**: 102–112.
- 40 Zaidi S, Maselli M, Laschi C, Cianchetti M. Actuation Technologies for Soft Robot Grippers and Manipulators: A Review. *Curr Robot Reports* 2021; **2**: 355–369.

- 41 Onal CD, Rus D. Autonomous undulatory serpentine locomotion utilizing body dynamics of a fluidic soft robot. *Bioinspir Biomim* 2013; **8**: 026003.
- 42 Polygerinos P, Wang Z, Galloway KC, Wood RJ, Walsh CJ. Soft robotic glove for combined assistance and at-home rehabilitation. *Rob Auton Syst* 2015; **73**: 135–143.
- 43 Yeo JC, Yap HK, Xi W, Wang Z, Yeow C-H, Lim CT. Flexible and Stretchable Strain Sensing Actuator for Wearable Soft Robotic Applications. *Adv Mater Technol* 2016; **1**: 1600018.
- 44 Tondu B. Modelling of the McKibben artificial muscle: A review. *J Intell Mater Syst Struct* 2012; **23**: 225–253.
- 45 Wakimoto S, Suzumori K, Kanda T. Development of intelligent McKibben actuator with built-in soft conductive rubber sensor. In: *The 13th International Conference on Solid-State Sensors, Actuators and Microsystems*. IEEE: Seoul, Korea, 2005, pp 745–748.
- 46 Wakimoto S, Suzumori K, Kanda T. Development of Intelligent McKibben Actuator. In: *2005 IEEE/RSJ International Conference on Intelligent Robots and Systems, IROS*. IEEE: Seoul, Korea, 2005, pp 487–492.
- 47 Chou C-P, Hannaford B. Measurement and Modeling of McKibben Pneumatic Artificial Muscles. *IEEE Trans Robot Autom* 1996; **12**: 90–102.
- 48 Thomalla SD, Van De Ven JD. Modeling and Implementation of the McKibben Actuator in Hydraulic Systems. *IEEE Trans Robot* 2018; **34**: 1593–1602.
- 49 Sangian D, Naficy S, Spinks GM, Tondu B. The effect of geometry and material properties on the performance of a small hydraulic McKibben muscle system. *Sensors Actuators A Phys* 2015; **234**: 150–157.
- 50 Tolley MT, Shepherd RF, Mosadegh B, Galloway KC, Wehner M, Karpelson M *et al*. A Resilient, Untethered Soft Robot. *Soft Robot* 2014; **1**: 213–223.
- 51 Katzschmann RK, Marchese AD, Rus D. Hydraulic Autonomous Soft Robotic Fish for 3D Swimming. In: Hsieh M, Khatib O, Kumar V (eds). *Experimental Robotics*. Springer, Cham, 2016, pp 405–420.
- 52 Galloway KC, Polygerinos P, Walsh CJ, Wood RJ. Mechanically Programmable Bend Radius for Fiber-Reinforced Soft Actuators. In: *2013 16th International Conference on Advanced Robotics (ICAR)*. IEEE: Montevideo, Uruguay, 2013, pp 1–6.
- 53 Deimel R, Brock O. A novel type of compliant and underactuated robotic hand for dexterous grasping. *Int J Rob Res* 2016; **35**: 161–185.
- 54 Haihang Wang B, Abu-Dakka FJ, Nguyen Le T, Kyrki V, Xu H. A Novel Soft Robotic Hand Design With Human-Inspired Soft Palm Achieving a Great Diversity of Grasps. *IEEE Robot Autom Mag* 2021; **28**: 37–49.
- 55 Tawk C, Spinks GM, In Het Panhuis M, Alici G. 3D Printable Linear Soft Vacuum Actuators: Their Modeling, Performance Quantification and Application in Soft Robotic Systems. *IEEE/ASME Trans Mechatronics* 2019; **24**: 2118–2129.
- 56 Jain S, Stalin T, Subramaniam V, Agarwal J, Valdivia y Alvarado P. A Soft Gripper with Retractable Nails for Advanced Grasping and Manipulation. In: *Proceedings - IEEE International Conference on Robotics and Automation*. IEEE: Paris, France, 2020, pp 6928–6934.
- 57 Fatahillah M, Oh N, Rodrigue H. A Novel Soft Bending Actuator Using Combined Positive and Negative Pressures. *Front Bioeng Biotechnol* 2020; **8**: 472.
- 58 Elsayes A, Koivikko A, Sariola V. Tactile Electronic Skin Based on Conductive Fabric for Robotic Hand Applications. In: *2019 IEEE SENSORS*. IEEE: Montreal, Canada, 2019, pp 1–4.
- 59 Lee K, Wang Y, Zheng C. TWISTER Hand: Underactuated Robotic Gripper Inspired by Origami Twisted Tower. *IEEE Trans Robot* 2020; **36**: 488–500.
- 60 Tawk C, Gillett A, in het Panhuis M, Spinks GM, Alici G. A 3D-Printed Omni-Purpose

- Soft Gripper. *IEEE Trans Robot* 2019; **35**: 1268–1275.
- 61 Behl M, Kratz K, Zotzmann J, Nöchel U, Lendlein A. Reversible Bidirectional Shape-Memory Polymers. *Adv Mater* 2013; **25**: 4466–4469.
- 62 Simone F, Rizzello G, Seelecke S. Metal muscles and nerves—a self-sensing SMA-actuated hand concept. *Smart Mater Struct* 2017; **26**: 095007.
- 63 Villoslada A, Flores A, Copaci D, Blanco D, Moreno L. High-displacement flexible Shape Memory Alloy actuator for soft wearable robots. *Rob Auton Syst* 2015; **73**: 91–101.
- 64 Kofod G, Wirges W, Paajanen M, Bauer S. Energy minimization for self-organized structure formation and actuation. *Appl Phys Lett* 2007; **90**: 081916.
- 65 Shintake J, Cacucciolo V, Shea H, Floreano D. Soft Biomimetic Fish Robot Made of Dielectric Elastomer Actuators. *Soft Robot* 2018; **5**: 466–474.
- 66 Richardson RC, Levesley MC, Brown MD, Hawkes JA, Watterson K, Walker PG. Control of Ionic Polymer Metal Composites. *IEEE/ASME Trans Mechatronics* 2003; **8**: 245–253.
- 67 Shahinpoor M, Bar-Cohen Y, Simpson JO, Smith J. Ionic Polymer-Metal Composites (IPMCs) as Biomimetic Sensors, Actuators and Artificial Muscles: A Review. *Smart Mater Struct* 1998; **7**: R15.
- 68 Li C, Lau GC, Yuan H, Aggarwal A, Dominguez VL, Liu S *et al*. Fast and programmable locomotion of hydrogel-metal hybrids under light and magnetic fields. *Sci Robot* 2020; **5**: eabb9822.
- 69 Wang L, Jian Y, Le X, Lu W, Ma C, Zhang J *et al*. Actuating and memorizing bilayer hydrogels for a self-deformed shape memory function. *Chem Commun* 2018; **54**: 1229–1232.
- 70 Hines L, Petersen K, Lum GZ, Sitti M. Soft Actuators for Small-Scale Robotics. *Adv Mater* 2017; **29**: 1603483.
- 71 Liu D, Tarakanova A, Hsu CC, Yu M, Zheng S, Yu L *et al*. Spider dragline silk as torsional actuator driven by humidity. *Sci Adv* 2019; **5**: eaau9183.
- 72 McDonald K, Rendos A, Woodman S, Brown KA, Ranzani T. Magnetorheological Fluid-Based Flow Control for Soft Robots. *Adv Intell Syst* 2020; **2**: 2000139.
- 73 Paek J, Cho I, Kim J. Microrobotic tentacles with spiral bending capability based on shape-engineered elastomeric microtubes. *Sci Rep* 2015; **5**: 10768.
- 74 Suzumori K, Iikura S, Tanaka H. Applying a Flexible Microactuator to Robotic Mechanisms. *IEEE Control Syst Mag* 1992; **12**: 21–27.
- 75 Tawk C, Gao Y, Mutlu R, Alici G. Fully 3D Printed Monolithic Soft Gripper with High Conformal Grasping Capability. In: *Proceedings of the 2019 IEEE/ASME International Conference on Advanced Intelligent Mechatronics*. IEEE: Hong Kong, China, 2019, pp 1139–1144.
- 76 Firouzeh A, Paik J. Grasp Mode and Compliance Control of an Underactuated Origami Gripper Using Adjustable Stiffness Joints. *IEEE/ASME Trans Mechatronics* 2017; **22**: 2165–2173.
- 77 Shintake J, Schubert B, Rosset S, Shea H, Floreano D. Variable Stiffness Actuator for Soft Robotics Using Dielectric Elastomer and Low-Melting-Point Alloy. In: *2015 IEEE/RJSJ International Conference on Intelligent Robots and Systems (IROS)*. IEEE: Hamburg, Germany, 2015, pp 1097–1102.
- 78 Nishida T, Okatani Y, Tadakuma K. Development of Universal Robot Gripper Using MR α Fluid. *Int J Humanoid Robot* 2016; **13**: 1650017.
- 79 Brown E, Rodenberg N, Amend J, Mozeika A, Steltz E, Zakin MR *et al*. Universal robotic gripper based on the jamming of granular material. *Proc Natl Acad Sci U S A* 2010; **107**: 18809–18814.
- 80 Amend J, Cheng N, Fakhouri S, Culley B. Soft Robotics Commercialization: Jamming

- Grippers from Research to Product. *Soft Robot* 2016; **3**: 213–222.
- 81 Hao Y, Wang T, Fang X, Yang K, Mao L, Guan J *et al.* A Variable Stiffness Soft Robotic Gripper with Low-Melting-Point Alloy. In: *Proceedings of the 36th Chinese Control Conference*. IEEE: Dalian, China, 2017, pp 6781–6786.
- 82 de Vicente J, Klingenberg J, Hidalgo-Ivarez R. Magnetorheological fluids : a review. *Soft Matter* 2011; **7**: 3701–3710.
- 83 Pettersson A, Davis S, Gray JO, Dodd TJ, Ohlsson T. Design of a magnetorheological robot gripper for handling of delicate food products with varying shapes. *J Food Eng* 2010; **98**: 332–338.
- 84 Kenaley GL, Cutkosky MR. Electrorheological Fluid-Based Robotic Fingers with Tactile Sensing. In: *Proceedings, 1989 International Conference on Robotics and Automation*. IEEE: Scottsdale, AZ, USA, 1989, pp 132–136.
- 85 Huber G, Mantz H, Spolenak R, Mecke K, Jacobs K, Gorb SN *et al.* Evidence for capillarity contributions to gecko adhesion from single spatula nanomechanical measurements. *Proc Natl Acad Sci* 2005; **102**: 16293–16296.
- 86 Song S, Drotlef D-M, Majidi C, Sitti M. Controllable load sharing for soft adhesive interfaces on three-dimensional surfaces. *Proc Natl Acad Sci U S A* 2017; **114**: E4344–E4353.
- 87 Hawkes EW, Christensen DL, Han AK, Jiang H, Cutkosky MR. Grasping without Squeezing: Shear Adhesion Gripper with Fibrillar Thin Film. In: *2015 IEEE International Conference on Robotics and Automation (ICRA)*. IEEE: Seattle, WA, USA, 2015, pp 2305–2312.
- 88 Song S, Drotlef D-M, Paik J, Majidi C, Sitti M. Mechanics of a pressure-controlled adhesive membrane for soft robotic gripping on curved surfaces. *Extrem Mech Lett* 2019; **30**: 100485.
- 89 Ruffatto D, Parness A, Spenko M. Improving controllable adhesion on both rough and smooth surfaces with a hybrid electrostatic/gecko-like adhesive. *J R Soc Interface* 2014; **11**: 20131089.
- 90 Shintake J, Rosset S, Schubert B, Floreano D, Shea H. Versatile Soft Grippers with Intrinsic Electroadhesion Based on Multifunctional Polymer Actuators. *Adv Mater* 2016; **28**: 231–238.
- 91 Guo J, Xiang C, Rossiter J. A soft and shape-adaptive electroadhesive composite gripper with proprioceptive and exteroceptive capabilities. *Mater Des* 2018; **156**: 586–587.
- 92 Iwasaki H, Lefevre F, Damian DD, Iwase E, Miyashita S. Autonomous and Reversible Adhesion Using Elastomeric Suction Cups for In-Vivo Medical Treatments. *IEEE Robot Autom Lett* 2020; **5**: 2015–2022.
- 93 Horie T, Sawano S, Konishi S. Micro Switchable Sucker for Fixable and Mobile Mechanism of Medical MEMS. In: *2007 IEEE 20th International Conference on Micro Electro Mechanical Systems (MEMS)*. IEEE: Kobe, Japan, 2007, pp 691–694.
- 94 Takahashi T, Suzuki M, Aoyagi S. Octopus Bioinspired Vacuum Gripper with Micro Bumps. In: *2016 IEEE 11th Annual International Conference on Nano/Micro Engineered and Molecular Systems (NEMS)*. IEEE: Sendai, Japan, 2016, pp 508–511.
- 95 Takahashi T, Kikuchi S, Suzuki M, Aoyagi S. Vacuum gripper imitated octopus sucker-effect of liquid membrane for absorption-. In: *2015 IEEE/RSJ International Conference on Intelligent Robots and Systems (IROS)*. IEEE: Hamburg, Germany, 2015, pp 2929–2936.
- 96 Hartzell CM, Choi YT, Wereley NM, Leps TJG. Performance of a Magnetorheological Fluid-Based Robotic End Effector. *Smart Mater Struct* 2019; **28**: 035030.
- 97 Schmalz. Bell suction cup (round) SPB4 20 SI-55 G1/8-AG Datasheet. ; : 1–3.
- 98 Mikkonen R, Puustola P, Jönkkäri I, Mäntysalo M. Inkjet Printable Polydimethylsiloxane for All-Inkjet-Printed Multilayered Soft Electrical Applications. *ACS Appl Mater Interfaces*

- 2020; **12**: 11990–11997.
- 99 Mengüç Y, Park Y-L, Pei H, Vogt D, Aubin PM, Winchell E *et al.* Wearable soft sensing suit for human gait measurement. *Int J Rob Res* 2014; **33**: 1748–1764.
- 100 Agaoglu S, Diep P, Martini M, KT S, Baday M, Araci IE. Ultra-sensitive microfluidic wearable strain sensor for intraocular pressure monitoring. *Lab Chip* 2018; **18**: 3471–3483.
- 101 Mikkonen R, Koivikko A, Vuorinen T, Sariola V, Mäntysalo M. Inkjet-printed, nanofiber-based soft capacitive pressure sensors for tactile sensing. *IEEE Sens J* 2021; **21**: 1–9.
- 102 Kenry, Yeo JC, Lim CT. Emerging flexible and wearable physical sensing platforms for healthcare and biomedical applications. *Microsystems Nanoeng* 2016; **2**: 16043.
- 103 Guo J, Zhou B, Zong R, Pan L, Li X, Yu X *et al.* Stretchable and Highly Sensitive Optical Strain Sensors for Human-Activity Monitoring and Healthcare. *ACS Appl Mater Interfaces* 2019; **11**: 33589–33598.
- 104 Elsayes A, Sharma V, Yiannacou K, Koivikko A, Rasheed A, Sariola V. Plant-Based Biodegradable Capacitive Tactile Pressure Sensor Using Flexible and Transparent Leaf Skeletons as Electrodes and Flower Petal as Dielectric Layer. *Adv Sustain Syst* 2020; **4**: 2000056.
- 105 Souri H, Banerjee H, Jusufi A, Radacsi N, Stokes AA, Park I *et al.* Wearable and Stretchable Strain Sensors: Materials, Sensing Mechanisms, and Applications. *Adv Intell Syst* 2020; **2**: 2000039.
- 106 Keil S. Historical review. In: *Technology and Practical Use of Strain Gages With Particular Consideration of Stress Analysis Using Strain Gages*. Wilhelm Ernst & Sohn: Berlin, Germany, 2017, pp 1–16.
- 107 Zhao H, O'Brien K, Li S, Shepherd RF. Optoelectronically innervated soft prosthetic hand via stretchable optical waveguides. *Sci Robot* 2016; **1**: eaai7529.
- 108 Amjadi M, Pichitpajongkit A, Lee S, Ryu S, Park I. Highly Stretchable and Sensitive Strain Sensor Based on Silver-Elastomer Nanocomposite. *ACS Nano* 2014; **8**: 5154–5163.
- 109 Pinto T, Cai L, Wang C, Tan X. CNT-based sensor arrays for local strain measurements in soft pneumatic actuators. *Int J Intell Robot Appl* 2017; **1**: 157–166.
- 110 White EL, Case JC, Kramer RK. Multi-mode strain and curvature sensors for soft robotic applications. *Sensors Actuators A Phys* 2017; **253**: 188–197.
- 111 Amjadi M, Kyung K-U, Park I, Sitti M. Stretchable, Skin-Mountable, and Wearable Strain Sensors and Their Potential Applications: A Review. *Adv Funct Mater* 2016; **26**: 1678–1698.
- 112 Sareh S, Noh Y, Li M, Ranzani T, Liu H, Althoefer K. Macrobend optical sensing for pose measurement in soft robot arms. *Smart Mater Struct* 2015; **24**: 125024.
- 113 Dagdeviren C, Joe P, Tuzman OL, Park K-I, Lee KJ, Shi Y *et al.* Recent progress in flexible and stretchable piezoelectric devices for mechanical energy harvesting, sensing and actuation. *Extrem Mech Lett* 2016; **9**: 269–281.
- 114 Xiong J, Lee PS. Progress on wearable triboelectric nanogenerators in shapes of fiber, yarn, and textile. *Sci Technol Adv Mater* 2019; **20**: 837–857.
- 115 Yang H, Chen Y, Sun Y, Hao L. A novel pneumatic soft sensor for measuring contact force and curvature of a soft gripper. *Sensors Actuators A Phys* 2017; **266**: 318–327.
- 116 Choi H, Kong K. A Soft Three-Axis Force Sensor Based on Radially Symmetric Pneumatic Chambers. *IEEE Sens J* 2019; **19**: 5229–5238.
- 117 Tawk C, in het Panhuis M, Spinks GM, Alici G. Soft Pneumatic Sensing Chambers for Generic and Interactive Human–Machine Interfaces. *Adv Intell Syst* 2019; **1**: 1900002.
- 118 Kusuda S, Sawano S, Konishi S. Fluid-resistive bending sensor having perfect compatibility with flexible pneumatic balloon actuator. In: *2007 IEEE 20th International*

- Conference on Micro Electro Mechanical Systems (MEMS)*. IEEE: Kobe, Japan, 2007, pp 615–618.
- 119 Gerboni G, Diodato A, Ciuti G, Cianchetti M, Menciassi A. Feedback control of soft robot actuators via commercial flex bend sensors. *IEEE/ASME Trans Mechatronics* 2017; **22**: 1881–1888.
- 120 Elgeneidy K, Lohse N, Jackson M. Bending angle prediction and control of soft pneumatic actuators with embedded flex sensors – A data-driven approach. *Mechatronics* 2018; **50**: 234–247.
- 121 Homberg BS, Katzschmann RK, Dogar MR, Rus D. Robust proprioceptive grasping with a soft robot hand. *Auton Robots* 2019; **43**: 681–696.
- 122 Kim DH, Lee SW, Park H-S. Sensor evaluation for soft robotic hand rehabilitation devices. In: *2016 6th IEEE International Conference on Biomedical Robotics and Biomechatronics (BioRob)*. IEEE: Singapore, 2016, pp 1220–1223.
- 123 Hamaguchi S, Kawasetsu T, Horii T, Ishihara H, Niyama R, Hosoda K *et al*. Soft Inductive Tactile Sensor Using Flow-Channel Enclosing Liquid Metal. *IEEE Robot Autom Lett* 2020; **5**: 4028–4034.
- 124 Park M, Jeong B, Park Y-L. Hybrid System Analysis and Control of a Soft Robotic Gripper with Embedded Proprioceptive Sensing for Enhanced Gripping Performance. *Adv Intell Syst* 2021; **3**: 2000061.
- 125 Lin Y-H, Siddall R, Schwab F, Fukushima T, Banerjee H, Baek Y *et al*. Modeling and Control of a Soft Robotic Fish with Integrated Soft Sensing. *Adv Intell Syst* 2021; **Preprint**: 2000244.
- 126 Wang S, Sun Z, Zhao Y, Zuo L. A highly stretchable hydrogel sensor for soft robot multi-modal perception. *Sensors Actuators A Phys* 2021; **331**: 113006.
- 127 Ozel S, Keskin NA, Khea D, Onal CD. A precise embedded curvature sensor module for soft-bodied robots. *Sensors Actuators A Phys* 2015; **236**: 349–356.
- 128 Wang C, Xia K, Wang H, Liang X, Yin Z, Zhang Y. Advanced Carbon for Flexible and Wearable Electronics. *Adv Mater* 2019; **31**: 1801072.
- 129 Nankali M, Nouri NM, Navidbakhsh M, Malek NG, Amindehghan MA, Shahtoori AM *et al*. Highly stretchable and sensitive strain sensors based on carbon nanotube-elastomer nanocomposites: the effect of environmental factors on strain sensing performance. *J Mater Chem C* 2020; **8**: 6185–6195.
- 130 Nur R, Matsuhisa N, Jiang Z, Nayeem OMG, Yokota T, Someya T. A Highly Sensitive Capacitive-type Strain Sensor Using Wrinkled Ultrathin Gold Films. *Nano Lett* 2018; **18**: 5610–5617.
- 131 Park Y-L, Wood RJ. Smart Pneumatic Artificial Muscle Actuator with Embedded Microfluidic Sensing. In: *SENSORS, 2013*. IEEE: Baltimore, MD, USA, 2013, pp 1–4.
- 132 Majidi C, Kramer R, Wood RJ. A non-differential elastomer curvature sensor for softer-than-skin electronics. *Smart Mater Struct* 2011; **20**: 105017.
- 133 Suikkola J, Björninen T, Mosallaei M, Kankkunen T, Iso-Ketola P, Ukkonen L *et al*. Screen-Printing Fabrication and Characterization of Stretchable Electronics. *Sci Rep* 2016; **6**: 25784.
- 134 Majidi C. Soft Robotics: A Perspective—Current Trends and Prospects for the Future. *Soft Robot* 2014; **1**: 5–11.
- 135 Qi HJ, Joyce K, Boyce MC. Durometer hardness and the stress-strain behavior of elastomeric materials. *Rubber Chem Technol* 2003; **76**: 419–435.
- 136 Larson K. Can You Estimate Modulus From Durometer Hardness for Silicones ? 2017.
- 137 Gent AN. On the Relation between Indentation Hardness and Young’s Modulus. *Rubber Chem Technol* 1958; **31**: 896–906.
- 138 Holland DP, Park EJ, Polygerinos P, Bennett GJ, Walsh CJ. The Soft Robotics Toolkit:

- Shared Resources for Research and Design. *Soft Robot* 2014; **1**: 224–230.
- 139 Koivikko A, Raei ES, Sariola V, Mosallaei M, Mäntysalo M. Soft actuators with screen-printed curvature sensors. In: *2017 IEEE SENSORS*. Glasgow, United Kingdom, 2017, pp 1–3.
- 140 Saggiomo V, Velders AH. Simple 3D Printed Scaffold-Removal Method for the Fabrication of Intricate Microfluidic Devices. *Adv Sci* 2015; **2**: 1500125.
- 141 Sourì H, Bhattacharyya D. Highly sensitive, stretchable and wearable strain sensors using fragmented conductive cotton fabric. *J Mater Chem C* 2018; **6**: 10524–10531.
- 142 Merilampi S, Björninen T, Haukka V, Ruuskanen P, Ukkonen L, Sydänheimo L. Analysis of electrically conductive silver ink on stretchable substrates under tensile load. *Microelectron Reliab* 2010; **50**: 2001–2011.
- 143 Phan K Le. Methods to correct for creep in elastomer-based sensors. In: *2008 SENSORS*. IEEE: Lecce, Italy, 2008, pp 1119–1122.

PUBLICATIONS

PUBLICATION

I

Fabrication of Soft Devices with Buried Fluid Channels by Using Sacrificial 3D Printed Molds

Anastasia Koivikko and Veikko Sariola

In Proceeding of 2019 2nd IEEE International Conference on Soft Robotics, 509-513
10.1109/ROBOSOFT.2019.8722741

Publication reprinted with the permission of the copyright holders.

Fabrication of Soft Devices with Buried Fluid Channels by Using Sacrificial 3D Printed Molds

Anastasia Koivikko and Veikko Sariola, *Member, IEEE*

Abstract— Casting silicone elastomers into 3D printed molds has seen a surge of applications in soft robots, soft manipulators, microfluidics, wearable technologies and stretchable sensors. In such devices, buried fluid channels are used to transport fluids, as fluidic actuators and as sensors with liquid metal. However, it is difficult to demold structures with buried channels and overhangs. As a solution, using sacrificial molds made of dissolvable materials has been proposed. In this paper, we evaluate different commercially available 3D printing materials as dissolvable mold materials. We tested dissolving prints made of high-impact polystyrene (HIPS), acrylonitrile butadiene styrene (ABS), polyvinyl butyral (PVB) and polyvinyl alcohol (PVA) in limonene, acetone, isopropanol/ethanol and water, respectively. We further studied the effect of magnetic stirring and ultrasonic bath on the dissolution times. Finally, we fabricated buried channels using different mold materials and silicone elastomers. The results show that at least ABS, PVB and PVA can be used as mold materials. In particular, PVA is a promising material as it is soluble in water. The studied method simplifies the fabrication of soft devices, allowing the fabrication of overhangs and buried channels in a single casting step.

I. INTRODUCTION

In past decades, rigid devices, such as manipulators and mobile robots, have served the needs of manufacturing industry well. Recently, new fabrication methods and materials have introduced soft devices to the world. These soft devices, composed of compliant materials, have found a number of new application areas beyond manufacturing, including soft manipulators [1], [2], wearable sensors [3], different bio-inspired robots [4], [5] and robots for challenging environments [6].

Conventional production methods used in the fabrication of rigid devices are often not directly applicable to soft materials. Therefore, old fabrication methods have been re-invented or adapted for new purposes: casting elastomers into 3D printed molds [6]–[8], 3D printing of soft materials [7] or sculpting [9]. All these manufacturing processes have their advantages, such as the sculpting and 3D printing methods are moldless, but producing structures with accurate dimensions and designs is challenging. By contrast, casting elastomers into hard molds can replicate the mold features down to nanometer accuracy [10]. Casting has a drawback of needing multipart or articulated molds when more complex designs are required [11], [12]. In particular, it is challenging to cast objects with overhangs and buried channels. For instance in our previous

work [13], we used PneuNet actuators [14] which need three different molds to fabricate two different parts, which are bonded in a post assembly process.

Consider the 3D printed mold in Fig. 1a. It is impossible to demold elastomer from this mold without breaking either the mold or the part, because the part design has a buried channel with a wider chamber in the middle. The traditional way to make such a channel is by casting two different pieces and then assembling and bonding them afterwards, which makes the whole process more complicated and time consuming. Adhesives bonds can also fail or leak.

One way to remove the mold material from the buried channel is by using sacrificial mold materials. Recently, many different sacrificial materials for filament-fusion 3D printers have been introduced on the market. Their intended use is to serve as support structures during 3D printing, to be removed after the print. The removal is by dissolving the material in solvent. Such materials could also be used as sacrificial mold materials in elastomer casting.

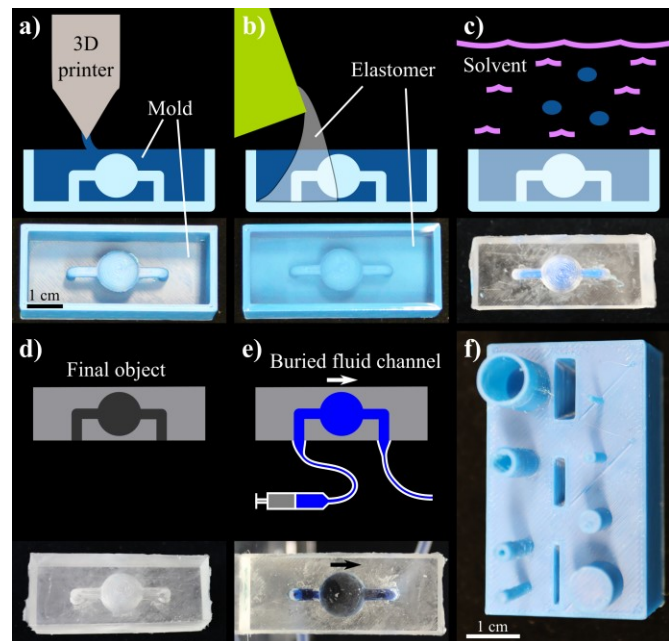


Figure 1. Fabrication process for sacrificial mold manufacturing. In fig. 1a, a sacrificial part is 3D printed, b) silicone elastomer is cast into the 3D printed mold, c) Sacrificial mold is dissolved in solvent, d) Final soft object with buried channel, e) Soft silicone device filled with dyed water and f) A photograph of a 3D printed test object. This object design was used in the dissolving experiments. a-e) have the same scale bar.

Research supported by the Academy of Finland (#299087, #306999).

A. Koivikko (e-mail: anastasia.koivikko@tuni.fi) and V. Sariola (phone: +358503625732, e-mail: veikko.sariola@tuni.fi) are with the Faculty of Medicine and Health Technology, Tampere University, Tampere, 33200 Finland.

Sacrificial 3D printed molds have been used in fabrication of scaffolds in tissue engineering, where polydimethylsiloxane (PDMS) elastomer and hydrogels have been cast into sacrificial polyvinyl alcohol (PVA) [15] and polyethylene glycol (PEG) [16] molds, respectively. Sacrificial 3D printed molds have also been used in the fabrication of complex 3D microfluidic chips, where acrylonitrile butadiene styrene (ABS) [17] and sugar alcohol isomalt [18] have been used as the sacrificial material. Additionally, a microcirculation phantom for visual analysis of hemodynamics has been fabricated by using sacrificial ABS molds in elastomer casting [19].

In this paper, we compare common filament materials as sacrificial mold materials for casting buried channels in silicone elastomers, with the goal of finding mold materials that are easy to print and soluble in benign solvents. Fig. 1 shows the fabrication steps of the studied method. First, the mold, including outer walls and complex inner structures, is 3D printed out of sacrificial material using a fused-filament 3D printer (Fig. 1a). Then, soft silicone elastomer is cast into the mold and cured (Fig. 1b). After curing, the composite object, including dissolvable mold and soft material, is placed in solvent (Fig. 1c). Silicones being resistant to most solvents, the solvent dissolves only the mold, leaving only the silicone with the buried channel (Fig. 1d). Fig. 1e shows that the channel can be filled with liquid.

II. MATERIALS AND METHODS

A. Filament materials

Nine different commercially available 3D printing filament materials were selected for the initial study. Table 1 shows the trade names, manufacturers and main component materials of the filaments, and the solvents used in sacrificial fabrication. Chosen filaments were intended to be used as support structure materials in fused filament fabrication or were used in previous studies in sacrificial manufacturing [15], [17]. The solvents used were chosen based on the solvents suggested by the filament manufacturers or based on previous work. The chosen filaments varied from commonly used ABS to recently presented filaments such as Ethy-Lay. The filaments can be divided in two categories by their printing temperature: high temperature filaments: HIPS, ABS, Lay-Cloud and High-t-Lay, and the lower temperature filaments: PVA, Ethy-Lay, Hydrosupport, PVA and LAYaPVA.

B. 3D printing

Molds and test objects were printed by using a fused filament fabrication 3D printer (Prusa i3 MK2, Prusa Research s.r.o., Czech Republic). The design of the test object is shown in Fig. 1f and was printed from all the different materials in Table 1. The printed test objects had same infill rate and surface pattern parameters in order to get as credible results from the solubility experiments as possible. In other words, the volume percentage occupied by the materials was the same and the surface roughness of objects made of different materials was close to each other.

TABLE I. TESTED 3D PRINTING FILAMENT MATERIALS AND SOLVENTS

Trade name	Manufacturer	Main Material	Solvent
HIPS	Orbi-Tech ¹	High impact polystyrene	Limonene
ABS	miniFactory ²	Acrylonitrile butadiene styrene	Acetone
PVB	Polymaker ³	Polyvinyl butyral	Isopropanol
Ethy-Lay	CC-Products ⁴	Polyvinyl butyral	Ethanol
Hydrosupport	3D-Fuel ⁵	Polyvinyl alcohol	Water
PVA	MatterHackers ⁶	Polyvinyl alcohol	Water
LAYaPVA	CC-Products ⁴	Polyvinyl alcohol	Water
Lay-Cloud	CC-Products ⁴	Undisclosed ⁷	Water
High-t-Lay	CC-Products ⁴	Undisclosed ⁷	Water

1. Orbi-Tech GmbH, Moltkestrasse 25, 42799 Leichlingen, Germany

2. miniFactory Oy LTD, Kampusranta 9 C 60320, Seinäjoki, Finland

3. Polymaker, Suzhou, Jiangsu, China

4. CC-PRODUCTS, Auenweg 173 / Halle 10, 51063 Köln, Germany

5. 3D-Fuel, Units 8/10 Moville Business Park, Glencrow, Moville, Co. Donegal, F93 DF84 Ireland

6. MatterHackers, Lake Forrest, California, USA

7. The exact material component was a trade secret.

C. Solubility experiments

In a preliminary solubility experiment, the 3D printed test objects (Fig. 1f) were placed in covered glass beakers filled with different solvents (Table 1). The beakers were kept in room temperature without stirring and photographed at selected time points for 24 hours. Time required to dissolve the test objects was examined visually.

Based on this first experiment, materials dissolvable within 24 hours were selected for further study. With the selected materials, we tested the effect of magnetic hotplate stirring (VWR, 1200 rpm) and ultrasonic bath (Mechanical Ultrasonic cleaner, VGT-1730QT) on the dissolution times. The total duration of these experiments were 18 and 6 hours, respectively.

D. Silicone casting

Two different silicones were cast into 3D printed molds: Sorta-Clear 18 (Smooth-on, Shore A hardness: 18) and Sylgard 184 (Dow corning, Shore A hardness: 50). Both elastomers were optically clear so that the buried channels could be visualized.

Both elastomers were two-component products, with 1:10 mixing ratio by weight. Their components were mixed in a mixer (Kurabo Mazerustar/KK-300SS) and then poured into the sacrificial molds. After pouring, the elastomers were degassed in a vacuum chamber. Finally, the elastomers were fully cured in room temperature (24 hours for Sorta-Clear 18 and 48 hours for Sylgard 184). Oven curing was not used to avoid any warping of the molds.

E. Removing sacrificial molds

To remove the sacrificial mold, the molds with the cured elastomers were placed in the designated solvent in a glass beaker inside an ultrasonic bath. For each solvent, the chosen

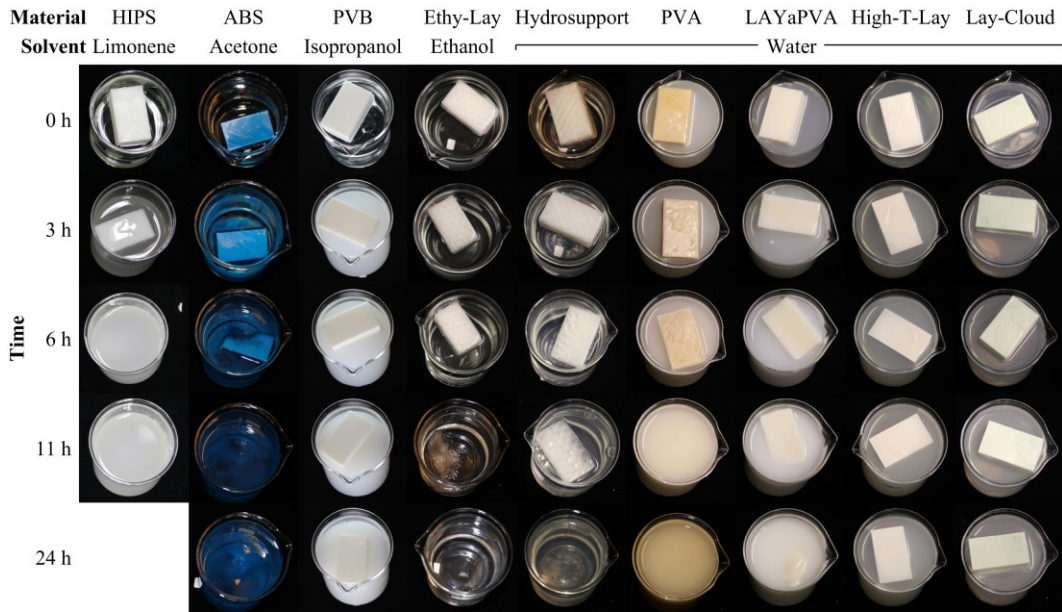


Figure 2. Dissolving different materials in their designed solvents in room temperature. Fig. 1f shows the design of the test object being dissolved. HIPS was fully dissolved already after 6 h.

mold material was the one that was fastest to dissolve in the earlier solubility experiments. The sonication was continued until the outer edges of the mold were fully removed. Finally, the material left in inner channel was cleaned by using a syringe to inject solvent through the channel.

III. RESULTS AND DISCUSSION

A. Dissolving without stirring

Fig. 2 shows the results from the solubility experiment where no stirring was used. The fastest to dissolve was HIPS (~ six hours), followed by ABS and Ethy-Lay (~ 11 hours). Hydrosupport, PVA and LAYaPVA were mostly dissolved in 24 hours. PVB, High-t-Lay and Lay-Cloud had barely

softened in 24 hours despite they being reported to be dissolvable support materials (Lay-Cloud and High-t-Lay) or were known to dissolve in certain solvent (PVB). Therefore, PVB, High-t-Lay and Lay-Cloud were excluded from further studies.

Note that ABS test object was considered as dissolved even if actually the material had only swelled, softened and flown to the bottom of the container. Nevertheless, the acetone was chosen to be the solvent because it was used in previous work [17] and found to be suitable for sacrificial manufacturing.

Other filament materials were known to dissolve in the selected solvents: HIPS in limonene [20], Ethy-Lay (PVB) in the ethanol [21] and PVA in the water [22] and it can be seen in the Fig. 2.

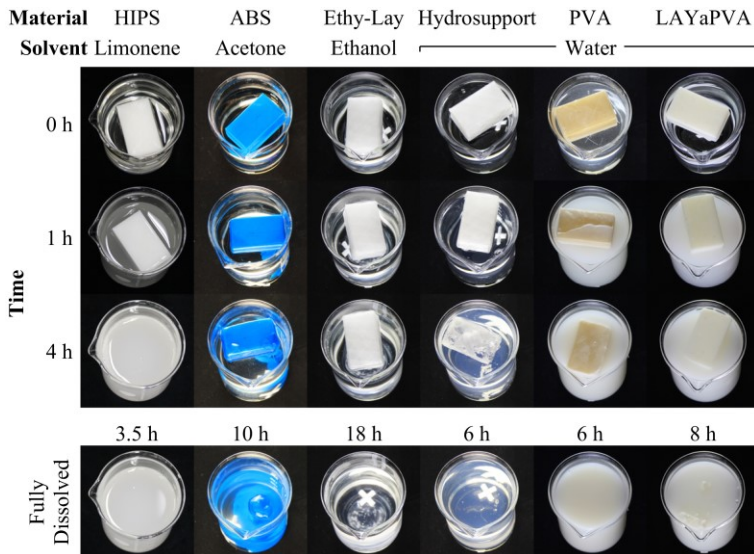


Figure 3. Dissolving with magnetic stirrer. The solvent was stirred (1200 rpm) while test objects were dissolved. Images on the bottom line show the fully dissolved test objects and times required for dissolving.

B. Dissolving with magnetic stirrer

Fig. 3 shows the results from the solubility experiment done with the magnetic stirrer. The fastest filament material to dissolve was HIPS (~3.5 hours). Then followed by Hydrosupport and PVA (~six hours), LAYaPVA (~eight hours), ABS (~ten hours) and Ethy-Lay (~18 hours). The ABS part was only softened and swelled and the stirring movement caused it to center in the middle of the beaker.

Comparing the times required to dissolve test objects in certain solvents with or without stirring, one can see that all the materials dissolved faster in stirred solvents, as expected. Nevertheless, the effect of the stirring to dissolving speed varied between materials. PVA based filament materials (Hydrosupport, PVA and LAYaPVA) dissolved in 24 hours without stirring, but in stirred water, the times required to

dissolve them were under eight hours. In contrast, the time required to dissolve PVB-based Ethy-Lay decreased only from 24 hours to 18 hours.

C. Dissolving in ultrasonic bath

Third solubility experiment was conducted in ultrasonic bath and results are shown in Fig. 4. The fastest material to dissolve was Ethy-Lay (~three hours), followed by HIPS (~four hours), ABS (~4.5 hours), Hydrosupport and PVA (~five hours) and LAYaPVA (~six hours). Excluding HIPS, the times required to dissolve the printed test objects decreased with all the materials when compared to the two previous experiments. For HIPS, the time required dissolving the test object increased by half an hour, so no significant difference was observed in the dissolving time.

In ultrasonic experiment, the times required for dissolving the test objects were more close to each other in contrast to two previous experiments. Specially, the Ethy-Lay, which needed 18 hours for dissolving in previous stirring experiment, needed only three hours in ultrasonic bath. This encourage us to use ultrasonic bath for dissolving the sacrificial molds in the casting experiment.

When considering all three experiments done, HIPS was the fastest material to dissolve. However, the solvent used with HIPS, limonene, is the most hazardous of the solvents tested. Furthermore, HIPS can suffer from warping in the printing process [23]. ABS was dissolved with acetone and Ethy-Lay with ethanol, which are more hazardous compared to water. The dissolving speeds of ABS and Ethy-Lay varied more among the dissolving experiments in contrast to HIPS and PVA filaments. This should be considered when choosing the sacrificial material and the way to dissolve it. One should also consider that HIPS and ABS contain styrene, which is emitted during 3D printing and is potentially carcinogenic. In contrast, PVA is relatively harmless and dissolves with benign water.

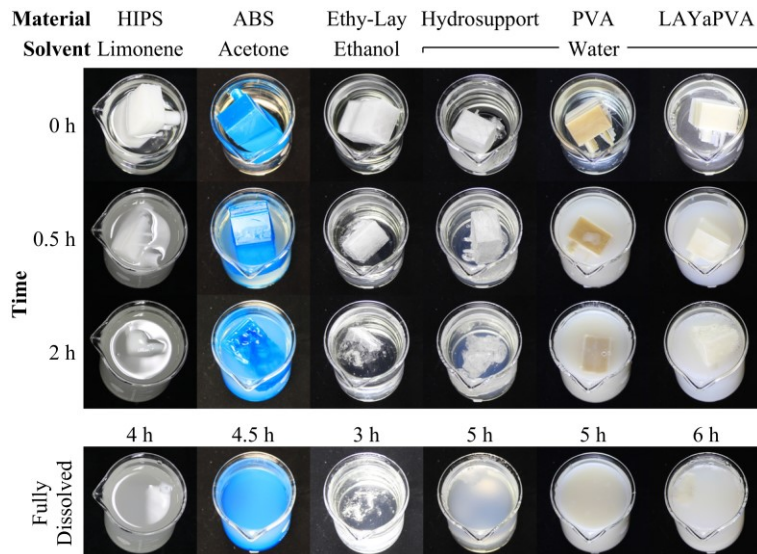


Figure 4. Ultrasound experiment. The object was placed in ultrasound bath during the solubility experiment. On the bottom line, can be seen the fully dissolved test objects and times required for that.

D. Fabrication of buried channels

To show that the sacrificial mold materials can be used to fabricate buried fluidic channels in elastomers, we 3D printed molds (Fig. 1a) out of four different materials and filled them with two different elastomers. Molds made of HIPS, ABS, Ethy-Lay (PVB) and Hydrosupport (PVA) were tested. These materials were soluble in limonene, acetone, ethanol and water, respectively. The two tested elastomers had varying hardness: Sylgard 184 and Sorta-Clear 18 had Shore A hardness of 50 and 18, respectively.

Fig. 5 shows the fabricated channels. The functionality of the fabricated channels structures was studied by filling them by dyed water so one can observe if the channel is open i.e. if there is no mold material left blocking the channel. Video 1 shows a channel buried in PDMS being filled, where ABS was used as the sacrificial mold material.

Fig. 5a shows a functional channel could be fabricated when ABS, Ethy-Lay and Hydrosupport were used as mold materials. Air bubbles can be seen in the channels, which might be caused by the roughness on the surface of the elastomer. The roughness could be avoided by smoothing the surface structures by improving printing quality or by using surface smoothing techniques such as vaporizing or coating [19]. On the other hand, if the structures are used for actuation in pneumatic actuators [14], the surface roughness is not so critical. When comparing the results from the two different elastomers, no big differences could be observed (Fig. 5a).

When HIPS was used as sacrificial mold material, limonene was used as the solvent. Silicones swelled in limonene and shrank while drying, as reported before [24]. In case of Sylgard 184, the shrinking caused the elastomer to crack while drying (Fig. 5b). Sorta-Clear 18 elastomer swelled as well, but the drying did not cause cracking. However, the drying made Sorta-Clear 18 less transparent and turned it yellow, which made it challenging to observe the channel structure visually. For both elastomers, the drying of the limonene took several days. Therefore, HIPS is less suitable as the mold material for the studied fabrication method.

IV. CONCLUSION

We evaluated different commercially available 3D printing materials as dissolvable mold materials for fabricating buried channels into silicone elastomers. We found that at least ABS, PVB and PVA based filaments could be used. HIPS was less suitable as a mold material, because the limonene used to dissolve HIPS could swell and crack the elastomer during drying. The fabrication process simplifies the elastomer casting because no multipart or articulated mold is needed. Additionally, we proved that the fabrication method is not limited only to a specific material or solvent.

The major limitation for presented fabrication method is that the material has to be 3D printable

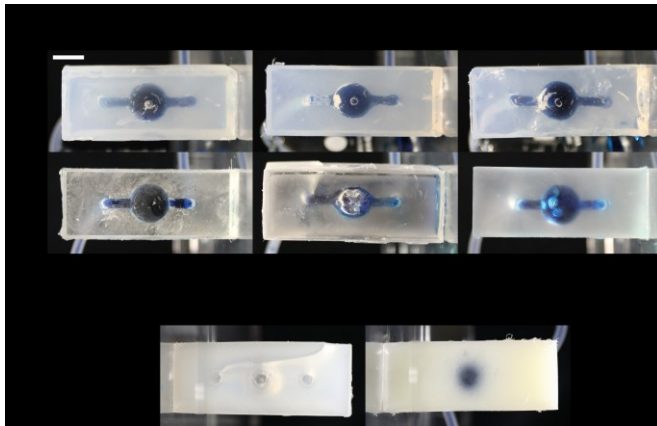


Figure 5. Fabricated soft devices with buried channels. a) Comparing the fabrication results with three different mold materials and two different silicone elastomers. b) Cracking of PDMS in Limonene (on the left), Filled channel in misted Sorta-Clear 18 (on the right) when HIPS was mold material. Scale bar: 1 cm.

and dissolvable. We found at least four materials (HIPS, ABS, PVB and PVA) which fulfil both of these requirements. These are some of the more commonly used 3D printing filament materials; it remains as a future work to expand this list of suitable materials and solvents.

Another shortcoming of this fabrication method is the limited resolution of fused filament 3D printers. However, the resolution of these printers has consistently improved during the past few years. For many applications e.g. pneumatic actuation, the resolution is already good enough.

In the future, this fabrication process will be adapted to elastomer casting of soft robots. The method might allow the casting of whole robot at once without post assembly. The possibility to use two or more sacrificial materials in a single mold should be also studied. Each of the materials could be dissolved sequentially and the channels filled with another material. This kind of sacrificial multimaterial molds could be used to create even more complex structures.

ACKNOWLEDGMENT

Ms. Koivikko did the experimental part. Ms. Koivikko and Dr. Sariola contributed both for the paper writing.

REFERENCES

- [1] S. Song and M. Sitti, "Soft grippers using micro-fibrillar adhesives for transfer printing," *Adv. Mater.*, vol. 26, no. 28, pp. 4901–4906, 2014.
- [2] F. Ilievski, A. D. Mazzeo, R. F. Shepherd, X. Chen, and G. M. Whitesides, "Soft robotics for chemists," *Angew. Chemie - Int. Ed.*, vol. 50, no. 8, pp. 1890–1895, 2011.
- [3] M. Amjadi, K. U. Kyung, I. Park, and M. Sitti, "Stretchable, Skin-Mountable, and Wearable Strain Sensors and Their Potential Applications: A Review," *Adv. Funct. Mater.*, vol. 26, no. 11, pp. 1678–1698, 2016.
- [4] C. Laschi, "Robot Octopus Points the Way to Soft Robotics With Eight Wiggly Arms," in *IEEE Spectrum*, 2016, pp. 1–8.
- [5] R. K. Katzschmann, A. D. Marchese, and D. Rus, "Hydraulic autonomous soft robotic fish for 3D swimming," *Springer Tracts Adv. Robot.*, vol. 109, no. 1122374, pp. 405–420, 2016.
- [6] R. F. Shepherd *et al.*, "Multigait soft robot," *Proc. Natl. Acad. Sci.*, vol. 108, no. 51, pp. 20400–20403, 2011.

- [7] N. W. Barlett *et al.*, "A 3D-printed, functionally graded soft robot powered by combustion," *Science (80-.)*, vol. 349, no. 6244, pp. 161–166, 2015.
- [8] M. Wehner *et al.*, "An integrated design and fabrication strategy for entirely soft, autonomous robots," *Nature*, vol. 536, no. 7617, pp. 451–455, 2016.
- [9] A. Argiolas *et al.*, "Sculpting Soft Machines," *Soft Robot.*, vol. 3, no. 3, pp. 101–108, 2016.
- [10] T. W. Odom, V. R. Thalladi, J. C. Love, and G. M. Whitesides, "Generation of 30–50 nm structures using easily fabricated, composite PDMS masks," *J. Am. Chem. Soc.*, vol. 124, no. 41, pp. 12112–12113, 2002.
- [11] R. V. Martinez *et al.*, "Robotic tentacles with three-dimensional mobility based on flexible elastomers," *Adv. Mater.*, vol. 25, no. 2, pp. 205–212, 2013.
- [12] H. Zhao, K. O'Brien, S. Li, and R. F. Shepherd, "Optoelectronically innervated soft prosthetic hand via stretchable optical waveguides," *Sci. Robot.*, vol. 1, no. 1, 2016.
- [13] A. Koivikko, E. Sadeghian Raei, M. Mosallaei, M. Mantysalo, and V. Sariola, "Screen-printed curvature sensors for soft robots," *IEEE Sens. J.*, vol. 18, no. 1, pp. 223–230, 2017.
- [14] B. Mosadegh *et al.*, "Pneumatic networks for soft robotics that actuate rapidly," *Adv. Funct. Mater.*, vol. 24, no. 15, pp. 2163–2170, 2014.
- [15] S. Mohanty *et al.*, "Fabrication of scalable and structured tissue engineering scaffolds using water dissolvable sacrificial 3D printed moulds," *Mater. Sci. Eng. C*, vol. 55, pp. 569–578, Oct. 2015.
- [16] J. S. Lee, J. M. Hong, J. W. Jung, J. H. Shim, J. H. Oh, and D. W. Cho, "3D printing of composite tissue with complex shape applied to ear regeneration," *Biofabrication*, vol. 6, no. 2, 2014.
- [17] V. Saggiomo and A. H. Velders, "Simple 3D Printed Scaffold-Removal Method for the Fabrication of Intricate Microfluidic Devices," *Adv. Sci.*, vol. 2, no. 9, pp. 1–5, 2015.
- [18] M. K. Gelber and R. Bhargava, "Monolithic multilayer microfluidics via sacrificial molding of 3D-printed isomalt," *Lab Chip*, vol. 15, pp. 1736–1741, 2015.
- [19] A. Buchoux, P. Valluri, S. Smith, A. A. Stokes, P. R. Hoskins, and V. Sboros, "Manufacturing of microcirculation phantoms using rapid prototyping technologies," *Proc. Annu. Int. Conf. IEEE Eng. Med. Biol. Soc. EMBS*, vol. 2015–Novem, pp. 5908–5911, 2015.
- [20] A. Zulfi, A. Fauzi, D. Edikresnha, M. M. Munir, and Khairurrijal, "Synthesis of High-Impact Polystyrene Fibers using Electrospinning," *IOP Conf. Ser. Mater. Sci. Eng.*, vol. 202, no. 1, 2017.
- [21] K. Nakane, T. Kurita, T. Ogihara, and N. Ogata, "Properties of poly(vinyl butyral)/TiO₂nanocomposites formed by sol - Gel process," *Compos. Part B Eng.*, vol. 35, no. 3, pp. 219–222, 2004.
- [22] C. Zhang, X. Yuan, L. Wu, Y. Han, and J. Sheng, "Study on morphology of electrospun poly(vinyl alcohol) mats," *Eur. Polym. J.*, vol. 41, no. 3, pp. 423–432, 2005.
- [23] J. Madamesila, P. McGeachy, J. E. Villarreal Barajas, and R. Khan, "Characterizing 3D printing in the fabrication of variable density phantoms for quality assurance of radiotherapy," *Phys. Medica*, vol. 32, no. 1, pp. 242–247, 2016.
- [24] D. J. Campbell and S. B. Rupe, "Solvent Swelling and Optical Rotation Demonstrated on the Overhead Projector," *J. Chem. Educ.*, vol. 77, no. 7, p. 876, 2000.

PUBLICATION II

3D-Printed Pneumatically Controlled Soft Suction Cups for Gripping Fragile, Small, and Rough Objects

Anastasia Koivikko, Dirk-Michael Drotlef, Cem Balda Dayan, Veikko Sariola and
Metin Sitti

Advanced Intelligent Systems 3, 2100034
<https://doi.org/10.1002/aisy.202100034>

Publication reprinted with the permission of the copyright holders.

3D-Printed Pneumatically Controlled Soft Suction Cups for Gripping Fragile, Small, and Rough Objects

Anastasia Koivikko, Dirk-Michael Drotlef, Cem Balda Dayan, Veikko Sariola, and Metin Sitti*

A 3D-printed pneumatically actuated soft suction gripper with an elastomer film is proposed. Suction in such gripper is actively controlled by applying a negative pressure behind the film. The elastomeric gripper body is 3D-printed, making it easy to customize and integrate into future robotic gripping systems. The gripper can pick a wide variety of objects, such as delicate fruits, small parts, and parts with uneven loads, with high pull-off forces (over 7.4 N with \varnothing 20 mm/55 kPa). The achieved pull-off forces are significantly higher than the previously reported suction cup grippers with films and more comparable with commercial vacuum grippers. The pull-off forces show no significant differences with surfaces of varying roughness (up to root-mean-square roughness of 5.66 μm) and the gripper is able to pick and release target objects repeatedly. The gripper is also compared with a commercial vacuum gripper with comparable dimensions. It outperforms the commercial gripper in the case of fragile objects, objects smaller than the gripper diameter, and objects with uneven loads. It can apply high pull-off forces while having controllable release, and is suitable for gripping a wide variety of real-world objects, including heavy, rough, small, thin, and fragile ones.

many different soft grippers have been proposed.^[1,2] Gentle gripping methods include capillary forces-based gripping,^[3,4] switchable electroadhesive surfaces,^[5–7] where a voltage applied to electrodes on the gripper induces a charge on the manipulated object, and switchable dry microfibrillar adhesive surfaces,^[8–11] inspired by the adhesive footpads of the gecko. However, capillary grippers and adhesive grippers generally do not achieve a very strong grip of the object: the applied pull-off forces to pick and lift the objects from these grippers are usually small. Strong grips can be achieved with claw grippers^[12–14] and with grippers that can control their shape and stiffness by using shape memory materials^[15–17] and granular jamming.^[18–20] Claw grippers can release the object very quickly, while thermal shape memory materials-based grippers tend to have longer response

1. Introduction

An ideal robotic gripper should be gentle, i.e., not deform or break the manipulated object by applying too large stresses on it, grip the object strongly, i.e., be able to lift at least the weight of the object and overcome the adhesion of the object to its substrate, be able to release the object from its grip easily at will, and be able to pick objects of varying sizes, shapes, roughness, and fragility. To fulfill the gentle handling requirement,


times because heating up and cooling down the material is slow. One limitation of claw grippers and granular jamming grippers is that they are limited to objects that they can enclose; flat objects being particularly challenging for both types of grippers. Meanwhile, adhesive and vacuum grippers excel at picking flat objects. Overall, all the different gripping techniques tend to excel in some aspects but have limitations in other aspects. A gripping technique that would excel in all these four different aspects would still be highly desirable.

Vacuum suction-based gripping is a fast and efficient way to handle objects.^[21] In industrial production lines, vacuum grippers are common due to their simple operation principle and fast speed. These grippers generate a negative pressure between the gripper and the target object to achieve a grasp.^[22] Grippers can use either passive or active vacuum for generating the suction effect. In passive vacuum, the adhesion is generated by pushing the fluid from under the gripper, thus creating a negative pressure between the gripper and the target object. In active vacuum, the suction is generated using a pump. Vacuum grippers are suitable for objects with a flat, smooth, and nonporous surface, which is wider than the gripper to achieve proper vacuum sealing.^[1]

Due to many advantages of the vacuum gripping, researchers have proposed different suction cup designs.^[21,23,24] Takahashi et al.^[25] proposed an octopus-inspired suction gripper with a film, using a combination of vacuum and jamming phenomena for

A. Koivikko, Dr. D.-M. Drotlef, C. B. Dayan, Prof. M. Sitti
Physical Intelligence Department
Max Planck Institute for Intelligent Systems
Heisenbergstr. 3, Stuttgart 70569, Germany
E-mail: sitti@is.mpg.de

A. Koivikko, Prof. V. Sariola
Faculty of Medicine and Health Technology
Tampere University
Korkeakoulunkatu 3, Tampere 33720, Finland

 The ORCID identification number(s) for the author(s) of this article can be found under <https://doi.org/10.1002/aisy.202100034>.

© 2021 The Authors. Advanced Intelligent Systems published by Wiley-VCH GmbH. This is an open access article under the terms of the Creative Commons Attribution License, which permits use, distribution and reproduction in any medium, provided the original work is properly cited.

DOI: 10.1002/aisy.202100034

the gripping. They fabricated a 14 mm wide gripper with micro-pumps and glass beads inside the gripper body. The maximum pull-off force they reported was 2.1 N. They also reported the enhancing effect of liquid on the surface^[26] when the same gripper design was used. Horie et al.^[27] reported an octopus-inspired microgripper for medical microelectromechanical systems. Mazzolai et al.^[28] reported an octopus-inspired actuator with integrated suction cups. Their suction cups had three different designs (a suction cup without film, with film underneath the cup, and with curve shaped film underneath the suction cup) depending on the desired function. They reached 3.3 N pull-off forces with the combination gripper.

Despite the many advantages of vacuum gripping, there are still some unsolved shortcomings. Due to the required preload in passive vacuum grippers or negative pressure in active vacuum grippers, the surface of the object cannot be neither soft nor delicate: the negative pressure of a vacuum gripper can leave a print on soft and delicate surfaces. The load of the vacuum gripper should also be even so that vacuum sealing is preserved during the object handling. In addition, the picked object should be able to be released after its transport. Finally, these challenges should be solved without compromising high pull-off forces to be able to carry heavy objects or to maintain grip during fast accelerations.

In our previous works,^[9,29] we proposed designs of soft cup-shaped grippers with thin silicone elastomer films. The adhesion could be actively controlled by applying a negative pressure behind the film. Two different films were demonstrated: a film with a gecko-inspired microfibrillar topography^[9] and a flat non-structured film.^[29] The operation principle of the gecko-inspired gripper relied on adhesion control by equal load sharing, whereas in the flat film gripper, the film acts as a suction cup when a negative pressure is applied behind the film. This, combined with the adhesion of the object to the elastomeric film, creates the force necessary to pick an object. We found that the pull-off forces of the flat film gripper against rough surfaces were larger than those of the gecko-inspired gripper. The fabrication of our previous gripper's body included several time-consuming and complex molding, silanization, demolding, and assembly steps. Also, the achieved pull-off forces were significantly lower than the commercial vacuum grippers of comparable size. To solve these issues, in this article, we propose an improved design of a 3D-printed soft vacuum gripper (Figure 1a,b). It is fabricated using direct 3D-printing (Carbon Digital Light Synthesis) with elastomeric silicone resins. The gripper consists of a 3D-printed gripper body with a negative pressure chamber, attached to a soft elastomer film. 3D-printing was selected to speed up and simplify the fabrication process of the gripper body. We were able to modify the design easily and 3D-printed multiple different designs at once. The film material and thickness were selected to be a balanced trade-off between the maximum pull-off force and conformation to rough surface, as reported in our previous study.^[29] The material of the gripper body was also stiffer than the one in our previous study. Unlike in our previous study, where the extremely soft material stretched significantly during the retraction and made the accurate positioning of the objects challenging, in this study the stiffer material reduces the stretching, and also prevents the gripper body to collapse on the soft film immediately after the withdrawal has been started.

We show that the gripper can handle objects smaller than its diameter because the film prevents the objects from being sucked into the gripper. In addition, we demonstrate that it handles highly uneven loads because the adhesion of the film enhances the sealing and thus prevents leaking. The improved gripper design can also achieve significantly higher pull-off forces even when the surface is rough. Finally, due to its softness and film, the gripper can pick soft and delicate objects without damaging them.

The grasping of the gripper is based on the vacuum suction principle. The pressure inside the vacuum chamber is called P_{neg} . Initially, it is same with the atmospheric pressure P_0 and the gripper has a dome shape (I in Figure 1c,d). When gripper is brought into contact with the target object and a preload F_{pre} is applied, small amount of air is captured between the film and the object (II in Figure 1c,d). Pressure in this volume is called P_S . After the preload, a negative pressure P_{neg} is applied inside the gripper by a syringe pump and then $P_{neg} < P_S = P_0$ (III in Figure 1c,d). When the gripper is retracted from the surface, the pressure between the gripper and the object starts to decrease and $P_{neg} < P_S < P_0$ (IV in Figure 1c,d). The pull-off force F_{off} is reached when (or a few seconds before) the gripper finally detaches from the surface (V in Figure 1c,d).

To see the effect of the negative pressure P_{neg} on the pull-off force F_{off} , we measured F_{off} against a smooth glass surface while varying P_{neg} from 0 to -55 kPa (Figure 1e). The maximum pull-off force was around 7.4 N, reached when a -55 kPa negative pressure was applied. The pull-off forces are higher with a larger negative pressure; however, the increase is nonlinear and saturates. To capture this nonlinearity, we fitted a second-order polynomial $y = -0.003683 - 0.4171x - 4.49x^2$, excluding the outlier when $P_{neg} = 0$, with an adjusted R^2 value of 0.996. We also tested linear fits for all the data and by excluding the $V = 0$ case and all these resulted in lower adjusted R^2 values. The good fit of the second-order polynomial implies reduced gains for high vacuums. Note that 55 kPa is already 0.54 atm, ≈ 1 atm being the theoretical maximum in the ambient environments.

To confirm how the elastic film affects the vacuum gripping forces, we repeated the pull-off experiments with the same gripper design, but without the film (Figure 1e). A fitted straight line had adjusted R^2 value of 0.8425. Without the film, the pull-off forces were always lower and more scattered than with the gripper with the film. The colors related to the applied withdrawal volumes also show that the achieved negative pressures were smaller and more scattered when the film was missing from the gripper. The gripper without the film fails as soon as there is a leakage from the edge, but the gripper with the film prevents the loss of vacuum under the gripper propagating immediately from one side to another. These results indicate that the film enhances the gripping forces. To see the effect of the object surface roughness, we measured pull-off forces against surfaces with varying roughness. To exclude the effect of the material, all surfaces were fabricated from the same material (EpoxAcast 690), by replicating the roughness of original surfaces through replica molding. For reference, we also tested the adhesion against a smooth glass surface. The masters for replicated surfaces were rough steel, 1000 and 2000 grit sandpaper, rough polymer, and concrete. The pull-off force results and R_{rms} (root-mean-squared

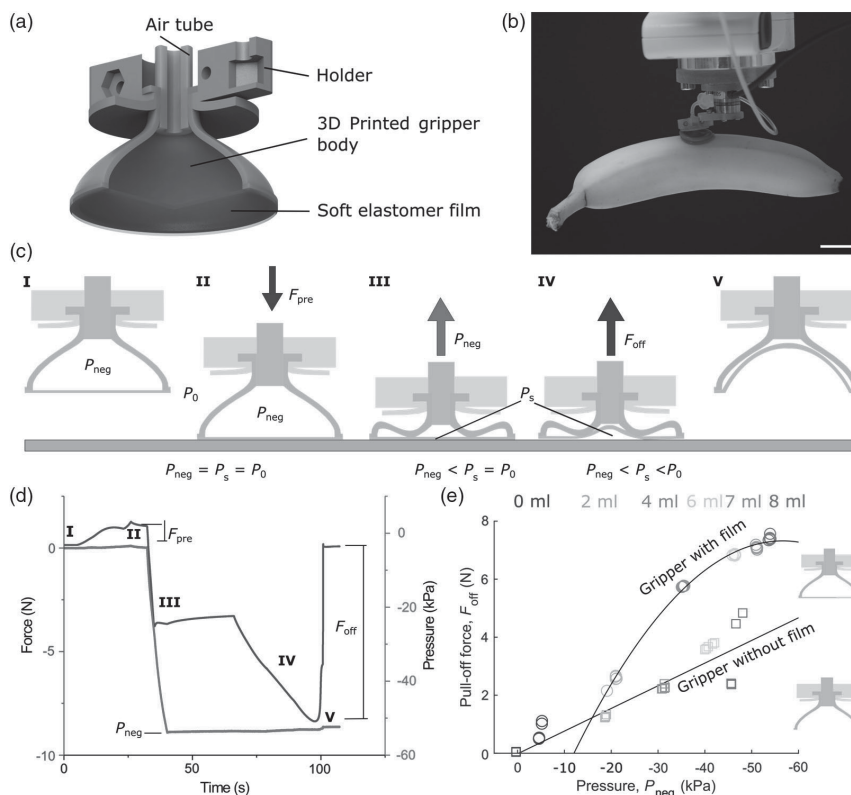


Figure 1. Concept and characterization of the 3D-printed soft vacuum gripper with an integrated elastomeric film. a) Schematic of the gripper and its holder. b) Photograph of the gripper holding a soft and delicate banana fruit (127 g), scale bar: 2 cm. c) Schematic of a pull-off force measurement and d) example data from a pull-off force measurement on a flat glass plate. I) The gripper is approaching the glass plate, II) a target preload F_{pre} (1 N) is applied after contacting the object, III) a negative pressure is applied in the gripper chamber, IV) the gripper is retracted from the object, V) the pull-off force F_{off} (the maximum force measured before the gripper detached from the object) is reached. e) Pull-off forces with different negative pressures on a smooth glass plate for grippers with (circles) and without (squares) the elastomeric film. With the film, the fitted line is a second-order polynomial with zero pressure point excluded. Without the film, the fitted line is linear. Different colors indicate the applied withdrawal volume in each measurement point.

surface roughness) values of the surface replicas are shown in **Figure 2a**, and micrographs for the corresponding surfaces are shown in **Figure 2b**. The selected surfaces are from the everyday objects, including also highly rough surfaces such as a sandpaper. The surface pattern in each object is different: in the sandpaper, the pattern is small with sharp peaks; in the rough polymer and concrete, the patterns are smoother and larger; and in the steel, there are long grooves and the structures are not as steep as the earlier ones. The measured pull-off forces were practically identical for all different test surfaces. However, the pull-off force did depend heavily on P_{neg} . This indicates that the operation principle of the gripper is mainly vacuum based. Thus, for reliable gripping, controlling P_{neg} is a much more important than the material/roughness of the object being picked, which is a promising result considering the practical applications of the gripper. **Figure 1e** also shows that the forces

start to saturate after the -55 kPa, which limits the maximum pull-force values that can be reached.

The film of the gripper makes it also possible to pick objects smaller than the diameter of the gripper. To demonstrate this, we tested picking of polymethyl methacrylate (PMMA) disks of varying diameters. The smallest disk we were able to pick had a diameter of 6 mm (30% of 20 mm gripper diameter) (**Figure 3f**). However, the gripper could not release this disk, but the disk remained adhered to the film. The smallest disk that we were able to both pick and release had a diameter of 16 mm. To better quantify the ability of the gripper to pick small objects, we measured the pull-off forces against two different diameter glass spheres, 30 mm and 15 mm. Spheres were used in these experiments because spheres do not require alignment of the gripper with the target object. The gripper adhered well to the bigger 30 mm sphere but did not adhere to the smaller 15 mm sphere.

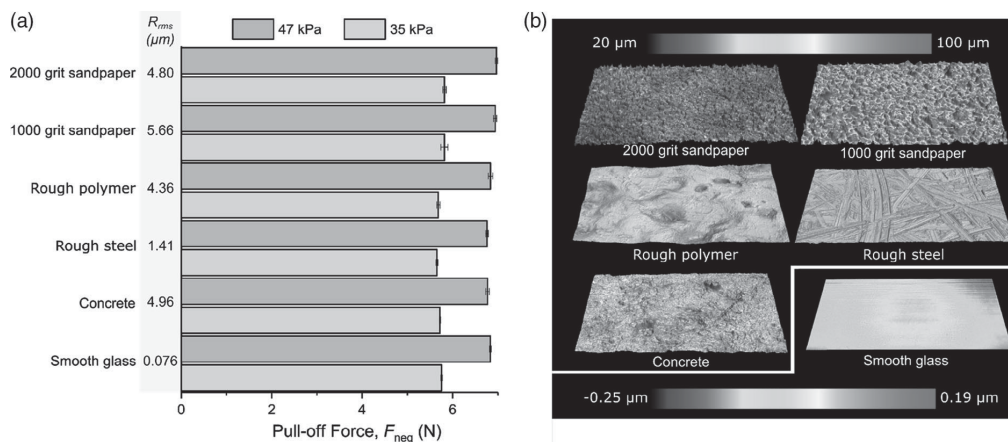


Figure 2. Pull-off forces for surfaces with varying roughness. a) Pull-off forces with smooth glass and replicas of rough surfaces (2000 and 1000 grit sandpaper, rough polymer, rough steel, and concrete) and R_{rms} values of the corresponding replicas. Pull-off force measurements were conducted with 35 and 47 kPa negative pressures. Each bar indicates an average of five measurements, and error bars show standard deviation. b) 3D topographies of the surfaces measured by a laser confocal microscope.

This is shown in Figure S3, Supporting Information. The results indicate that the gripper is able to grip small, flat, and light parts, due to its soft film, but would fail with highly curved objects.

The repeatability of the gripper was tested by attaching the gripper to a robotic arm with a three-axis force sensor (Figure 3c). The pick-and-place operation (Video S1, Supporting Information and snapshots in Figure 3b) was repeated 15 times for the same five surface replicas as before and two small PMMA parts with diameters of 18 and 16 mm. The target objects were selected to be light (≈ 10 g), to test the adhesion of the gripper to the objects. Even in the absence of vacuum, the gripper might adhere to the object simply due to van der Waals and capillary forces (sticky finger phenomenon). An example (concrete replica) of the force data recorded during one of these repeatability experiments is shown in Figure 3a. In each pick-and-place cycle, the force profile stays similar and the gripper was able to reliably and reproducibly pick and release every tested object. This shows that the gripper would not be limited only to smooth surfaces in potential future applications and it is capable to release also light objects.

To test whether the gripper leaves marks or dints on surfaces, we picked two delicate objects: a pear (170 g) and a banana (130 g), as shown in Figure 1b and 3e. Picking and releasing the fruits was successful, and the gripper did not leave any visible dints on the surface. We attribute that as the gripper, including the gripper body, is entirely soft, there is no risk of local high stresses and thus the gripping is gentler. As a control experiment, we did the same manipulation tasks with a commercial suction cup (Bellow suction cup SPB4 20 SI-55 G1/8-AG, Schmalz GmbH, Germany). The commercial suction cup was used with a vacuum generator (Vacuum Unit VER 15, Schmalz GmbH, Germany), set to -60 kPa pressure as recommended by the manufacturer for continuous suction. Figures S1a,b, Supporting Information, show that the commercial suction cup left visible prints on both surfaces. To test if

the gripper leaves visible contamination on picked surfaces, we picked a cleaned glass plate and a silicon wafer with the gripper (Figure S4, Supporting Information). Both surfaces and the gripper were cleaned before the picking with acetone, isopropyl alcohol, and deionized water. We did not observe any visible contamination on the surfaces after inspecting them with an optical microscope. However, silicone elastomers are known to contaminate surfaces in nonvisible ways,^[30] which can be reduced, for example, by oxidating the silicone elastomer before picking.^[31] We conclude that our gripper can handle significant loads without leaving visible dints on the soft surfaces of the objects that can be easily damaged. Also, it does not leave visible contamination marks on the clean surfaces.

Thin objects and films are often a challenge to robotic grippers: both grasping and suction grippers may inadvertently wrinkle or even crumple the film. To demonstrate that our gripper can pick thin objects, the gripper was used to flip the pages of a book (Video S2, Supporting Information and snapshots in Figure 3g). The gripper managed to grip and release the pages, without leaving visible crumples on the pages of the book.

Objects with uneven load distribution are difficult for many robotic grippers, as such loads results in torque, leading to an uneven stress distribution between the gripper and the object. To see if our gripper can pick uneven loads, we tested picking a fluid-containing bottle (429 g) from the edge of the bottle (Figure 3d). For comparison, we tested gripping the bottle using the same commercial vacuum gripper as before (Video S3, Supporting Information and snapshots in Figure S1c, Supporting Information). Our gripper could pick the bottle from the edge, i.e., when the load was uneven, whereas the commercial gripper could grip the bottle only from the middle, i.e., when the load was even. This ability to grip uneven loads could be from the soft silicone film that maintains the seal between the gripper and the object, preventing a small opening developing into a catastrophic loss of vacuum. This reduces the need to carefully plan

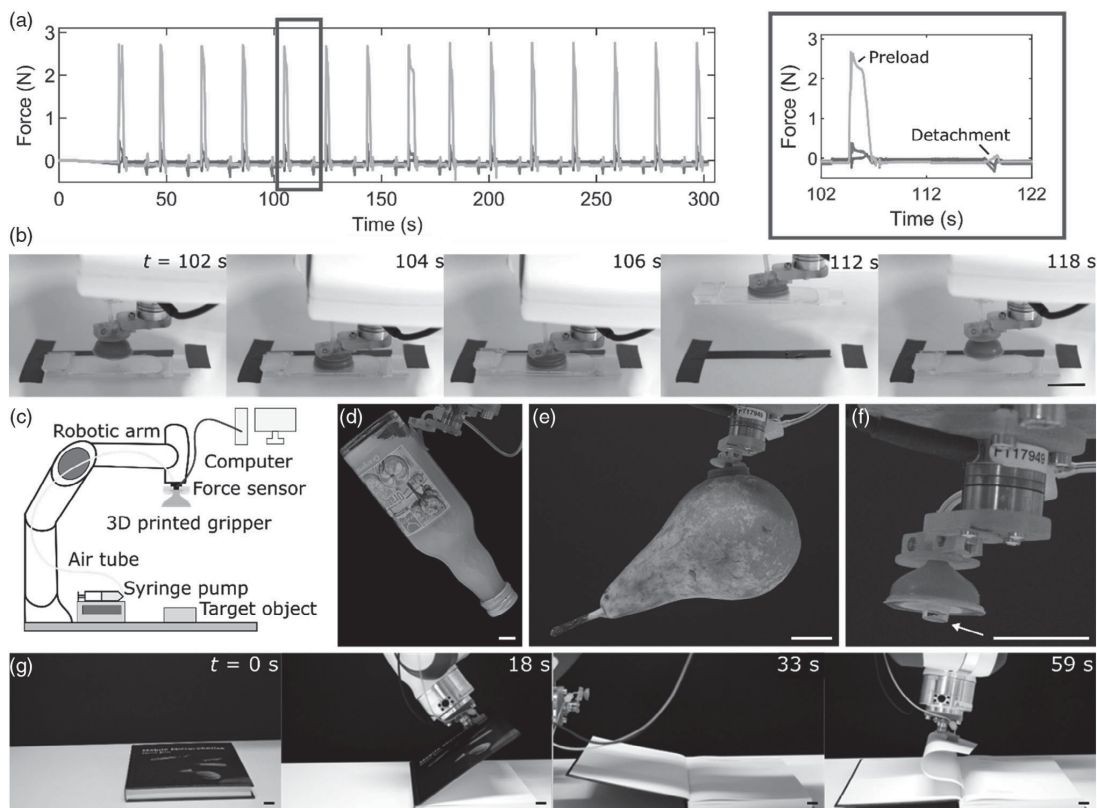


Figure 3. Pick-and-place repeatability tests and demonstrations using a robotic arm. a) Three-axis force data (x = blue, y = red, and z = orange) from the 15 repeated measurements with concrete replica and inset of that data. b) Snapshots from a repeatability measurement. At $t = 102$ s, the gripper approaches the target object. The gripper contacts the object with preload at $t = 104$ s, and then a negative pressure is applied inside the chamber ($t = 106$ s). At $t = 112$ s, the object is carried, and then released ($t = 118$ s). c) Schematic of the robotic arm setup: gripper is mounted at tip of the robotic arm and connected to the syringe pump using silicone tubing. A force sensor is between the gripper and the robotic arm, and the sensor is connected to a computer. d–g) Demonstration with the robotic arm: d–f) photographs of the gripper holding different objects: an orange juice bottle (429 g, highly uneven load), a pear (167 g), a soft object, and a small object (6 mm). g) Snapshots of the video: the gripper turns the pages of a book. Scale bar in all photographs: 2 cm.

the gripping. The angle and spot to grip the object do not have to be exact, making it especially suitable for situations where visual inspection of the object is limited.

In conclusion, we fabricated and characterized a 3D-printed soft suction cup gripper with a thin film underneath it. 3D-printing the gripper is faster and simpler than our previously^[9,25,28,29] reported casting techniques: there are less fabrication steps, they take less time to complete, and they are more reproducible. This rapid prototyping also makes it easier to integrate our gripper into future applications in fully 3D-printed soft robotic systems including actuators and sensors. The design of the proposed gripper is closed unlike in traditional suction cup grippers. The closed design prevents particles from entering and clogging the pneumatic channel, making the gripper more reliable in dirty environments. The design also allows the gripping of objects smaller than the gripper diameter. The soft gripper

conforms to the 3D shape of the object, which reduces the need to position the gripper accurately when picking objects. Because of these features, the gripper can have future various industrial manipulation or assembly applications, where the objects often have varying sizes and the position of the target objects may vary, for example, when they arrive on a conveyor belt. Finally, compared with previously reported soft suction grippers,^[9,29] the pull-off force of our gripper is significantly higher (7.4 N), as shown in Table 1. The pull-off force was also higher when compared with the gripper diameter and area normalized pull-off forces. The exception is the gripper proposed by Tomokazu et al.,^[26] which has higher pull-off force and diameter normalized pull-off force. However, their measurements were conducted with liquid enhancing in the gripper-object contact so the comparison is not straightforward. We attribute the higher pull-off forces are due to improved design and materials of the gripper

Table 1. Comparison of the proposed 3D-printed suction gripper and previously reported suction-based grippers.

Gripper name	Diameter [mm]	Pull-of force per area [[N] mm ⁻²]	Pull-off force per diameter [[N] mm ⁻¹]	Pull-off force [N]	Fabrication method	Max. Surface roughness picked (R_{rms}) [μm]	Reference
Dielectric suction cup	12	–	–	–	Thin films stacked together	–	[21]
Magnetically switchable gripper	10	0.012	0.09	0.9	Casting	–	[23]
Octopus-inspired gripper	14	0.014	0.15	2.1	Casting	–	[25]
Octopus-inspired gripper with liquid membrane	60	0.016	0.77	46 ^{a)}	Casting	1.2	[26]
Micro sucker	3–10	0.0035	0.03	≈0.1 ^{b)}	Casting	–	[27]
Octopus-inspired gripper	9–14	–	–	3.3 ^{c)}	Casting	^{d)}	[28]
Soft suction gripper	18	0.011	0.15	2.7	Casting, bar coating	1.6	[29]
Commercial Suction gripper	20	0.035	0.55	11	–	–	Schmalz
3D-printed soft suction gripper	20	0.024	0.37	7.4	3D-printing, bar coating	5.66	This work

^{a)}Force measured with a liquid membrane between the gripper and the object; ^{b)}Measurement was conducted with a chicken breast (wet), estimated from Figure 4 in ref. [27];

^{c)}Measurement was conducted by using the whole robotic arm and many suction cups, the whole diameter not known; ^{d)}Rough surfaces tested, where $R_z = 36.5 \mu\text{m}$.

body which were able to achieve due to fat fabrication methods. This pull-off force is comparable with industrial suction grippers and that is why we compared our gripper to the same size commercial suction cup gripper with 11 N pull-off force. We demonstrated that our gripper can perform the same tasks as the commercial gripper in the given pull-off force limit, but additionally our gripper could perform tasks that are challenging for the commercial gripper, such as picking uneven loads, delicate surfaces, and smaller objects than the diameter of the suction cup. The operation speed of our 3D-printed gripper is slower than the commercial suction cup. The speed of the proposed gripper is currently limited by the used vacuum pump, and by changing the vacuum unit, the operation speed can be increased. Because of such versatility of our gripper, we believe that it could find use in future warehouse applications, where objects can be expected to vary in surface material, size, and shape.

2. Experimental Section

Design and Fabrication of the Soft Gripper: The fabrication steps of the soft gripper are shown in Figure S2, Supporting Information. The gripper consists of a 3D-printed soft gripper body with 700 μm wall thickness, a soft silicone film, air tubing, and a rigid 3D-printed holder. The diameter of bottom part of the body is 20 mm with 0.3 mm wider outer ring to enhance the sealing when in contact. The inner volume of the gripper is 1.4 mL. The 3D-printed part was fabricated by using Carbon Digital Light Synthesis (Carbon DLS) and M2 Printer (Carbon, CA, USA) by using a soft silicone urethane resin (SIL 30, Carbon, CA, USA. Shore hardness: A35). 3D-printer had a 75 μm xy-resolution and 100 μm z-resolution. After the 3D-printing, the parts were cleaned with isopropyl alcohol to get rid of any residual resin. Then, the parts were placed in the oven for 8 h at 120 °C. After that, the supporting structures were removed from the gripper bodies. Then, the 3D-printed gripper body was bonded onto 400 μm-thick bar-coated soft silicone film (Ecoflex, Smooth-On Inc., USA. Shore hardness: 00–50) with a silicone adhesive (Sil-Poxy™, Smooth-On, USA). Then air tubing was attached into upper part of the gripper and sealed by using the same silicone adhesive. Finally, the gripper was attached to a 3D-printed rigid plastic holder designed for the gripper.

Fabrication of the Rough Surface Replicas: The rough surface replicas were fabricated by first creating a negative mold of the original surface, by pressing a glass plate with a layer of uncured vinylsiloxane polymer

(Flexitime medium flow, Heraeus Kulzer GmbH) onto the original surface. The mold was cured for 5 min at room temperature, and then removed from the surface. Next, a positive replica of the original surface was made by casting clear epoxy (EpoxyAcast 690, Smooth-On Inc., 10:3 ratio by weight) into the mold, with another glass plate pressed on top. The positive replica was cured for 48 h before removing it from the mold.

Adhesion Measurements: To characterize the adhesion and pull-off forces of the gripper, the gripper was attached to a high-resolution load cell (GSO-1K, Transducer Techniques), measuring the reaction forces normal to a smooth glass substrate. High-precision piezo motion stages (LPS-65 2", Physik Instrumente GmbH & Co. KG) were used to move the gripper vertically. The interface between the gripper film and the glass substrate was observed from below using an inverted optical microscope (Axio Observer A1, Zeiss) with a video camera (Grasshopper3, Point Gray Research Inc.). A programmable syringe pump (Legato 210p, KD Scientific, USA) was used to control the pressure inside the gripper body.

Repeatability Tests and Demonstrations: The repeatability of the gripper was tested with 7 degrees of freedom robotic arm (Franka Emika, Panda Research, Germany). Figure 3c shows the measurement setup. We attached the gripper and the holder to a six-axis torque sensor (Nano 17 Titanium, ATI Industrial Automation, USA) which was attached to the tip of the robotic arm. In these experiments, we used the same syringe pump as before to apply the negative pressure inside the gripper chamber. In the repeatability tests, the robotic arm was programmed to pick and place the objects 15 times and the syringe pump was operated accordingly.

Supporting Information

Supporting Information is available from the Wiley Online Library or from the author.

Acknowledgements

The project was funded by Suomen Kulttuurirahasto (Pirkanmaan rahasto, grant "Robots and Us"), the Finnish Science Foundation for Technology and Economics, Academy of Finland (grant nos. 299087 and 306999), and Max Planck Society. C.B.D. thanks the International Max Planck Research School for Intelligent Systems (IMPRS-IS) for his Ph.D. fellowship.

Conflict of Interest

The authors declare no conflict of interest.

Data Availability Statement

Research data are not shared.

Keywords

adhesion, pick and place manipulation, soft grippers, soft robotics, vacuum grippers

Received: February 23, 2021

Revised: May 12, 2021

Published online: July 1, 2021

-
- [1] J. Shintake, V. Cacucciolo, D. Floreano, H. Shea, *Adv. Mater.* **2018**, *30*, 1707035.
- [2] S. I. Rich, R. J. Wood, C. Majidi, *Nat. Electron.* **2018**, *1*, 102.
- [3] J. Giltinan, E. Diller, M. Sitti, *Lab Chip* **2016**, *16*, 4445.
- [4] A. Iazzolino, Y. Tourtit, A. Chafai, T. Gilet, P. Lambert, L. Tadrist, *Soft Matter* **2020**, *16*, 754.
- [5] J. Shintake, S. Rosset, B. Schubert, D. Floreano, H. Shea, *Adv. Mater.* **2016**, *28*, 231.
- [6] X. Gao, C. Cao, J. Guo, A. Conn, *Adv. Mater. Technol.* **2019**, *4*, 1800378.
- [7] G. Gu, J. Zou, R. Zhao, X. Zhao, X. Zhu, *Sci. Robotics* **2018**, *3*, 2874.
- [8] M. Sitti, R. S. Fearing, *J. Adhes. Sci. Technol.* **2003**, *17*, 1055.
- [9] S. Song, D.-M. Drotlef, C. Majidi, M. Sitti, *Proc. Natl. Acad. Sci. U. S. A.* **2017**, *114*, E4344.
- [10] E. W. Hawkes, D. L. Christensen, A. K. Han, H. Jiang, M. R. Cutkosky, in *Proc. IEEE Int. Conf. on Robotics and Automation*. IEEE, Seattle, WA, USA **2015**, pp. 2305–2312.
- [11] D.-M. Drotlef, P. Blümler, A. del Campo, *Adv. Mater.* **2014**, *26*, 775.
- [12] A. Elsayes, A. Koivikko, V. Sariola, in *Proc. of IEEE Sensors*, IEEE, Montreal, Canada **2019**, pp. 1–4.
- [13] A. Koivikko, E. Sadeghian Raei, M. Mosallaei, M. Mantysalo, V. Sariola, *IEEE Sens. J.* **2018**, *18*, 223.
- [14] B. Mosadegh, P. Polygerinos, C. Keplinger, S. Wennstedt, R. F. Shepherd, U. Gupta, J. Shim, K. Bertoldi, C. J. Walsh, G. M. Whitesides, *Adv. Funct. Mater.* **2014**, *24*, 2163.
- [15] M. Behl, K. Kratz, Jörg. Zotzmann, U. Nöchel, A. Lendlein, *Adv. Mater.* **2013**, *25*, 4466.
- [16] Q. Ze, X. Kuang, S. Wu, J. Wong, S. M. Montgomery, R. Zhang, J. M. Kovitz, F. Yang, H. Jerry Qi, R. Zhao, *Adv. Mater.* **2020**; *32*: 1906657.
- [17] A. Firouzeh, M. Salerno, J. Paik, *IEEE Trans. Rob.* **2017**, *33*, 765.
- [18] J. R. Amend, E. Brown, N. Rodenberg, H. M. Jaeger, H. Lipson, *IEEE Trans. Rob.* **2012**, *28*, 341.
- [19] J. Amend, N. Cheng, S. Fakhouri, B. Culley, *Soft Rob.* **2016**, *3*, 213.
- [20] I. De Falco, M. Cianchetti, A. Menciassi, *Bioinspiration Biomimetics* **2017**, *12*, 056008.
- [21] M. Follador, F. Tramacere, B. Mazzolai, *Bioinspiration Biomimetics* **2014**, *9*, 046002.
- [22] G. J. Monkman, S. Hesse, R. Steinmann, H. Schunk, *Robot Grippers*, Wiley, Hoboken, New Jersey **2007**, 169–220 <https://doi.org/10.1002/9783527610280>.
- [23] H. Iwasaki, F. Lefevre, D. D. Damian, E. Iwase, S. Miyashita, *IEEE Rob. Autom. Lett.* **2020**, *5*, 2015.
- [24] C. Tawk, A. Gillet, M. in het Panhuis, G. M. Spinks, G. Alici, *IEEE Trans. Rob.* **2019**, *35*, 1268.
- [25] T. Takahashi, M. Suzuki, S. Aoyagi, in *IEEE 11th Annual Int. Conf. on Nano/Micro Engineered and Molecular Systems, NEMS*, IEEE, Sendai, Japan **2016**, pp. 508–511.
- [26] T. Takahashi, S. Kikuchi, M. Suzuki, S. Aoyagi, in *IEEE Int. Conf. on Intelligent Robots and Systems*, IEEE, Hamburg, Germany **2015**, pp. 2929–2936.
- [27] T. Horie, S. Sawano, S. Konishi, in *Proc. of the IEEE Int. Conf. on Micro Electro Mechanical Systems (MEMS)*, IEEE, Kobe, Japan **2007**, pp. 691–694.
- [28] B. Mazzolai, A. Mondini, F. Tramacere, G. Ricconi, A. Sadeghi, G. Giordano, E. Del Dottore, M. Scaccia, M. Zampato, S. Carminati, *Adv. Intell. Syst.* **2019**, *1*, 1900041.
- [29] S. Song, D.-M. Drotlef, D. Son, A. Koivikko, M. Sitti, *arXiv* **2020**, <http://arxiv.org/abs/2009.08156>.
- [30] D. J. Graham, D. D. Price, B. D. Ratner, *Langmuir* **2002**, *18*, 1518.
- [31] K. Glasmästar, J. Gold, A.-S. Andersson, D. S. Sutherland, B. Kasemo, *Langmuir* **2003**, *19*, 5475.

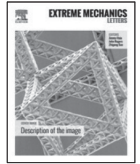
PUBLICATION III

3D-Printed Pneumatically Controlled Soft Suction Cups for Gripping Fragile, Small, and Rough Objects

Anastasia Koivikko, Dirk-Michael Drotlef, Metin Sitti and Veikko Sariola

Extreme Mechanics Letters, 44, 101263
<https://doi.org/10.1016/j.eml.2021.101263>

Publication reprinted with the permission of the copyright holders.



Magnetically switchable soft suction grippers

Anastasia Koivikko^a, Dirk-Michael Drotlef^b, Metin Sitti^b, Veikko Sariola^{a,*}

^a Faculty of Medicine and Health Technology, Tampere University, 33720 Tampere, Finland

^b Physical Intelligence Department, Max Planck Institute for Intelligent Systems, 70569 Stuttgart, Germany



ARTICLE INFO

Article history:

Received 17 November 2020

Received in revised form 27 January 2021

Accepted 27 February 2021

Available online 5 March 2021

Keywords:

Soft gripper

Magnetorheological fluid

Hydraulic actuator

Suction

ABSTRACT

Grasping is one of the key tasks for robots. Gripping fragile and complex three-dimensional (3D) objects without applying excessive contact forces has been a challenge for traditional rigid robot grippers. To solve this challenge, soft robotic grippers have been recently proposed for applying small forces and for conforming to complex 3D object shapes passively and easily. However, rigid grippers are still able to exert larger forces, necessary for picking heavy objects. Therefore, in this study, we propose a magnetically switchable soft suction gripper (diameter: 20 mm) to be able to apply both small and large forces. The suction gripper is in its soft state during approach and attachment while it is switched to its rigid state during picking. Such stiffness switching is enabled by filling the soft suction cup with a magnetorheological fluid (MR fluid), which is switched between low-viscosity (soft) and high-viscosity (rigid) states using a strong magnetic field. We characterized the gripper by measuring the force required to pull the gripper from a smooth glass surface. The force was up to 90% larger when the magnetic field was applied (7.1 N vs. 3.8 N). We also demonstrated picking of curved, rough, and wet 3D objects, and thin and delicate films. The proposed stiffness-switchable gripper can also carry heavy objects and still be delicate while handling fragile objects, which is very beneficial for future potential industrial part pick-and-place applications.

© 2021 The Authors. Published by Elsevier Ltd. This is an open access article under the CC BY license (<http://creativecommons.org/licenses/by/4.0/>).

1. Introduction

Grasping is one of the most important tasks for robots in manufacturing lines, food industry and warehouses. When manipulated objects are not fragile and their shape is well-defined, traditional rigid grippers perform well due to their ability to exert large forces and to maintain their shape during grasping. However, they struggle with fragile objects as they may damage the objects by applying too much local stress at the contact points. Furthermore, when the object shape is not well-defined (e.g. most biological objects), the grasping needs to be carefully planned, based on vision or otherwise, to account for variations in the object shape.

To overcome these challenges, soft robotic grippers [1] have been proposed. Being made of soft material, they can conform to the shape of the target object, distributing the stress more evenly. Multiple different soft grippers have been proposed: bioinspired suction cups [2,3], grippers with controlled adhesive surfaces [4–8], grippers with multiple soft fingers [9–13], grippers based on state change [14,15] and so-called jamming grippers [16–19], which envelope the target object with a switchable material that turns from soft to rigid (e.g. granular material [16,17] or magnetorheological fluids (MR fluids) [18–20]).

All of the aforementioned gripping methods have their shortcomings: (1) suction cups and adhesive grippers generally exert smaller forces than rigid and jamming grippers; (2) jamming grippers can only pick objects that can be partially or completely enveloped by the gripper; and (3) adhesive grippers are mostly limited to dry and clean surfaces. To develop a gripping method without such shortcomings, we decided to explore how the gripping forces of our existing soft suction cup gripper design [21] could be improved, without compromising its soft touch.

In this paper, we show that a soft suction cup gripper, filled with an MR fluid, can act as a switchable soft/hard gripper (Fig. 1a and b). The gripper consists of a 3D-printed bell-shaped gripper body, attached to a cast soft elastomer film (Fig. 1a and b). Between the body and the film is an internal cavity. At the top of the bell shaped body is an inlet, through which the cavity can be filled with an MR fluid. The inlet is connected to a syringe pump with silicone tubing. The basic gripper design is same as in our previous works [4,21]; however, unlike in our previous works, where the gripper cavity was filled with air, here the gripper is filled with an MR fluid, which enables the switchable stiffness.

During approach in Fig. 1c, I, the magnetic field is off, and the gripper is soft, conforming to the target object to get the best possible attachment without damaging the surface in Fig. 1c, II. Then, the magnetic field is applied in Fig. 1c, III; in this work by bringing a permanent magnet near the gripper. The magnetic field

* Corresponding author.

E-mail address: veikko.sariola@tuni.fi (V. Sariola).

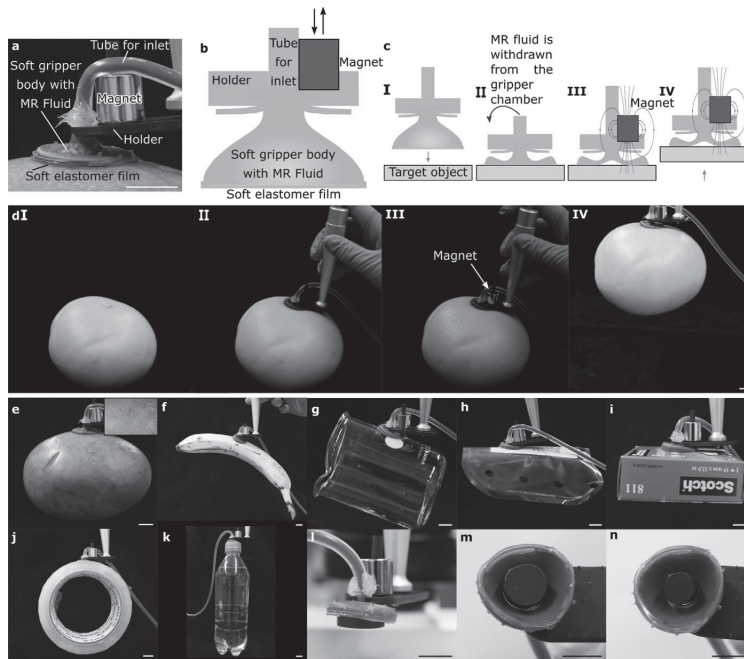


Fig. 1. Schematic of the proposed stiffness-switchable gripper and its gripping demonstrations. (a) A photograph and (b) a schematic of the gripper. The soft gripper body is 3D-printed and attached onto a soft elastomer film. A silicone tube is attached to the inlet for the hydraulic connection. The gripper is filled with an MR fluid and attached to a 3D-printed holder including a removable magnet. (c) Schematic of the pick-and-place manipulation process and (d) corresponding photographs from a real experiment. (I) The gripper approaches the target object. (II) A preload is applied while withdrawing the MR fluid from the inside the gripper chamber. (III) A magnet is placed on top of the gripper for enhancing the pull-off force. (IV) The gripper picks the object. Gripping demonstrations: (e) a mango (inset: a close-up of the surface of the mango), (f) a banana, (g) a wet beaker, (h) a thin plastic sheet, (i) a cardboard packet, (j) a tape roll, (k) a plastic water bottle, (l) \varnothing 16 mm 3D-printed disc, (m) \varnothing 10 mm 3D-printed disc and (n) \varnothing 8 mm 3D-printed disc. Scale bars: 1 cm.

stiffens the MR fluid, so it does not move inside the gripper during the picking process in Fig. 1c, IV. The stiffness of the gripper prevents the object from peeling off and helps maintaining a good suction, effectively increasing the pull-off force. The entire gripping sequence is illustrated in Fig. 1c and d and demonstrations with varying objects in Fig. 1e–n.

MR fluids are often mineral or silicone oils containing micron sized iron particles. Under the external magnetic field, they show a reversible transformation from a liquid to a nearly solid-like state in less than milliseconds [22]. They are typically used in hydraulic dampers, brakes and control valves [22,23], but also as a semi-active actuation method in robotic grippers [24]. In soft grippers, they have been used by mixing them into silicones to create magnetic elastomers [25], by filling empty structures with them to create jamming effect based grippers [18–20], and in controllable wet adhesive grippers [26].

The main advantages of our new approach are: (1) the adhesion can be switched to apply large and small gripping forces as needed to grip heavy or fragile objects, respectively; (2) the softness of the gripper during approach allows it to conform to the shape of the object; (3) the gripper can pick both small and large objects (relative to its size); and (4) the gripper can adhere to many different surfaces, including curved, soft, rough, wet or oily ones.

2. Material and methods

2.1. Gripper design and fabrication

The gripper body was stereolithography printed (Form 2, Formlabs, Somerville, MA, USA) with an elastic resin (Elastic V1,

Shore A 50). The body is a hollow bell-like structure, with an inner diameter of 20 mm, a height of 12.5 mm and a wall thickness of 700 μm . An inlet with a diameter of 4 mm is at the apex of the bell-like structure. To fabricate the soft elastomer film, we spread silicone elastomer (EcoflexTM 00–50, Smooth-On Inc., Macungie, PA, USA) onto a polyethylene terephthalate (PET) sheet by using a universal film applicator (UA 3000, Mtv Messtechnik oHG, Germany). The thickness of the elastomer film after curing was \sim 400 μm .

To bond the film to the gripper, we cleaned the gripper with oxygen plasma (PICO with RF Generator, Diener electronic, 20 s at 30 W). Immediately after plasma treatment, we dipped the gripper in a silicone adhesive (Sil-PoxyTM, Smooth-On Inc., Macungie, PA, USA) and pressed onto the cured elastomer film. The same silicone adhesive was used to attach a silicone tube (\varnothing 2/4 mm) to the inlet. Fig. S1 shows a schematic of the fabrication method.

2.2. Magnetorheological fluid

We tested filling the gripper with two different magnetorheological fluids (122EG and 140CG, Parker Lord, Macungie, PA, USA). The properties of the fluids are summarized in Table 1. To fill the gripper without having air bubbles, we first evacuated air from the gripper using an empty syringe, creating a near vacuum inside the gripper. Then, we swapped the syringe to one filled with an MR fluid and the vacuum was let to suck the fluid into the gripper cavity (Fig. S1). The total mass of the gripper with the fluid was approximately 9 g.

Table 1
Properties of the two MR fluids tested.

MR fluid property	122EG	140CG
Viscosity (mPa s)	42 ± 20	280 ± 70
Yield stress at 100 kA/m (kPa)	20	44
Density (g/cm ³)	2.28–2.48	3.54–3.74
Solid content by weight (%)	72	85.44

2.3. Characterization setup

A mechanical tester (TA.XT Plus, Stable Micro Systems, Surrey, UK) was used to characterize the gripping forces. The approach and retraction speeds of the tester were set to 0.1 mm/s. The gripper was attached to a 10 kg load cell, using a custom-made 3D-printed holder. The holder included a pole to which a ring-shaped neodymium magnet (grade N42, \varnothing 5/12 mm, height: 12 mm, 4.4 kg holding power, weight: 8.5 g) could be placed. The center of the magnet was approximately 15 mm from the center of the gripper.

The characterization experiments were done against a smooth and clean glass surface unless otherwise noted. A 45° mirror was mounted beneath the glass surface for observing the attachment of the soft film during the experiments. To control the MR fluid flow, a syringe pump (Aladdin Single-Syringe Pump, High Pressure, World Precision Instruments) was used. The pump was computer controlled over a serial port interface. The flowrate was 1 ml/min in all the experiments. Fig. 2a and b show the characterization setup.

Example of a typical characterization experiment is shown in Fig. 2c. First, the gripper approaches the target surface and once in contact, a preload force F_{pre} of 1.47 N is applied. Then, a volume V of the MR fluid is withdrawn from the gripper, which flattens the gripper body and creates vacuum under the film. A closed-loop controller maintains the preload during fluid withdrawal. After the withdrawal is finished, the external magnetic field is applied by placing the magnet on top of the gripper. The gripper then retracts and detaches from the surface. We call the peak force during the retraction as the pull-off force F_{off} and integral of the tensile part of the force–distance curve as the tensile work W_T (Fig. 3a).

3. Results and discussion

To confirm the effect of the magnetic field and suction on the gripping forces, we performed characterization experiments with and without the magnetic field applied and with varying volumes V of fluid withdrawn from the gripper. The representative force–distance curves from such experiments are shown in Fig. 3a and b.

The gripper film detached in multiple sudden jumps from the surface, which is seen as spikes in both Fig. 3a and b. The number and placement of the spikes varied between experiments, but they could be seen in almost all the experiments with and without external magnetic field applied. However, the overall shape of the curve, including the location and magnitude of the pull-off force peak, is quite comparable between the experiments, despite the smaller spikes seen in the experiments. The smaller spikes are due to parts of the film detaching at different times and vacuum readjusting under the gripper in a step-like manner. Another reason for the spikes is the step-like detachment of the gripper body from the soft film. When the MR fluid was withdrawn from the cavity, the gripper body collapsed onto the soft film. When the gripper started to retract from the surface, the gripper body detached from the soft film also in a step-like manner. The collapse of the gripper body onto the soft film is further illustrated in Fig. 5.

The average pull-off forces and tensile works from five repeats with different combinations of experimental parameters are shown in Fig. 4a. The largest increase (90%, from 3.8 N to 7.1 N) in pull-off force with the magnet is seen when $V = 1.5$ ml. Note that, in the undeformed shape, the volume of the gripper chamber is ~ 1.5 ml, so $V = 1.5$ ml corresponds to 100% of the gripper chamber volume and majority of the MR fluid is already withdrawn from the chamber. When V was only 0.5 ml (33% of the chamber volume), the pull-off force was not observed to increase with the magnet. The pull-off forces increased with V until 1.5 ml, but no difference was seen in pull-off forces between 1.5 ml and 2 ml (133% of the gripper volume) when the magnetic field was applied. At such a large V , majority of the MR fluid is already withdrawn from the chamber and the extra withdrawn volume results in the compression of the silicone tubing connecting pump to the gripper, which is likely why the pull-off force was not observed to increase significantly after $V = 1.5$ ml. The tensile work was increased with the magnet for all tested withdrawal volumes from 1 ml and up. We conclude that, as long as a sufficient volume of fluid is withdrawn, the magnet can increase the adhesion significantly.

Many switchable adhesive grippers, such as electroadhesives and gecko inspired adhesives, fail to grasp surfaces wetted by water or oil [1]. However, most suction grippers do not suffer from this limitation [2]. To see how our gripper adheres to wet surfaces, we measured its adhesion against a glass surface wetted with deionized water or heavy mineral oil (CAS 8042-47-5, Sigma-Aldrich). The results are shown in Fig. 4b. The results show that the adhesion was largest to dry surfaces, and smallest to oily surfaces. However, the drop in pull-off forces was less than 20% between dry and oily surfaces. These results show that, due to merit of still working based on the vacuum principle, our gripper can adhere not only to dry surfaces, but also to wet and oily ones, unlike many previously reported switchable adhesive grippers that do not enclose the object.

Another challenge for switchable adhesive grippers can be gripping soft and deformable objects. To study our suction-based soft gripper's performance in this challenge, we characterized how our gripper adheres to soft surfaces. We measured the maximum pull-off forces against ~ 0.7 cm thick flat objects having Shore-00 hardness ranging from 10 to 80. Note that these objects are still much softer than the gripper body (Shore $\sim A50$). The objects were made by casting 20 g of elastomer into a petri dish, from which they were removed after being cured. Fig. 4c shows the results. The pull-off forces decreased as the Shore hardness decreased. Shore-00 30 corresponds approximately to human skin and even at this softness, the gripper was able to reach almost 5 N forces. We conclude that our gripper can pick also soft objects, although with reduced gripping forces, unlike many other switchable adhesive grippers [1].

The pull-off forces and tensile works are expected to vary with the MR fluid, due to different MR fluids having different properties, as documented in Table 1. To see the effect of MR fluid on the adhesion, we did the same characterization experiments for two different MR fluids, 122EG and 140CG. The representative curves are shown in Fig. S2. A gripper filled with 140CG fluid had much smaller pull-off force than a gripper filled with 122EG. The high viscosity and solid content of the 140CG fluid makes withdrawing it difficult: the fluid does not move smoothly inside the gripper during the withdrawal. With 140CG, all pull-off forces were observed to be less than 1 N. We conclude that the viscosity of the MR fluid is a highly critical parameter for successful gripping, because (a) the viscosity limits how quickly the fluid can be withdrawn from the cavity; and (b) high viscosity is related to high solid content, which can result in agglomeration of the magnetic particles at the inlet, clogging the inlet.

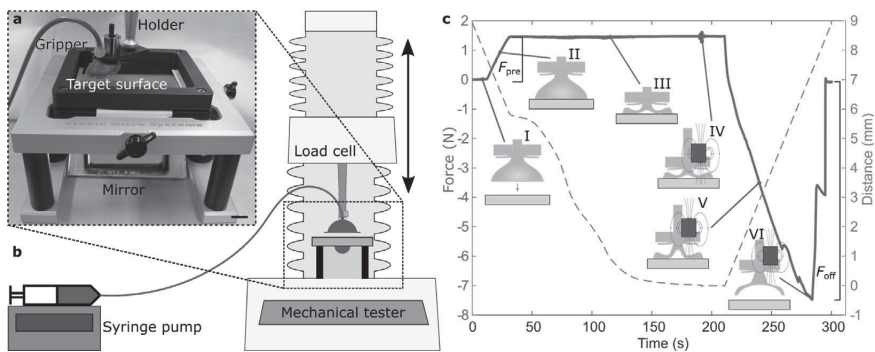


Fig. 2. Pull-off force measurement method schematic and details. (a) Photograph of the experimental setup and (b) schematic. Experimental setup includes a syringe pump with a MR fluid and the gripper attached to a load cell of the mechanical tester. The target surface under the gripper is mounted to a holder containing a mirror for observing the attachment of the gripper during the experiment. Scale bar in the photograph: 1 cm. (c) An example of the measurement data. (I) The gripper approaches the target surface. (II) Once in contact, a preload force F_{pre} of 1.47 N is applied. (III) A volume V of the MR fluid is withdrawn while maintaining the preload. In this example, $V = 1.5$ ml and the fluid is 122EG. To maintain the preload while the gripper collapses, the controller decreases the distance as can be seen in the distance curve. (IV) The magnet is placed on top of the gripper. (V) The gripper retracts from the surface. (VI) The gripper comes off from the surface and the pull-off force F_{off} is measured. In this example, $F_{off} = 7.47$ N. The pull-off is not instantaneous but several peaks can be seen, due to parts of the film detaching at different times, until the gripper comes off completely.

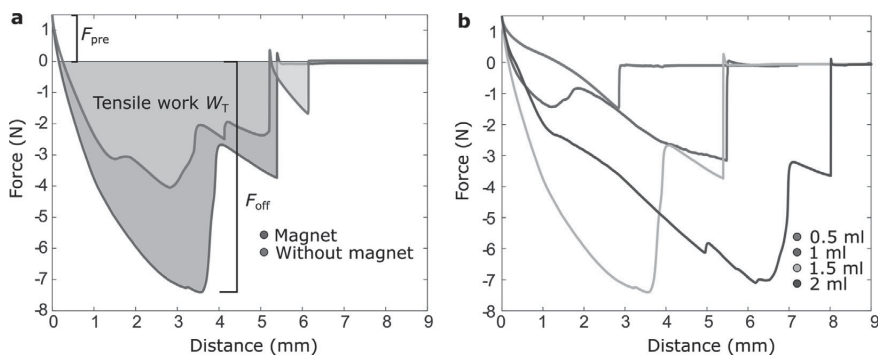


Fig. 3. (a) Representative force–distance curves for the tensile part of the characterization experiment with and without the magnet. The retraction speed is 0.1 mm/s after constant preload F_{pre} of 1.47 N. The force needed for complete detachment is called F_{off} (here 4.05 N without magnetic field and 7.41 N with magnetic field applied). The area under the curve represents the tensile work W_T needed for detachment (here $W_T = 13.65$ mJ without magnetic field and 24.39 mJ with magnetic field applied). (b) Representative force–distance curves with different volumes V of fluid withdrawn (fluid:122EG). The magnetic field was applied in all these experiments.

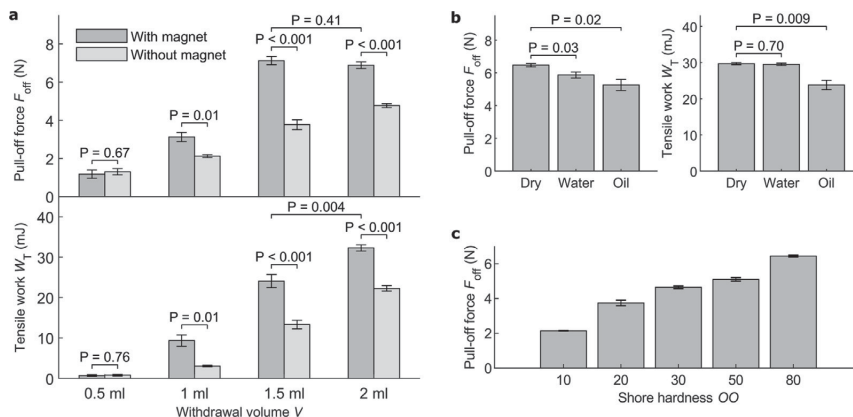


Fig. 4. Characterization of the gripper. (a) Pull-off forces and tensile works for the gripper with different withdrawal volumes (fluid: 122EG). (b) Pull-off forces and tensile works for different surface conditions: dry, deionized water and heavy mineral (MR fluid: 122EG, $V = 1.5$ ml). (c) Pull-off forces for the gripper with objects with different softness. The error bars show standard error ($n = 5$) and the P-values are calculated using Welch's unequal variances t-test.

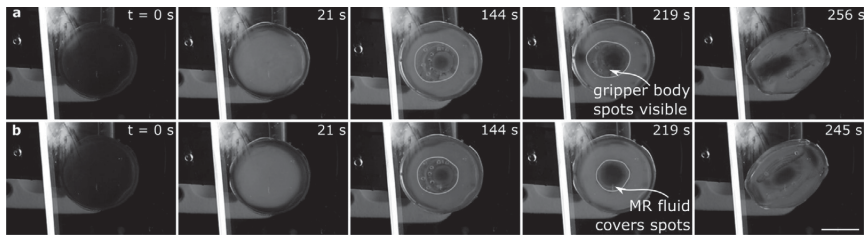


Fig. 5. The behavior of the soft film of the 3D-printed gripper. Snapshots of the video showing the film of the gripper (a) under magnetic field and (b) without magnetic field. Orange circle indicates where the soft gripper body touches the soft film during the retraction. The body collapses against the film when the fluid is withdrawn. Due to the way the body is manufactured, it has small spots. The spots are clearly visible in some of the photographs. When the spots are visible, we know that there is a thin enough layer of MR fluid between the film and the body to allow the spots to be seen through the fluid. At the 219 s time point, there is a marked difference between (a) and (b): when the magnetic field is applied, the MR fluid does not flow and the body remains collapsed against the film, whereas the fluid can rearrange itself from the edges to the center when magnetic field is applied. Scale bar in all the photographs 1 cm.

Rough surfaces can be challenging for adhesive grippers. To demonstrate that our gripper does not suffer from similar limitations, we picked up a red grapefruit (441 g, Fig. 1c) and a cardboard packet (44 g, Fig. 1i). The red grapefruit was rough ($R_z = 17.7 \mu\text{m}$, measured using an optical profilometer) with a visible pattern. These demonstrations show that the gripper can pick relatively heavy parts even with rough surfaces, which are typical for many everyday objects.

Fragile and thin objects can be difficult for jamming and vacuum grippers because the objects can break, or thin sheets can be sucked into the gripper. To demonstrate that our gripper can handle such objects, we picked up a mango fruit (418 g, $R_z = 9.9 \mu\text{m}$, Fig. 1e) and a thin plastic sheet (0.83 g, Fig. 1h). The gripper did not leave visible print onto the surface of the mango (Fig. 1e inset), even though the load was relatively large, and the surface was delicate and soft. Similarly, the plastic sheet did not show any visible marks, despite being thin.

Further gripping demonstrations included a banana fruit (143 g, Fig. 1f, uneven load/torque), a wetted glass beaker (116 g, Fig. 1g, a practical example of a wet surface), a tape roll (164 g, Fig. 1j, an example of a curved object), and a water bottle (518 g, Fig. 1k, a relatively heavy object). Taking all these demonstrations together, we conclude that the gripper is not highly specific to a particular material or surface type but can robustly pick many different types of everyday objects.

One potential drawback of suction cup grippers is that they might fail to pick objects smaller than the cup diameter, due to no vacuum forming between the film and the object. To see how our gripper fares with such objects, we tested picking disc-shaped objects with progressively smaller diameters (Fig. 1l–n). The smallest disc we could pick was $\varnothing 8 \text{ mm}$, which is already markedly smaller than the cup diameter ($\varnothing 20 \text{ mm}$). These results show that the gripper cannot only pick objects larger than its diameter, but also objects slightly smaller than its diameter.

To confirm that the magnetic field has an effect on the MR fluid inside the gripper and to observe how this affects the detachment of the film from the substrate, we recorded a video of the film detaching from the substrate with and without the external magnetic field applied. Video S1 and snapshots in Fig. 5 show the results. In the video, it can be observed that the fluid moves less when the magnetic field is applied (there is MR fluid in the middle of the gripper without external magnetic field applied). In the snapshots, this is most visible by comparing the snapshots from 219 s to the snapshots from 144 s: with the magnetic field is applied, the shape of the film and the fluid changes less than without the magnetic field. We take these results as an evidence that the magnetic field inhibits the movement of the fluid inside the gripper.

During all the experiments, we observed a few different ways the gripper can fail or break. The bonding between the film

and the gripper body is a critical weak point and can tear (Fig. S3a) when excessive loads are gripped. In future, we aim to improve the film bonding by using different silicone adhesives and bonding surface treatments. Another failure mode is the sedimentation of the MR fluid in the silicone tube (Fig. S3b): if the gripper is unused for a few days, the magnetic particles start to sediment, separating the oil and the iron particles. This failure is not catastrophic, as the particles can be resuspended in the oil by repeatedly withdrawing the fluid from the cavity or by applying strong, varying external magnetic field. Finally, the silicone elastomers are air permeable and in a long period of time (\sim days), some air can be found inside the gripper cavity and the inlet tube. This failure can be remedied by refilling the gripper with the MR fluid.

Table 2 compares the performance of our gripper to some of the grippers previously reported in the literature. Shintake et al. [1] reviewed different soft robotic grippers and grouped different reported grippers whether they are based on actuation, controlled stiffness, or controlled adhesion. To our comparison table, we selected a few representative grippers belonging to each of these groups. For a more thorough review of the literature, we refer to the excellent review by Shintake et al. [1]. Compared to granular jamming and MR fluid jamming gripper, both stiffness-controlled grippers, our gripper can handle objects much heavier than its own mass. Also, unlike jamming grippers, our gripper does not need to completely enclose the target object or part of it. Jamming-based grippers are still faster than the current prototype of our gripper. Currently, the total time of the pick-and-place cycle of our gripper is limited by two different things: (1) it takes approximately 10 s for the syringe pump to withdraw the fluid (1.5 ml) from the cavity; and (2) manually placing the neodymium magnet to apply the magnetic field takes a few seconds. We do not think these are fundamental limitations of our gripper: faster pumps surely exist and MR fluids known to switch states less than in milliseconds [22]. A strong electromagnet could be used to quickly turn on the magnetic field. Typically, adhesion-controlled grippers (e.g., so-called gecko grippers) require the surface to be dry. There are attempts to enhance gecko-inspired adhesives so they adhere under water [27], but such adhesives require complex surface coatings which may degrade over time. Adhesive surfaces also struggle with contaminations, requiring careful consideration how to clean such surfaces to maintain their stickiness [28]. Our gripper does not require the surface to be dry and it is also very easy to clean our gripper, as the gripping surface is just a flat silicone film.

Finally, compared to commercial vacuum grippers, our gripper can handle a larger variety of objects: our proposed gripper, with its thin film, can pick thin films and objects somewhat smaller than its diameter. Wet/oily surfaces are also challenges

Table 2
Comparison of few proposed gripping methods to fabricated gripper with MR fluid.

Gripper type	Ref.	Max. Preload (N)	Gripper diameter (mm)	Max. Pull-off force (N)	Max. lifting ratio ^a	Diameter ratio limits ^b	Surface conditions			Max. Surface roughness tested R_z (μm)	Time to acquire grip (s)	Power required to maintain grasp (W)
							Dry	Watery	Oily			
Granular jamming	[16]	150	86	100	?	0.1–0.85	Yes	?	?	?	0.1–1.1	^c
MR fluid jamming	[20]	40	108	50	1.7	0.2–0.4	Yes	?	?	?	<0.1	75
Bioinspired suction gripper	[2]	0.5–1	9–14 ^d	3.3	3.9	>2 ^e	Yes	Yes	Yes	36.5	20 ^f	?
Magnet-embedded suction cup	[29]	0.3	10	0.9	?	>3	Yes	Yes	Yes	?	140 ^g	0
Same size commercial suction cup for uneven workpieces	[30]	?	20	11	>48	>1	Yes	Yes ^h	Yes ^h	?	<0.1 ⁱ	^c
Gecko-inspired gripper	[31]	?	180 ^j	43	200	>0.5 ^k	Yes	?	?	?	<0.1	0
This work		1.5	20	7.5	80	>0.4	Yes	Yes	Yes	17.7	10	0

^aObject mass/gripper mass.

^bObject diameter/gripper diameter.

^cPower the vacuum unit needs.

^dDiameter of a single suction cup.

^eEstimated from Fig. 5 in [2].

^fEstimated from the video in [2].

^gEstimated from the video in [29].

^hSeparated filtering system for liquids is needed.

ⁱDepends the vacuum system used.

^jEstimated from the Fig. 1 in [30].

^kEstimated from the Figures in [31].

to traditional open vacuum grippers, as liquids may contaminate the vacuum line. One advantage of our gripping method is that the film seals the fluidic line completely from the environment.

4. Conclusion

We have demonstrated a magnetically switchable soft suction gripper which can handle a wide range of fragile and complex 3D objects and surfaces. The switching mechanism is based on a magnetorheological fluid, which allows the gripper to stiffen under the presence of an external magnetic field. The gripper can handle over 7 N loads while the diameter of the gripper is only ~20 mm.

We envision that our gripper will be particularly useful for future packaging and warehouse applications, which typically involve gripping many different types of objects. The strength of our gripper in such applications is that it can pick rough, soft, wet, oily and curved surfaces and objects of various sizes. Another advantage of our gripper is that the gripping force can be carefully controlled: delicate light objects could be gripped with small suction and without the magnetic field, while heavy objects can use a combination of strong suction and magnetic field.

Another potential future application of our gripper is in industrial assembly. When soft, our gripper can conform to the shape of the object, allowing greater tolerances during picking and releasing. High precision tasks e.g. precision assembly will benefit from the gripper being in rigid state. Our proposed gripper design may also simplify the overall system complexity, by reducing the need for carefully measuring the object position before picking, or even by completely eliminating the need for visual feedback during picking.

Finally, our gripper is light-weight, relatively easy to fabricate, and can tolerate alignment errors during picking. These aspects suggest it will be feasible to use several of such grippers in parallel: multiple grippers picking multiple objects simultaneously. Every gripper would not need its own fluid line and magnet, but a single line and a magnet could be shared by several grippers. In parallel operation, our gripper has potential to greatly increase the throughput of industrial pick-and-place operations.

Declaration of competing interest

The authors declare that they have no known competing financial interests or personal relationships that could have appeared to influence the work reported in this paper.

Acknowledgments

M. Sitti and V. Sariola conceived the research. All authors contributed to the planning of the research. A. Koivikko and D.-M. Drotlef designed the gripper. A. Koivikko fabricated the gripper and did the characterization and demonstration experiments. A. Koivikko and V. Sariola wrote the paper together with inputs from all authors. We thank Marika Janka for measuring the surface roughness values. This work was funded by the Academy of Finland projects #299087 and #306999, Pirkanmaan Kulttuurirahasto grant "Robots and Us", the Finnish Science Foundation for Technology and Economics, the Max Planck Society, Germany, and European Research Council (ERC) Advanced Grant SoMMoR project with grant no. 834531.

Appendix A. Supplementary data

Supplementary material related to this article can be found online at <https://doi.org/10.1016/j.eml.2021.101263>.

References

- [1] J. Shintake, V. Caccuciolo, D. Floreano, H. Shea, Soft robotic grippers, *Adv. Mater.* 30 (29) (2018) 1707035, <http://dx.doi.org/10.1002/adma.201707035>.
- [2] B. Mazzolai, et al., Octopus-inspired soft arm with suction cups for enhanced grasping tasks in confined environments, *Adv. Intell. Syst.* 1 (6) (2019) 1900041, <http://dx.doi.org/10.1002/aisy.201900041>.
- [3] T. Takahashi, M. Suzuki, S. Aoyagi, Octopus bioinspired vacuum gripper with micro bumps, in: 2016 IEEE 11th Annual International Conference on Nano/Micro Engineered and Molecular Systems, NEMS 2016, pp. 508–511, <http://dx.doi.org/10.1109/NEMS.2016.7758301>.
- [4] S. Song, D.-M. Drotlef, C. Majidi, M. Sitti, Controllable load sharing for soft adhesive interfaces on three-dimensional surfaces, *Proc. Natl. Acad. Sci. USA* 114 (22) (2017) E4344–E4353, <http://dx.doi.org/10.1073/pnas.1620344114>.
- [5] J. Shintake, S. Rosset, B. Schubert, D. Floreano, H. Shea, Versatile soft grippers with intrinsic electroadhesion based on multifunctional polymer actuators, *Adv. Mater.* 28 (2) (2016) 231–238, <http://dx.doi.org/10.1002/adma.201504264>.
- [6] S. Song, M. Sitti, Soft grippers using micro-fibrillar adhesives for transfer printing, *Adv. Mater.* 26 (28) (2014) 4901–4906, <http://dx.doi.org/10.1002/adma.201400630>.
- [7] V. Sariola, M. Sitti, Mechanically switchable elastomeric microfibrillar adhesive surfaces for transfer printing, *Adv. Mater. Interfaces* 1 (4) (2014) 1300159, <http://dx.doi.org/10.1002/admi.201300159>.
- [8] S. Song, D.-M. Drotlef, J. Paik, C. Majidi, M. Sitti, Mechanics of a pressure-controlled adhesive membrane for soft robotic gripping on curved surfaces, *Extreme Mech. Lett.* 30 (2019) 100485, <http://dx.doi.org/10.1016/j.eml.2019.100485>.
- [9] F. Ilievski, A.D. Mazzeo, R.F. Shepherd, X. Chen, G.M. Whitesides, Soft robotics for chemists, *Angew. Chem. - Int. Ed.* 50 (8) (2011) 1890–1895, <http://dx.doi.org/10.1002/anie.201006464>.
- [10] H. Zhao, K. O'Brien, S. Li, R.F. Shepherd, Optoelectronically innervated soft prosthetic hand via stretchable optical waveguides, *Sci. Robot.* 1 (1) (2016) eaai7529, <http://dx.doi.org/10.1126/scirobotics.aai7529>.
- [11] A. Koivikko, et al., Screen-printed curvature sensors for soft robots, *IEEE Sens. J.* 18 (1) (2017) 223–230, <http://dx.doi.org/10.1109/JSEN.2017.2765745>.
- [12] A. Elsayes, A. Koivikko, V. Sariola, Tactile electronic skin based on conductive fabric for robotic hand applications, in: *Proceedings of IEEE Sensors*, Vol. 2019–October, 2019, pp. 1–4, <http://dx.doi.org/10.1109/SENSOR43011.2019.8956811>.
- [13] D. McCoul, S. Rosset, N. Besse, H. Shea, Multifunctional shape memory electrodes for dielectric elastomer actuators enabling high holding force and low-voltage multisegment addressing, *Smart Mater. Struct.* 26 (2) (2017) 025015, <http://dx.doi.org/10.1088/1361-665X/26/2/025015>.
- [14] M. Yunusa, G.J. Amador, D.-M. Drotlef, M. Sitti, Wrinkling instability and adhesion of a highly bendable gallium oxide nanofilm encapsulating a liquid-gallium droplet, *Nano Lett.* 18 (4) (2018) 2498–2504, <http://dx.doi.org/10.1021/acs.nanolett.8b00164>.
- [15] Z. Ye, G.Z. Lum, S. Song, S. Rich, M. Sitti, Phase change of gallium enables highly reversible and switchable adhesion, *Adv. Mater.* 28 (25) (2016) 5088–5092, <http://dx.doi.org/10.1002/adma.201505754>.
- [16] J.R. Amend, E. Brown, N. Rodenberg, H.M. Jaeger, H. Lipson, A positive pressure universal gripper based on the jamming of granular material, *IEEE Trans. Robot.* 28 (2) (2012) 341–350, <http://dx.doi.org/10.1109/TRO.2011.2171093>.
- [17] J. Amend, N. Cheng, S. Fakhouri, B. Culley, Soft robotics commercialization: Jamming grippers from research to product, *Soft Robot.* 3 (4) (2016) 213–222, <http://dx.doi.org/10.1089/soro.2016.0021>.
- [18] A. Pettersson, S. Davis, J.O. Gray, T.J. Dodd, T. Ohlsson, Design of a magnetorheological robot gripper for handling of delicate food products with varying shapes, *J. Food Eng.* 98 (3) (2010) 332–338, <http://dx.doi.org/10.1016/j.jfoodeng.2009.11.020>.
- [19] T. Nishida, Y. Okatani, K. Tadakuma, Development of universal robot gripper using MR α fluid, *Int. J. Humanoid Robot.* 13 (4) (2016) 1–13, <http://dx.doi.org/10.1142/S0219843616500171>.
- [20] C.M. Hartzell, Y.T. Choi, N.M. Wereley, T.J.G. Leps, Performance of a magnetorheological fluid-based robotic end effector, *Smart Mater. Struct.* 28 (3) (2019) 035030, <http://dx.doi.org/10.1088/1361-665x/aafe2b>.
- [21] S. Song, D.-M. Drotlef, D. Son, A. Koivikko, M. Sitti, Suction-based soft robotic gripping of rough and irregular parts, 2020, <http://arxiv.org/abs/2009.08156>.
- [22] J. de Vicente, D.J. Klingenberg, R. Hidalgo-Alvarez, Magnetorheological fluids: a review, *Soft Matter* 7 (2011) 3701–3710, <http://dx.doi.org/10.1039/c0sm01221a>.
- [23] K. McDonald, A. Rendos, S. Woodman, K.A. Brown, T. Ranzani, Magnetorheological fluid-based flow control for soft robots, *Adv. Intell. Syst.* 2 (11) (2020) 2000139, <http://dx.doi.org/10.1002/aisy.202000139>.
- [24] J. Cramer, M. Cramer, E. Demeester, K. Kellens, Exploring the potential of magnetorheology in robotic grippers, in: *Procedia CIRP*, Vol. 76, 2018, pp. 127–132, <http://dx.doi.org/10.1016/j.procir.2018.01.038>.
- [25] S. Kashima, F. Miyasaka, K. Hirata, Novel soft actuator using magnetorheological elastomer, *IEEE Trans. Magn.* 48 (4) (2012) 1649–1652, <http://dx.doi.org/10.1109/TMAG.2011.2173669>.
- [26] M. Lanzetta, K. Iagnemma, Gripping by controllable wet adhesion using a magnetorheological fluid, *CIRP Ann. - Manuf. Technol.* 62 (1) (2013) 21–25, <http://dx.doi.org/10.1016/j.cirp.2013.03.002>.
- [27] H. Lee, B.P. Lee, P.B. Messersmith, A reversible wet/dry adhesive inspired by mussels and geckos., *Nature* 448 (2007) 338–341, <http://dx.doi.org/10.1038/nature05968>.
- [28] Y. Mengüç, M. Röhrig, U. Abusomwan, H. Hölscher, M. Sitti, Staying sticky: Contact self-cleaning of gecko-inspired adhesives, *J. R. Soc. Interface* 11 (94) (2014) <http://dx.doi.org/10.1098/rsif.2013.1205>.
- [29] H. Iwasaki, F. Lefevre, D.D. Damian, E. Iwase, S. Miyashita, Autonomous and reversible adhesion using elastomeric suction cups for in-vivo medical treatments, *IEEE Robot. Autom. Lett.* 5 (2) (2020) 2015–2022.
- [30] Schmalz, Bell suction cup (round) SPB4 20 SI-55 G1/8-AG Datasheet. 1–3.
- [31] E.W. Hawkes, D.L. Christensen, A.K. Han, H. Jiang, M.R. Cutkosky, Grasping without squeezing: Shear adhesion gripper with fibrillar thin film, in: *Proceedings - IEEE International Conference on Robotics and Automation*, 2015, pp. 2305–2312, <http://dx.doi.org/10.1109/ICRA.2015.7139505>.

PUBLICATION IV

Screen-Printed Curvature Sensors for Soft Robots

Anastasia Koivikko, Ehsan Sadeghian Raei, Mahmoud Mosallaei, Matti Mäntysalo
and Veikko Sariola

IEEE Sensors Journal, 18, 1, 223-230
10.1109/JSEN.2017.2765745

Publication reprinted with the permission of the copyright holders.

Screen-Printed Curvature Sensors for Soft Robots

Anastasia Koivikko, Ehsan Sadeghian Raei, Mahmoud Mosallaei, Matti Mäntysalo¹, *Member, IEEE*,
and Veikko Sariola², *Member, IEEE*

Abstract—Castable elastomers have been used to fabricate soft robotic devices and it has been shown that the technique scales well from prototyping to mass manufacturing. However, similarly scalable techniques for integrating strain or curvature sensors into such devices are still lacking. In this paper, we show that screen-printed silver conductors serve well as curvature sensors for soft robotic devices. The sensors are produced onto elastomer substrates in a single printing step and integrated into soft pneumatic actuators. We characterized the resistance-curvature relationship of the sensors, which allows the curvature of the actuators to be estimated from the sensor measurements. Hysteresis was observed, which does limit the absolute accuracy of the sensors. However, temperature characterizations showed that the sensor measurements are not significantly affected by temperature fluctuations during normal operation. Dynamic experiments showed that the bandwidth of the sensors is larger than the bandwidth of the actuators. We experimentally validated that these sensors can be used to detect whether the motion of an actuator has been blocked, clearing the way toward simple-to-fabricate soft robots that react to their surroundings. Finally, we demonstrate a three-fingered soft robotic gripper with integrated sensors. We conclude that screen-printing is a promising way to integrate curvature sensors into soft robots.

Index Terms—Mechanical sensors, flexible printed circuit, soft robotics, strain measurement.

I. INTRODUCTION

SOFT robots [1]–[4] made of easily deformable materials are a recent innovation with promising applications in manipulators/grippers [2], [5]–[7], mobile robots [8]–[10], exoskeletons/rehabilitation [11] and monitoring human motion [12]. Soft actuators have been made by embedding small fluidic channels in an elastomer, and then inflating them by gas [2], [13], [14] or liquid [15]. The quick, monolithic fabrication technique of casting elastomers into 3D printed molds has enabled the rapid prototyping of different soft robot designs [2], [10], [16], and this technique scales well for mass manufacturing. However, in their simplest form,

the fluidic actuators do not include any strain or curvature sensors. Such sensors would enable closed-loop position control or the ability to detect whether an obstacle is blocking the motions of the robot.

The first approach to integrating sensors into soft robots was to embed commercially available bending sensors [17], [18] or custom-designed sensor modules [19] into the casting/assembly. However, this approach is not ideal as the sensor design cannot be adapted quickly to new robot designs. The second approach was to fabricate flexible/stretchable sensors [20]–[23] as needed. Flexible or stretchable strain sensors based on carbon [24], carbon black particles [25], liquid metals [12], [26], and silver nanowires [27], [28] have all been proposed. In particular, carbon nanotubes [29], hydrogels [30], liquid metals [31] and optical sensing [32], [33] have been utilised for curvature sensing in soft fluidic actuators. However, many of these examples involve multistep fabrication or materials which are difficult to handle, so they are not suitable for mass manufacturing. There is still a clear need for a simple, low-cost and scalable method for manufacturing sensors for soft robots.

Printed electronics as an additive manufacturing method is a good candidate to fulfill these needs. Functional materials have been printed to fabricate flexible circuits [34], temperature sensors [35] and electrodes [36]. Screen-printing, in particular, is the most common printing method used in electronics. Screen-printing is one of the oldest printing technologies in existence, originating in China over a thousand years ago. Today, screen-printing is applied not only in electronics, but also in textiles, signs, product labels and many other products. Consequently, screens, inks and automated printing machines are widely available.

Recently, our coauthors have shown that screen-printing with conductive inks can be used to produce stretchable conductors directly onto elastomer substrates [37]. Here we show that these conductors, printed in a single step, can serve as resistive curvature sensors for soft robots. These sensors yield information about the true curvature of a soft robotic actuator within the limits of the hysteresis and the creep of the sensor. By creep, we mean slow change observed in the sensor output, even when the actuator is not moving. The main advantages of these sensors are that they: a) can be fabricated in a matter of hours; b) require only a little extra effort in the fabrication of the actuators; and c) are based on widely available equipment and materials.

II. MATERIALS AND METHODS

A. Overview of the Fabrication Method

The fabrication method is illustrated in Fig. 1. Conductive ink was added onto a screen lying on a

Manuscript received August 28, 2017; revised October 6, 2017; accepted October 6, 2017. Date of publication October 23, 2017; date of current version December 7, 2017. This work was supported by the Academy of Finland, under Project 299087, Project 306999, Project 288945, and Project 294119. The associate editor coordinating the review of this paper and approving it for publication was Prof. Subhas C. Mukhopadhyay. This paper was presented at the IEEE Sensors 2017 Conference, Glasgow, U.K. (A. Koivikko and E. Sadeghian Raei contributed equally to this work.) (Corresponding author: Veikko Sariola.)

A. Koivikko, E. Sadeghian Raei, and V. Sariola are with the Faculty of Biomedical Sciences and Engineering, BioMediTech Institute, Tampere University of Technology, 33720 Tampere, Finland (e-mail: veikko.sariola@tut.fi).

M. Mosallaei and M. Mäntysalo are with the Laboratory of Electronics and Communications Engineering, Tampere University of Technology, 33720 Tampere, Finland (e-mail: matti.mantysalo@tut.fi).

This paper has supplementary downloadable multimedia material available at <http://ieeexplore.ieee.org> provided by the authors. The Supplementary material contains a video showing a three-fingered soft robotic gripper with screen-printed silver ink sensors. This material is 1.58 MB in size.

Digital Object Identifier 10.1109/JSEN.2017.2765745

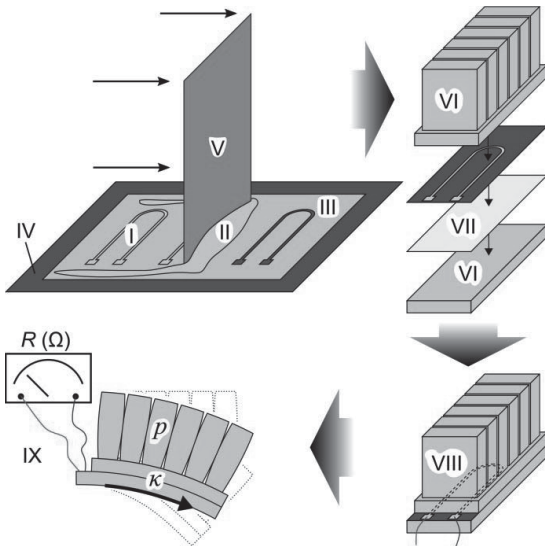


Fig. 1. The concept of soft actuators with sensors. The sensors (I) are screen-printed by applying a resistive silver or carbon ink (II) on a screen (III) lying on top of a polyurethane elastomer substrate (IV). The ink is spread by a squeegee (V). By assembling a stack of silicone components (VI), a fiberglass strain-limiting layer (VII) and a sensor, a smart pneumatic actuator (VIII) is produced. The actuator is pressurized with the pressure p . The measuring resistance R (IX) gives the curvature κ of the actuator.

thermoplastic polyurethane elastomer sheet. The ink is transferred to the substrate through a mesh, except in the areas covered by a stencil.

In a single step, we fabricate a shape with two pads and a long, conductive path (Fig. 2a). We used a silver flake-based ink for the sensors. A photograph of the screen-printing process is shown in Fig. 2b. After printing, the sensors are wired, cut and integrated into the pneumatic actuators. The actuator consists of two parts: an upper part with pneumatic chambers and a base with a strain-limiting layer (fiberglass). Upon pressurizing, the pneumatic chambers expand, resulting in the bending of the actuator. The sensors are stacked on top of the strain-limiting layer before the assembly of the actuator. Resistance measurement can be used to estimate the curvature κ of the actuator. Photographs of the fabricated silver sensors and actuators are shown in Fig. 2 c-d. A scanning electron micrograph (Fig. 2e) shows the flaked structure of the screen-printed silver. The stretchability of these conductors comes from this microstructure [37].

B. Fabrication of the Curvature Sensors

The sensors were fabricated on thermoplastic polyurethane substrate (Epurex Platilon / U4201), which is a stretchable, abrasion resistant, chemically inert, 50 μm thick, transparent sheet. Most of the results in this paper were done using silver ink (ECM / CI-1036), but we also tested carbon ink (ECM / CI-2051) for comparison. The silver ink had a quoted sheet resistance of $< 10 \text{ m}\Omega \text{ sq}^{-1}$ at 25.4 μm and a curing

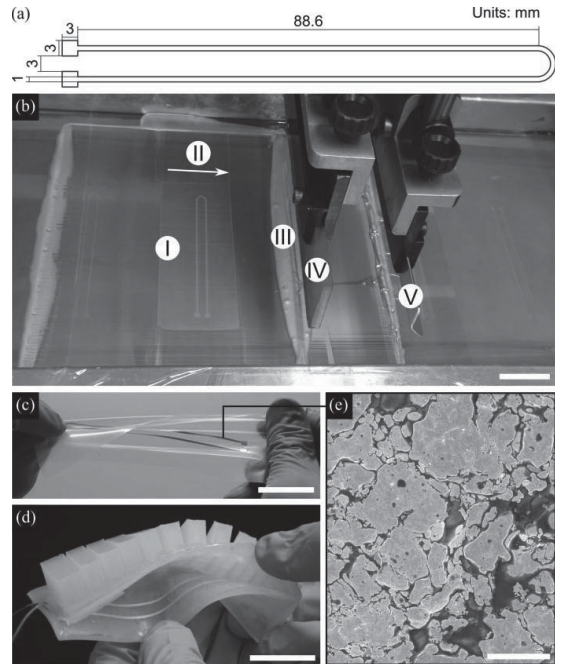


Fig. 2. Fabrication results. (a) Print design of the sensors. Units: mm. (b) Photograph of the screen-printing process. I: Mesh/screen. II: Print direction. III: Silver ink. IV: Rubber squeegee. V: Metal squeegee. (c) Photograph of the sensor. (d) Photograph of the actuator. Scale bars in all photographs: 3 cm. (e) Scanning electron micrograph of the screen-printed silver sensors. The light areas are silver flakes and the darker background is polymer. Scale bar: 10 μm .

temperature of 120°C for 10 minutes, which is lower than the softening range of the elastomer. The carbon ink had a quoted sheet resistance of $< 40 \Omega \text{ sq}^{-1}$ at 25.4 μm . The screens (Finnseri Oy) had a mesh count of 79 threads cm^{-1} and a mesh opening of 69 μm^{-1} .

The screen-printing starts by slightly stretching the substrate and attaching it to an aluminum plate. The substrates are then cleaned with isopropyl alcohol. The printing is done in two continuous printing cycles by a semi-automatic screen-printing machine (TIC / SCF-300). The process is completed with an oven annealing (silver ink: 30 min at 125 °C, and carbon: 10 min at 90 °C). The annealing temperature and time were increased for the silver due to the heat absorption of the aluminum carriers [35]. The sheet resistances of the silver and carbon traces (measured after the annealing) are approximately 45 $\text{m}\Omega \text{ sq}^{-1}$ and 300 $\Omega \text{ sq}^{-1}$, respectively. Finally, wires are attached to the pads of the conductive print using silver paint (MG Chemicals / 8331-14G).

C. Fabrication of the Soft Pneumatic Actuators

The pneumatic actuator design is from Mosadegh *et al.* [14] and detailed drawings can be found in the Soft Robotics Toolkit (<http://softroboticstoolkit.com/>) [16]. We cast silicone (Smooth-On / Dragon skin 30. Shore A hardness: 30)

into 3D-printed plastic molds. The actuator consists of an upper part, with the pneumatic chambers, and a lower part, the base. The base is a stack of several layers: Dragon Skin 30, a fiberglass strain limiting layer, a sensor on polyurethane facing away from the fiberglass, and another layer of Dragon Skin 30. We bonded all the parts using a silicone adhesive.

In our initial trials, when we placed the sensor on the outer bottom wall of the actuator, the sensors delaminated easily. In our final design, the sensors were placed inside the actuator to avoid this delamination. The last layer of Dragon Skin 30 on the sensors prevents slipping and delamination of the sensors while the actuators are moving.

D. Resistance Measurements

We measured the resistance R of the sensors using a digital multimeter (National Instruments / USB-4065). Multichannel strain measurements were made using a strain/bridge input module (National Instruments / NI-9237). For the bridge measurements, 100 Ω or 102 Ω resistors were added in series with the sensors, while the quarter-bridge was made into a half-bridge with 120 Ω resistors.

E. Pressure Control

The fluidic control board was based on the instructions from the Soft Robotics Toolkit (<http://softroboticstoolkit.com/>) [16]. Briefly, solenoid valves were driven by an Arduino microcontroller using pulse-width modulation at 56 Hz. The pressure p was controlled by changing the duty cycle of the valves. Pressure sensors measured the pressure p at the control board. Supply pressure was from a regulator at ~ 2 bar.

F. Curvature Measurements

The actuator was mounted on an aluminum frame from the air inlet side (Supplementary Fig. 1). A computer-controlled digital camera took photographs. The photographs were saved along with the pressure and resistance data. The images were analyzed by a custom-designed Matlab script, which used an optimization algorithm to find a circular arc that best fit the pixels on the bottom edge of the actuator. The inverse of the arc radius is taken as a measure of the curvature κ . Note that the soft bending actuators do not have constant curvature κ , but it is still a reasonable estimate [38].

G. Temperature Measurements

We used K- and J-type thermocouples to monitor the temperature of the actuator during the experiments.

III. RESULTS AND DISCUSSION

A. Resistance – Curvature Relationship of the Silver Sensors

To characterize the silver sensors, we measured the resistance R and curvature κ while repeatedly cycling the pressure p of the actuator (30 cycles). Each cycle was slow (~ 5 min) to avoid dynamic effects from the viscoelasticity of the elastomers. The results of the measurements are shown in Fig. 3. In the initial state, $R = 15.8 \Omega$, $p = 12$ kPa, and

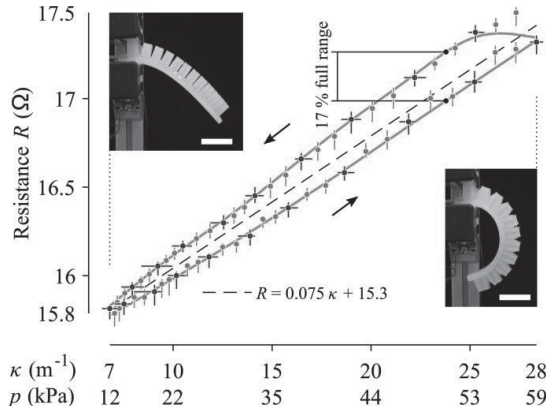


Fig. 3. Resistance R versus curvature κ and pressure p for the silver sensor. Curvature κ was estimated from photographs (insets). The data points are medians of 150 resistance measurements and 30 curvature measurements (blue points). The curvature κ had to be linearly interpolated between frames (gray data points). The error bars show interquartile range. The cycle was repeated 30 times. Scale bars in photographs: 3 cm.

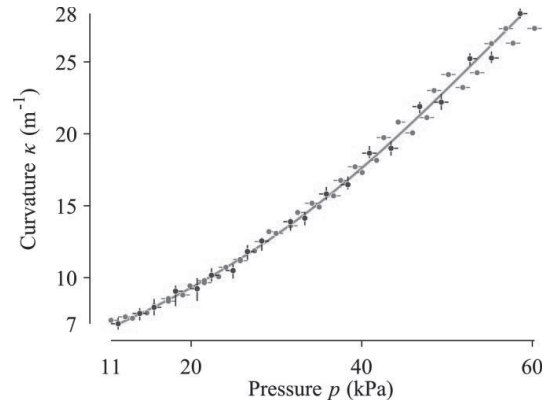


Fig. 4. Pressure-curvature relationship for the actuator used in Fig. 3. The return curve points are slightly above the fitted curve, but the effect is much smaller than in Fig. 3.

$\kappa = 7 \text{ m}^{-1}$. At their peak, $\Delta R = 1.7 \Omega$, $\Delta p = 47 \text{ kPa}$ and $\Delta \kappa = 21 \text{ m}^{-1}$. The sensitivity was $0.075 \Omega/\text{m}^{-1}$.

The relationship between resistance R and curvature κ is linear and hysteretic, with a maximum hysteresis of 17% (Fig. 3). The relationship between pressure p and curvature κ is non-linear and without hysteresis (Fig. 4). This data is consistent with the previous reports of the hysteretic behavior of conductive inks [39]. However, even a linear resistance-curvature model has an R^2 -statistic of 0.92. We conclude that the silver sensor can yield useful proprioceptive information from the actuator, limited by the hysteresis of the sensor material.

Note that the sensor is ~ 90 mm long, while the whole actuator is ~ 110 mm long. Each small segment of the sensor is responsive to local strains and thus to local curvatures of the actuator, but when we measure the total resistance of the sensor, we are measuring the average curvature κ of the

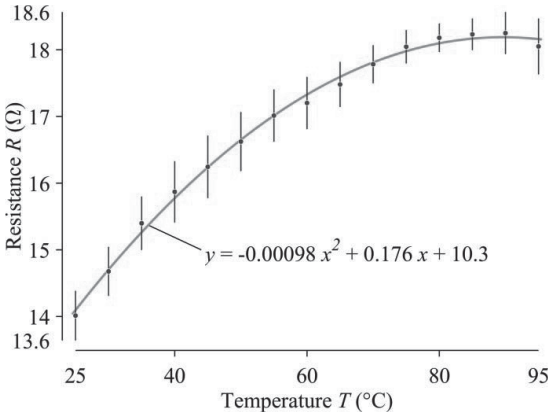


Fig. 5. Resistance R of a silver sensor as a function of the temperature T . Data points are means of six measurements, error bars show standard error.

actuator, except in the small area at the tip not covered by the sensor. In practice, the local curvatures do not deviate much from the average curvature κ for these types of actuators [38].

B. Temperature – Resistance Relationship for the Silver Sensors

The data in Fig. 3 does not rule out that the hysteresis is caused by temperature fluctuations within each cycle. To rule out this possibility, we measured the temperature coefficient of resistance and the normal temperature fluctuations during the experiments. We placed the actuator flat on a hot plate and measured the resistance R as a function of the temperature. The thermocouple was inserted into the pneumatic chamber inside the actuator. The resistance R was recorded at the moment when the temperature was first reached. The results of these measurements are shown in Fig. 5. The temperature coefficient of the resistance is $(dR/dT)/R|_{T=20\text{ }^\circ\text{C}} \approx 0.01\text{ }^\circ\text{C}^{-1}$, which is slightly higher than the temperature coefficient of pure silver: $0.0038\text{ }^\circ\text{C}^{-1}$.

To see if this could contribute to the hysteresis in our cycling experiments, we measured the temperature fluctuations of the air entering or leaving the actuator. The air temperature was taken from the air entering / exiting the actuator, right next to the inlet. The results (Fig. 6) show that during the first cycle, the air heated up from $25.0\text{ }^\circ\text{C}$ to $25.7\text{ }^\circ\text{C}$, but after the first few cycles, the temperature fluctuations are within $\Delta T \approx 0.3\text{ }^\circ\text{C}$. These fluctuations are caused by our pressure controller, and the estimated contribution to resistance change is $(dR/dT)\Delta T \approx 0.04\text{ }\Omega$. Thus, we conclude that the air temperature fluctuations cannot be the dominant effect to explain the hysteresis in Fig. 3.

C. Linear Strain Estimates

To estimate the linear strain ε for our silver sensors, our first approach was to use the ideal bending relationship

$$\Delta\varepsilon = d\Delta\kappa, \quad (1)$$

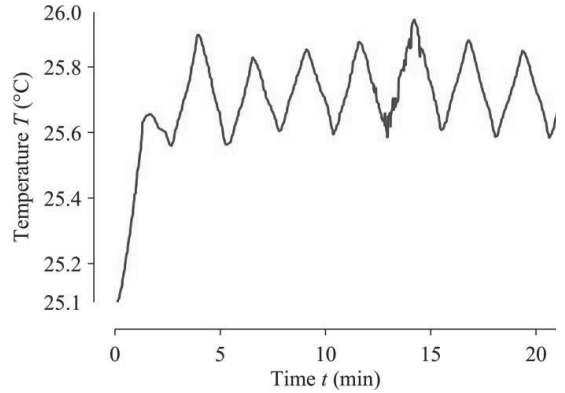


Fig. 6. Temperature fluctuations during the cycling experiment in Fig. 3.

where d is the distance from the neutral plane. Assuming that the neutral plane is half-way through the fiberglass, the stack between the sensor and neutral plane is: fiberglass ($d = 125\text{ }\mu\text{m}$, half of the nominal thickness), silicone adhesive (we take $d = 500\text{ }\mu\text{m}$, but this is difficult to measure and varies from one sample to another) and polyurethane ($d = 50\text{ }\mu\text{m}$, nominal), the total distance from the neutral plane is $d = 675\text{ }\mu\text{m}$. Thus, using (1), we estimate $\Delta\varepsilon \approx 675\text{ }\mu\text{m} \cdot 21\text{m}^{-1} \approx 1\%$. Our second approach was to use ΔR and the previously reported [37] small-strain gauge factor of $GF \approx 5.759$ and the relationship

$$\Delta\varepsilon = \frac{\Delta R}{R \cdot GF}, \quad (2)$$

to estimate $\Delta\varepsilon \approx 2\%$. Because of the difficulties of measuring the thickness of the soft sensor stack and the distance from the neutral plane d , we consider the resistance-based estimate of 2% strains to be more trustworthy.

D. Carbon Sensors

To show that our approach is not limited to silver-based inks, we also tested printing the sensors using carbon-based inks. The resistance-curvature characterization for the actuator with a carbon sensor is shown in Fig. 7. Due to the specific resistance of the ink being higher, the absolute resistances are also higher; in a neutral state, the resistance $R_{\text{carbon}} = 56.5\text{ k}\Omega$. The sensitivity of the carbon sensor was $0.31\text{ k}\Omega/\text{m}^{-1}$, and the maximum hysteresis 27%. Compared to the silver sensors, there is more non-linearity and creep in the carbon sensors, which is why we focused on the silver sensors in our studies. Nevertheless, a linear resistance-curvature model still has a R^2 -statistic of 0.64, supporting our claim that carbon sensors can also be used to estimate the bending of the actuator.

E. Decoupling Pressure Contribution From the Curvature Measurement

We then checked whether the pressure changes make a direct contribution to the silver sensor measurements. We measured the curvature κ , resistance R and pressure p in four different states (Fig. 8), where the actuator was bent or prevented

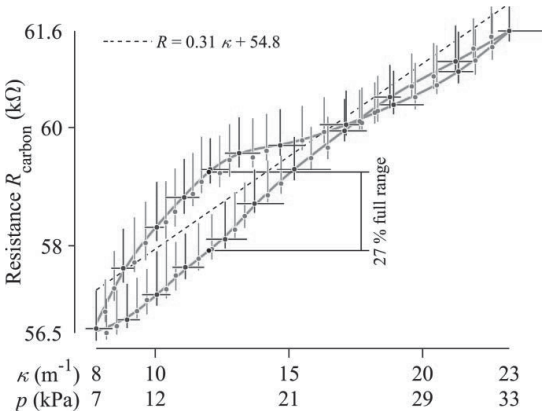


Fig. 7. Resistance R_{carbon} versus curvature κ and pressure p for the carbon sensor. Data points are medians of 150 resistance measurements and 30 curvature measurements (blue points). The curvature was interpolated for the gray data points. The error bars show interquartile range.

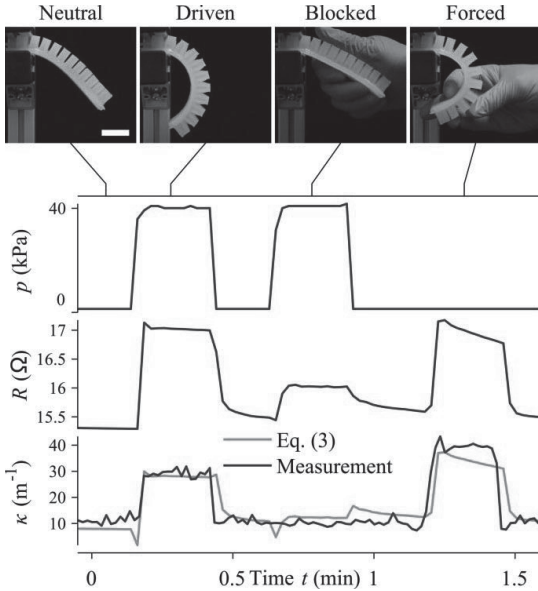


Fig. 8. Pressure p , resistance R and curvature κ recordings from the external blocking experiment. Snapshots are from a video. Scale bar: 3 cm.

from bending by an external force (a hand) in addition to being driven by internal pressure. The resistance measurement is closer to the curvature measurement, but also shows some response to the pressure changes. The underlying reason for the pressure response is that the sensor responds to strains, but during pressurization of the actuator, not all strains are just from ideal bending. Simple linear decoupling found using the method of least-squares

$$\kappa_{\text{estimate}} = \alpha R + \beta p + \gamma, \quad (3)$$

where $\alpha = 17.1 \text{ m}^{-1}\Omega^{-1}$, $\beta = -0.230 \text{ m}^{-1}\text{kPa}^{-1}$ and $\gamma = -254 \text{ m}^{-1}$ yielded the estimate shown in Fig. 8. Thus,

TABLE I
COMPARISON TO LITERATURE

Material /Product	Method ^a	Tested strains (%)	GF ^b	Hyste-resis (%)	Ref.
Silver ink	R	2	6	17	This work
Carbon ink	R	2	7	27	This work
Carbon nanotube ink	R	5	250 ^c	29 ^d	[29]
Gallium-Indium	R	23	2 ^e	5 ^f	[31]
Flex sensor®	R	< 10	7 ^g	13	[17]
Bend sensor®	R	< 10	40 ^g	10	[17]
Ionic hydrogels	C	490	0.7 ^h	-	[30]
Elastomer waveguide	O	100	-	~0	[33]
Polyethylene optical fiber	O	400	-	~0	[32]

^a R = Resistive, C = Capacitive, O = Optical

^b Gauge factor, $\Delta R/(R\epsilon)$ for resistive sensors, $\Delta C/(C\epsilon)$ for capacitive

^c Estimated from Fig. 6a in [29]

^d Estimated from Fig. 9a in [29]

^e Value from [42]

^f Estimated from Fig. 5 in [31]

^g From Table 1 in [17] and using relation $\epsilon = \theta r/L_0$, $L_0 = 50.8 \text{ mm}$, $r = 10 \text{ mm}$

^h Estimated from Fig. 2b in [30]

approximately $\frac{\Delta\kappa}{\alpha\Delta R} \approx 70\%$ of the sensor signal comes from the curvature changes alone. Furthermore, comparing κ_{estimate} to the pressure curve allows the detection of whether the actuator has been blocked or is being forced. We conclude that the sensor is mainly a curvature sensor and an external pressure measurement can be used to decouple the curvature estimate.

F. Dynamic Response of the Actuator and the Sensor

To study the dynamics of the system, we performed step experiments by fully opening or closing the valve, with the supply pressure adjusted to $\sim 50 \text{ kPa}$. Ground truth was recorded using a 50 fps video. Fig. 9 shows the results. The actuator exhibits approximately underdamped, second-order dynamics, with a damping ratio of ~ 0.03 and a damped natural frequency of $\sim 2.8 \text{ Hz}$. This is comparable to the previously reported response times of 130 ms for similar actuators [14]. These oscillations are clearly visible in the sensor signal. However, there is additional slow creep in the sensor, which is not seen in the ground truth. Such creep is typical for elastomer-based sensors and mathematical models have been developed to compensate for it [40]. We conclude that the dynamic response of the sensor is faster than that of the actuator, so the sensor is not limiting the sensor-actuator system bandwidth, but the slow creep limits the absolute accuracy of the sensor.

G. Integrating Sensors Into a Three-Fingered Soft Robotic Gripper

To show a practical application of the smart actuators in soft robots, we fabricated a three-fingered gripper with sensors (Fig. 10). The fingers can be driven independently. One base was shared between the fingers and included the sensors. Fig. 10b shows the gripper picking up an object. Fig. 10c shows snapshots of an experiment where each of the fingers was sequentially actuated (see also the Supplementary Video for the experiment). Fig. 10d shows the resistances

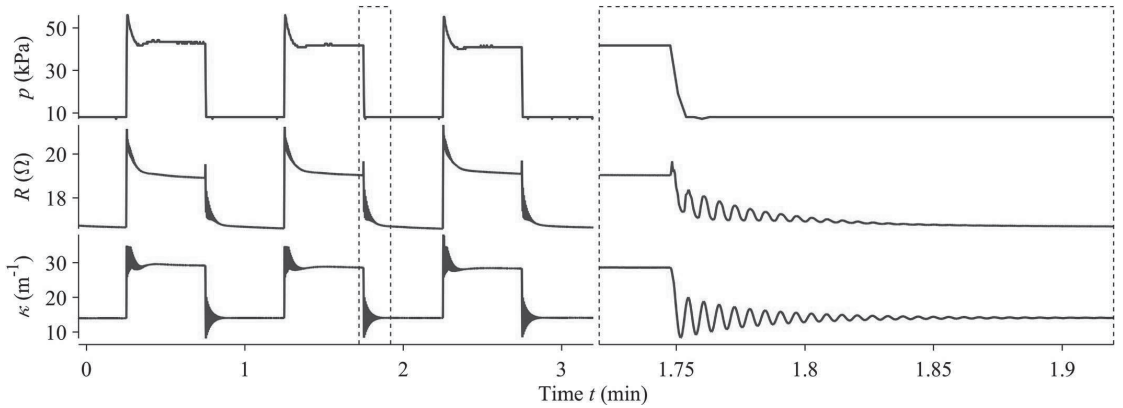


Fig. 9. Dynamics experiment. Several step experiments were done by fully opening or closing the valve. The actuator has approximately second-order dynamics and oscillates at around 2.8 Hz after a pressure step. The oscillations can easily be seen by the sensor, but there is additional slow creep in the sensor.

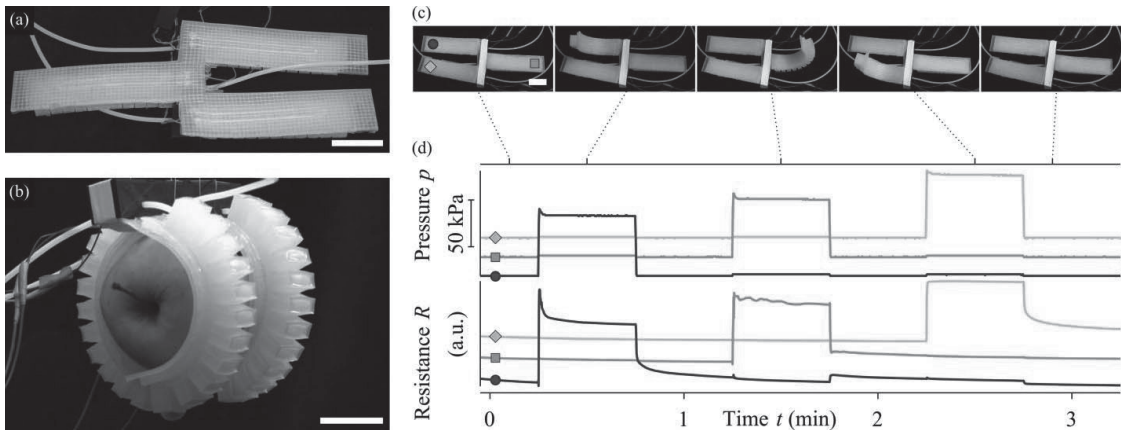


Fig. 10. Demonstration of the fabricated sensors in a soft robotic gripper. (a-b) A three-finger gripper in open and closed state. (c) Snapshots from the supplementary video, showing an experiment where all three fingers are actuated sequentially. (d) Pressure p and resistance R of the fingers during the experiment. Scale bars: 3 cm.

and pressures during the experiment. The channels are mostly independent. This demonstration shows that the sensors can be applied in practical robot designs.

IV. CONCLUSIONS

The screens and inks we used are readily available and the sensors can be printed directly onto elastomeric substrates in a timeframe of hours. Different sensor designs can be achieved simply by changing the screen stencil. The gauge factors, neutral resistances and dynamic characteristics vary from one sample to another, due to variations in the printing runs. We recommend calibrating every sensor individually. Also, the effects of hysteresis, temperature and creep limit the absolute accuracy of the sensors. We foresee using Preisach-type hysteresis models [41] to compensate for the hysteresis. Temperature effects could be reduced by using half-/full-bridge measurements. However, many practical robotic applications do not need absolute accuracy, only relative. For example, only relative

measurement is needed to detect whether a soft robot finger has just collided with an object, as we have demonstrated.

Table I compares our results to the literature in which strain sensors have been applied for soft robotic actuators. In particular, Pinto *et al.* [29] have printed their carbon nanotube-based sensors with the aid of a stencil. Compared to that work, the main advantages of our method are: a) our sensors can be fabricated in a single print, instead of the two prints required in their method; b) using a mesh and a semi-automated screen-printer, the thickness can be controlled better than it can when the ink is applied manually through a stencil.

In Table I, we also see that the hysteresis values reported here are quite typical for resistive sensors. In particular, compared to [29], the hysteresis of our silver sensors was slightly lower. However, optical sensors generally have much lower hysteresis than resistive sensors, so they might be a better choice for applications where high-accuracy absolute measurements are needed. The main advantage of resistive sensing is the ease of measurement.

Finally, Table I shows that the strains we tested are quite low compared to other studies. This is not due to a fundamental limitation of our sensor, but a consequence of the sensor placement in our actuators. Our coauthors have previously shown that the silver ink does not fail, even at 50 % strains [37]. In summary, we have shown that screen-printing is a promising route for the integration of curvature sensors into soft robots. This clears the path towards soft robots that react to their surroundings.

ACKNOWLEDGEMENT

V. S. and M. Mäntysalo conceived the research. Ehsan Sadeghian Raei built the characterization setup. Anastasia Koivikko performed the characterization experiments. Anastasia Koivikko and Ehsan Sadeghian Raei fabricated the actuators. V. S. analyzed the results. M. Mosallaei fabricated the sensors. Anastasia Koivikko, Ehsan Sadeghian Raei, and Veikko Sariola wrote the paper with inputs from all authors. The authors thank Timo Aho for the scanning electron micrograph, and Sampo Tuukkanen, Ville Liimatainen and Pasi Kallio for insightful comments on the draft of this manuscript.

REFERENCES

- [1] D. Trivedi, C. D. Rahn, W. M. Kier, and I. D. Walker, "Soft robotics: Biological inspiration, state of the art, and future research," *Appl. Bionics Biomech.*, vol. 5, no. 3, pp. 99–117, 2008.
- [2] F. Ilievski, A. D. Mazzeo, R. F. Shepherd, X. Chen, and G. M. Whitesides, "Soft robotics for chemists," *Angew. Chem.-Int. Ed.*, vol. 50, no. 8, pp. 1890–1895, 2011.
- [3] C. Majidi, "Soft robotics: A perspective—Current trends and prospects for the future," *Soft Robot.*, vol. 1, no. 1, pp. 5–11, 2013.
- [4] D. Rus and M. T. Tolley, "Design, fabrication and control of soft robots," *Nature*, vol. 521, no. 7553, pp. 467–475, May 2015.
- [5] E. Brown *et al.*, "Universal robotic gripper based on the jamming of granular material," *Proc. Nat. Acad. Sci. USA*, vol. 107, no. 44, pp. 18809–18814, 2010.
- [6] S. Song and M. Sitti, "Soft grippers using micro-fibrillar adhesives for transfer printing," *Adv. Mater.*, vol. 26, no. 28, pp. 4901–4906, 2014.
- [7] R. Deimel and O. Brock, "A novel type of compliant and underactuated robotic hand for dexterous grasping," *Int. J. Robot. Res.*, vol. 35, nos. 1–3, pp. 161–185, 2016.
- [8] K. Suzumori, S. Endo, T. Kanda, N. Kato, and H. Suzuki, "A bending pneumatic rubber actuator realizing soft-bodied manta swimming robot," in *Proc. IEEE Int. Conf. Robot. Autom.*, Apr. 2007, pp. 4975–4980.
- [9] S.-J. Park *et al.*, "Phototactic guidance of a tissue-engineered soft-robotic ray," *Science*, vol. 353, no. 6295, pp. 158–162, 2016.
- [10] R. F. Shepherd *et al.*, "Multigait soft robot," *Proc. Nat. Acad. Sci. USA*, vol. 108, no. 51, pp. 20400–20403, 2011.
- [11] P. Polygerinos, Z. Wang, K. C. Galloway, R. J. Wood, and C. J. Walsh, "Soft robotic glove for combined assistance and at-home rehabilitation," *Robot. Auton. Syst.*, vol. 73, pp. 135–143, Nov. 2015.
- [12] Y. Mengüç *et al.*, "Wearable soft sensing suit for human gait measurement," *Int. J. Robot. Res.*, vol. 33, no. 14, pp. 1748–1764, 2014.
- [13] K. Ogura, S. Wakimoto, K. Suzumori, and Y. Nishioka, "Micro pneumatic curling actuator—Nematode actuator," in *Proc. IEEE Int. Conf. Robot. Biomimetics*, Feb. 2008, pp. 462–467.
- [14] B. Mosadegh *et al.*, "Pneumatic networks for soft robotics that actuate rapidly," *Adv. Funct. Mater.*, vol. 24, no. 15, pp. 2163–2170, 2014.
- [15] R. K. Katzschmann, A. D. Marchese, and D. Rus, "Hydraulic autonomous soft robotic fish for 3D swimming," in *Experimental Robotics*, (Springer Tracts in Advanced Robotics), vol. 109. Cham, Switzerland: Springer, 2016, pp. 405–420.
- [16] D. P. Holland, E. J. Park, P. Polygerinos, G. J. Bennett, and C. J. Walsh, "The soft robotics toolkit: Shared resources for research and design," *Soft Robot.*, vol. 1, no. 3, pp. 224–230, 2014.
- [17] D. H. Kim, S. W. Lee, and H.-S. Park, "Sensor evaluation for soft robotic hand rehabilitation devices," in *Proc. IEEE RAS EMBS Int. Conf. Biomed. Robot. Biomech.*, Jun. 2016, pp. 1220–1223.
- [18] G. Gerboni, A. Diodato, G. Ciuti, M. Cianchetti, and A. Mencassi, "Feedback control of soft robot actuators via commercial flex bend sensors," *IEEE/ASME Trans. Mechatronics*, vol. 22, no. 4, pp. 1881–1888, Aug. 2017.
- [19] S. Ozel, N. A. Keskin, D. Khea, and C. D. Onal, "A precise embedded curvature sensor module for soft-bodied robots," *Sens. Actuators A, Phys.*, vol. 236, pp. 349–356, Dec. 2015.
- [20] M. Amjadi, K.-U. Kyung, I. Park, and M. Sitti, "Stretchable, skin-mountable, and wearable strain sensors and their potential applications: A review," *Adv. Funct. Mater.*, vol. 26, no. 11, pp. 1678–1698, 2016.
- [21] J. C. Yeo and C. T. Lim, "Emerging flexible and wearable physical sensing platforms for healthcare and biomedical applications," *Microsyst. Nanoeng.*, vol. 2, Sep. 2016, Art. no. 16043.
- [22] H. Nakamoto, H. Ootaka, M. Tada, I. Hirata, F. Kobayashi, and F. Kojima, "Stretchable strain sensor with anisotropy and application for joint angle measurement," *IEEE Sensors J.*, vol. 16, no. 10, pp. 3572–3579, May 2016.
- [23] H. Nakamoto, H. Ootaka, M. Tada, I. Hirata, F. Kobayashi, and F. Kojima, "Stretchable strain sensor based on areal change of carbon nanotube electrode," *IEEE Sensors J.*, vol. 15, no. 4, pp. 2212–2218, Apr. 2015.
- [24] J. Shi *et al.*, "Graphene reinforced carbon nanotube networks for wearable strain sensors," *Adv. Funct. Mater.*, vol. 26, no. 13, pp. 2078–2084, 2016.
- [25] C. Mattmann, F. Clemens, and G. Tröster, "Sensor for measuring strain in textile," *Sensors*, vol. 8, no. 6, pp. 3719–3732, 2008.
- [26] E. L. White, J. C. Case, and R. K. Kramer, "Multi-mode strain and curvature sensors for soft robotic applications," *Sens. Actuators A, Phys.*, vol. 253, pp. 188–197, Jan. 2017.
- [27] M. Amjadi, A. Pichitpajongkit, S. Lee, S. Ryu, and I. Park, "Highly stretchable and sensitive strain sensor based on silver nanowire–elastomer nanocomposite," *ACS Nano*, vol. 8, no. 5, pp. 5154–5163, 2014.
- [28] F. Xu and Y. Zhu, "Highly conductive and stretchable silver nanowire conductors," *Adv. Mater.*, vol. 24, no. 37, pp. 5117–5122, 2012.
- [29] T. Pinto, L. Cai, C. Wang, and X. Tan, "CNT-based sensor arrays for local strain measurements in soft pneumatic actuators," *Int. J. Intell. Robot. Appl.*, vol. 1, no. 2, pp. 157–166, 2017.
- [30] C. Larson *et al.*, "Highly stretchable electroluminescent skin for optical signaling and tactile sensing," *Science*, vol. 351, no. 6277, pp. 1071–1074, 2016.
- [31] Y.-L. Park and R. J. Wood, "Smart pneumatic artificial muscle actuator with embedded microfluidic sensing," in *Proc. IEEE SENSORS*, Nov. 2013, pp. 1–4.
- [32] S. Sareh, Y. Noh, M. Li, T. Ranzani, H. Liu, and K. Althoefer, "Macrobend optical sensing for pose measurement in soft robot arms," *Smart Mater. Struct.*, vol. 24, no. 12, p. 125024, 2015.
- [33] H. Zhao, K. O'Brien, S. Li, and R. F. Shepherd, "Optoelectronically innervated soft prosthetic hand via stretchable optical waveguides," *Sci. Robot.*, vol. 1, no. 1, p. eaai7529, 2016.
- [34] C. M. Homenick *et al.*, "Fully printed and encapsulated SWCNT-based thin film transistors via a combination of R2R gravure and inkjet printing," *ACS Appl. Mater. Interfaces*, vol. 8, no. 41, pp. 27900–27910, 2016.
- [35] T. Vuorinen, J. Niittynen, T. Kankkunen, T. M. Kraft, and M. Mäntysalo, "Inkjet-printed graphene/PEDOT:PSS temperature sensors on a skin-conformable polyurethane substrate," *Sci. Rep.*, vol. 6, Oct. 2016, Art. no. 35289.
- [36] S. L. Swisher *et al.*, "Impedance sensing device enables early detection of pressure ulcers *in vivo*," *Nature Commun.*, vol. 6, Mar. 2015, Art. no. 6575.
- [37] J. Suikkola *et al.*, "Screen-printing fabrication and characterization of stretchable electronics," *Sci. Rep.*, vol. 6, May 2016, Art. no. 25784.
- [38] R. J. Webster, III, and B. A. Jones, "Design and kinematic modeling of constant curvature continuum robots: A review," *Int. J. Robot. Res.*, vol. 29, no. 13, pp. 1661–1683, 2010.
- [39] S. Merilampi, T. Björninen, V. Haukka, P. Ruuskanen, L. Ukkonen, and L. Sydänheimo, "Analysis of electrically conductive silver ink on stretchable substrates under tensile load," *Microelectron. Rel.*, vol. 50, no. 12, pp. 2001–2011, 2010.
- [40] K. Le Phan, "Methods to correct for creep in elastomer-based sensors," in *Proc. IEEE SENSORS*, Oct. 2008, pp. 1119–1122.
- [41] I. D. Mayergoyz, "Mathematical models of hysteresis," *IEEE Trans. Magn.*, vol. MAG-22, no. 5, pp. 603–608, Sep. 1986.
- [42] C. Majidi, R. Kramer, and R. J. Wood, "A non-differential elastomer curvature sensor for softer-than-skin electronics," *Smart Mater. Struct.*, vol. 20, no. 20, pp. 105017–1–105017-7, 2011.

Anastasia Koivikko received the B.Sc. and M.Sc. degrees in biomedical engineering from the Tampere University of Technology, Tampere, Finland, in 2015 and 2017, respectively, where she is currently pursuing the Ph.D. degree. Her research interests include fabrication of soft robots.

Ehsan Sadeghian Raei received the B.Sc. degree in biomedical engineering from Azad University, Mashhad, Iran, in 2011, and the M.Sc. degree in electrical engineering from the Tampere University of Technology, Tampere, Finland, in 2016, where he is currently pursuing the Ph.D. degree in biomedical engineering. His research interests include energy-harvesting, thermoelectric materials, pneumatic actuators, and sensors for biomedical soft robots.

Mahmoud Mosallaei received the B.Sc. degree in polymer industries engineering from Shiraz Azad University, Shiraz, Iran, in 2007, and the M.Sc. degree in materials science from the Tampere University of Technology (TUT), Tampere, Finland, in 2015, where he is currently pursuing the Ph.D. degree in computing and electrical engineering. He finished his master's thesis with IMEC, Leuven, Belgium, in 2015. His research interests are mainly printed electronics and soft and deformable materials toward the development of stretchable electronic devices.



Matti Mäntysalo (M'09) received the M.Sc. and D.Sc. (Tech.) degrees in electrical engineering from the Tampere University of Technology, Tampere, Finland, in 2004 and 2008, respectively. He was an Adjunct Professor of Digital Fabrication. He is currently an Associate Professor of Electronics Materials and Manufacturing. He has authored or coauthored more than 100 international journal and conference articles. His research interests include printed electronics materials, fabrication processes, stretchable and soft electronics, and integration of printed electronics with silicon-based technology (hybrid systems). He is an Academy of Finland Research Fellow. He has been active in IEEE CMPT, IEC TC119 printed electronics standardization, and Organic Electronics Association.



Veikko Sariola (M'17) received the Dr. Tech. degree in electrical engineering from Aalto University, Finland, in 2012. From 2013 to 2015, he was a Post-Doctoral Researcher with Carnegie Mellon University. In 2016, he was appointed as a Research Fellow with the Academy of Finland. He is currently an Assistant Professor of Biomedical Microelectromechanical Systems with the Tampere University of Technology, Finland. His current research interests include bio-inspired materials and robotics.

MANUSCRIPT

V

Highly stretchable pneumatic strain gauges

Anastasia Koivikko, Vilma Lampinen, Mika Pihlajamäki, Kyriacos Yiannacou,
Vipul Sharma and Veikko Sariola

Unpublished manuscript

